ÉCOLE DE TECHNOLOGIE SUPÉRIEURE
UNIVERSITÉ DU QUÉBEC

THÈSE PAR ARTICLES PRÉSENTÉE À
L'ÉCOLE DE TECHNOLOGIE SUPÉRIEURE

COMME EXIGENCE PARTIELLE
À L'OBTENTION DU
DOCTORAT EN GÉNIE
Ph. D.

PAR
Pierre-Luc VACHON

ÉTUDE COMPARATIVE SUR LA PROPAGATION DE L'ENDOMMAGEMENT APRÈS IMPACT DES COMPOSITES CARBONE/ÉPOXY RENFORCÉS PAR PIQUAGE AU FIL KEVLAR ET TI-NI

MONTRÉAL, LE 14 DÉCEMBRE 2012

Pierre-Luc Vachon, 2012

Cette licence Creative Commons signifie qu'il est permis de diffuser, d'imprimer ou de sauvegarder sur un autre support une partie ou la totalité de cette œuvre à condition de mentionner l'auteur, que ces utilisations soient faites à des fins non commerciales et que le contenu de l'œuvre n'ait pas été modifié.

PRÉSENTATION DU JURY

CETTE THÈSE A ÉTÉ ÉVALUÉE

PAR UN JURY COMPOSÉ DE :

M. Vladimir Brailovski, directeur de thèse
Département de génie mécanique à l'École de technologie supérieure

M. Patrick Terriault, codirecteur de thèse
Département de génie mécanique à l'École de technologie supérieure

M. Omar Chaallal, président du jury
Département de génie de la construction à l'École de technologie supérieure

M. Anh Dung Ngo, membre du jury
Département de génie mécanique à l'École de technologie supérieure

Mme. Martine Dubé, membre du jury
Département de génie mécanique à l'École de technologie supérieure

M. Larry Lessard, examinateur externe
Département de génie mécanique à l'Université McGill

ELLE A FAIT L'OBJET D'UNE SOUTENANCE DEVANT JURY ET PUBLIC

LE 5 NOVEMBRE 2012

À L'ÉCOLE DE TECHNOLOGIE SUPÉRIEURE

REMERCIEMENTS

J'aimerais d'abord remercier mon directeur de recherche, M. Vladimir Brailovski, pour le support constant qu'il a démontré tout au long de ce projet. Sa présence, sa patience, son écoute et sa capacité de motivation ont été grandement appréciées tout au long de ces années. Un grand merci également à mon codirecteur, M. Patrick Terriault, qui a su me guider dans certains aspects de mon projet, toujours avec ouverture et disponibilité.

J'aimerais remercier également les professeurs Martin Viens et Larry Lessard pour m'avoir facilité l'accès à certains équipements. Ces remerciements vont également à M. Harold Hébert, de l'IMI, pour son soutien technique et sa disponibilité.

Je tiens à souligner aussi le support indispensable des techniciens du département de génie mécanique, qui sont toujours prêts à nous faire bénéficier de leurs compétences, de leur savoir-faire et de leur bonne humeur pour nous aider dans nos projets.

Évidemment, je ne peux passer sous silence tous mes collègues du LAMSI, la ligue du vieux poêle autant que les jeunesses, qui ont su rendre agréable ces années de travail. À Vincent, Thomas, Pierre, Karina, Yan, Yann et Yannick, Charles, Daniel, Sébastien, Jean-Sébastien, Émeric, Simon Simoneau, Fanny, Sergey, Guillaume : merci! Votre apport à la vie sociale de l'équipe fut inestimable!

Un merci spécial à mes parents, qui m'ont soutenu et encouragé durant toutes ces années. Cette fois, c'est vrai, c'est ma dernière année!

Et finalement, un gros merci à celle qui m'a enduré durant toute cette étape, dans les bons moments comme dans les moments de doute, ma copine, Dominique. Ton support indéfectible, ta compréhension, ton proverbial optimisme et ta bonne humeur m'ont rendu cette période de ma vie plus agréable!

ÉTUDE COMPARATIVE SUR LA PROPAGATION DE L'ENDOMMAGEMENT APRÈS IMPACT DES COMPOSITES CARBONE/ÉPOXY RENFORCÉS PAR PIQUAGE AU FIL KEVLAR ET TI-NI

Pierre-Luc VACHON

RÉSUMÉ

Les matériaux composites stratifiés présentent des propriétés mécaniques enviables dans le plan des couches de fibres, mais ils ont également une faiblesse naturelle dans la direction de l'épaisseur. Cette faiblesse peut donner lieu à l'apparition de zones délaminées invisibles à l'œil nu, particulièrement lors d'un impact à faible vitesse. Par conséquent, beaucoup de travaux de recherche ont été dédiés à l'étude de méthodes de renfort interlaminaire pour les stratifiés, dont notamment l'insertion de coutures transversales. Ce projet de recherche propose donc d'utiliser la technique de couture avec un fil métallique en alliage TiNi présentant un comportement superélastique. La combinaison de ces deux éléments devrait permettre l'amélioration de la résistance à la propagation du délaminage lors d'un chargement en flexion.

En premier lieu, un modèle numérique a été développé pour servir d'outil d'analyse des structures composites. Le modèle 3-D a été construit dans l'environnement ANSYS à partir d'éléments solides à 20 nœuds et d'éléments shell à 8 nœuds. La technique d'endommagement progressif a été implémentée, permettant ainsi de prédire la propagation du délaminage dans une plaque stratifiée soumise à différents chargements. Le modèle a d'abord été validé en traction quasi-statique avant d'être utilisé pour simuler des essais de flexion trois-points.

Par la suite, des plaques de composite carbone/époxy ont été fabriquées, chaque plaque comprenant des échantillons renforcés de couture et d'autres non renforcés. Deux types de renforts ont été utilisés : des fils TiNi superélastiques et des fils de Kevlar, à titre de référence. Les plaques renforcées ont été découpées pour permettre l'observation des coutures internes au microscope optique.

Des essais standardisés d'impact à faible vitesse et de compression résiduelle après impact ont été menés (ASTM D7136 et D7137) sur les échantillons renforcés et non renforcés. Les renforts de Kevlar se sont montrés les plus performants pour réduire la zone endommagée après impact, ainsi que pour améliorer la résistance résiduelle en compression. Les renforts de TiNi ont tout de même présenté une amélioration encourageante pour ce qui est de la performance lors de l'impact, alors que la différence lors de l'essai de compression s'est avérée très faible par rapport aux échantillons non renforcés.

En troisième lieu, la performance en flexion trois-points des échantillons a été quantifiée expérimentalement en calculant l'énergie nécessaire pour créer un volume unitaire de matériau endommagé (G_v, J/mm^3). Ce paramètre s'apparente au taux de restitution de l'énergie de déformation (*Strain Energy Release Rate*) communément rencontré dans les

travaux sur le délaminage. Les résultats ont montré que bien que les renforts de Kevlar permettaient d'améliorer la ténacité à l'endommagement lors de l'impact, cette performance n'était pas entièrement reportée sur la ténacité à l'endommagement durant l'essai de flexion. Ainsi, en relativisant l'énergie de déformation dégagée lors de la propagation du délaminage par rapport au volume de délaminage engendré, on constate que les renforts de TiNi augmentent la valeur de cette résistance à l'endommagement.

Finalement, l'étude numérique du comportement des renforts a permis d'identifier des différences qui étaient imperceptibles sur les courbes Force-Déplacement. Les deux types de renforts semblent favoriser la propagation interlaminaire du délaminage lors de la flexion, bien que ce comportement soit moins prononcé dans le cas du TiNi. Cependant, les fils de Kevlar semblent plus efficaces pour freiner la propagation latérale du délaminage entre les lignes de couture.

Mots-clés : matériaux composites, couture, modèle numérique, alliage à mémoire de forme, flexion trois-points, impact à faible vitesse, imagerie par ultrasons.

COMPARATIVE STUDY ON THE POST-IMPACT DAMAGE PROPAGATION OF CARBON/EPOXY COMPOSITES STITCHED WITH KEVLAR AND TI-NI THREADS

Pierre-Luc VACHON

ABSTRACT

Composite laminates have strong in-plane mechanical properties, but they are generally weaker through their thickness. This specificity makes the laminates prone to delamination, particularly under low-velocity impact loads. Consequently numerous research efforts have been dedicated to developing interlaminar reinforcing methods, such as transverse stitching. The present project proposes the use of the stitching technique combined with a special stitching thread made of superelastic TiNi alloy. This technology is intended to improve the delamination toughness in composite laminates loaded in bending.

In the first part of this study a numerical model was developed for analyzing composite structures. The 3-D finite element model was built with the ANSYS commercial software using 20-node solid and 8-node shell elements. The progressive damage modeling technique was used, allowing the prediction of delamination propagation in a laminate submitted to various loading modes. The model was validated for a plate under quasi-static traction load, and it was then used to simulate three-point bending tests.

Secondly, carbon/epoxy composite panels were fabricated, with each panel containing unstitched and stitched specimens. Two different materials were used for the stitching thread: superelastic TiNi wires and Kevlar threads as a reference. Some stitched specimens were cut in slices in order to make some observations of the internal stitch using an optical microscope.

Standardized low-velocity impact tests and compression after impact tests were carried out on stitched and unstitched specimens (ASTM D7136 and D7137). The Kevlar reinforcements have shown great performance in reducing the delaminated zone after impact, as well as in improving the residual compression strength. The TiNi reinforcements provided encouraging results during the impact tests, though being less effective than the Kevlar threads. During the compression after impact tests, only a slight difference could be measured between the TiNi-stitched and the unstitched specimens.

Then the bending performance of the specimens was quantified experimentally by calculating the energy required to create a unit volume of damaged material (G_v, J/mm^3). This metric is similar to the Strain Energy Release Rate (SERR) commonly used in studies on delamination. According to the experimental results, the damage resistance in three-point bending was not improved by the Kevlar reinforcements, despite the reduced damaged zone after the impact test. Indeed, when the strain energy in bending is relativized to the induced damaged volume during propagation, it turns out that the TiNi reinforcements are more effective than the Kevlar's for improving the damage resistance.

Finally, the numerical study on the behavior of both types of stitched reinforcements allowed identifying subtle differences between those. Indeed, both stitching threads (TiNi and Kevlar) promoted the interlaminar propagation of the delamination during simulation of the bending test, with this behavior being less pronounced for the TiNi-stitched plate. However the Kevlar threads seemed more effective for stopping this propagation in the zones between the stitches.

Keywords: composite materials, stitching, numerical model, shape memory alloy, three-point bending, low-velocity impact, ultrasound imaging.

TABLE DES MATIÈRES

Page

INTRODUCTION 1
Problématique 2
Objectifs des travaux de recherche 2
Méthodologie et organisation de la thèse 3
Contributions scientifiques 5

CHAPITRE 1 REVUE DE LA LITTÉRATURE 7
1.1 Matériaux composites 7
1.1.1 Généralités 7
1.1.2 Amélioration des propriétés interlaminaires des matériaux composites 10
1.1.2.1 Tissage et tressage 3-D 11
1.1.2.2 Insertion de tiges de renfort (*Z-pinning*) 13
1.1.2.3 Couture 15
1.1.3 Impacts à basse vitesse sur les matériaux composites et propriétés résiduelles après impact 20
1.2 Modélisation numérique 23
1.2.1 Modélisation du délaminage dans les matériaux composites 24
1.2.2 Modèle d'endommagement progressif 27
1.2.3 Dégradation des propriétés mécaniques 28
1.2.4 Modélisation de la couture dans les stratifiés 30
1.3 Alliages à mémoire de forme 32
1.3.1 Transformations martensitiques thermoélastiques 32
1.3.2 Mécanismes de transformation et de déformation 34
1.3.3 Propriétés fonctionnelles de l'alliage Ti-Ni 35
1.3.3.1 Effet mémoire de forme simple sens 35
1.3.3.2 Génération de contrainte 37
1.3.3.3 Superélasticité 37

CHAPITRE 2 ARTICLE #1 : MODELING OF DELAMINATION INITIATION AND PROPAGATION IN COMPOSITE LAMINATES UNDER MONOTONIC TENSILE LOADING USING THE PROGRESSIVE DAMAGE MODELING TECHNIQUE 39
2.1 Résumé (français) 39
2.2 Abstract 40
2.3 Introduction 40
2.4 Literature Review 42
2.5 Problem Statement 43
2.6 Development of the Model 44
2.6.1 Stress Analysis 45
2.6.2 Static Failure Analysis and Degradation of Mechanical Properties 45
2.7 Validation of the Model 46

2.7.1 Validation of the Model: Stress Analysis 47
2.7.1.1 Choice of Element Type 47
2.7.1.2 Numerical Study on the Use of Symmetry 53
2.7.2 Validation of the model: Failure analysis and degradation of mechanical properties 60
2.8 Conclusions 63
2.9 References 64

CHAPITRE 3 ARTICLE DE CONFÉRENCE : SUPPRESSION OF DELAMINATION PROPAGATION IN CARBON/EPOXY LAMINATES BY THE USE OF SUPERELASTIC STITCHING WIRES: PRELIMINARY RESULTS 69
3.1 Résumé (français) 69
3.2 Abstract 70
3.3 Introduction 70
3.4 Experimentations 71
3.4.1 Equipments 71
3.4.2 Specimen Preparation 72
3.4.3 Impact Testing 74
3.4.4 Compression After Impact (CAI) Testing 74
3.5 Results and Discussion 75
3.5.1 Impact Testing 75
3.5.2 CAI Testing 76
3.6 Conclusions 81
3.7 Acknowledgements 81
3.8 References 82

CHAPITRE 4 ARTICLE #2 : PREDICTION OF THE PROPAGATION OF IMPACT-INDUCED DELAMINATION IN CARBON/EPOXY LAMINATES 85
4.1 Résumé (français) 85
4.2 Abstract 85
4.3 Introduction 86
4.4 Experimentations 88
4.4.1 Specimen Preparation 88
4.4.2 Low-Velocity Impact Testing 88
4.4.3 Ultrasonic Imaging 89
4.4.4 Bending after Impact Testing 89
4.5 Finite Element Model 90
4.6 Results and Discussion 95
4.6.1 Bending after Impact Testing 95
4.6.2 Finite Element Modeling 98
4.7 Conclusions 102
4.8 Acknowledgements 103
4.9 References 103

CHAPITRE 5 ARTICLE #3 : IMPACT-INDUCED DAMAGE AND DAMAGE PROPAGATION UNDER FLEXURAL LOAD IN TINI AND KEVLAR-STITCHED CARBON/EPOXY LAMINATES.....107
5.1 Résumé (français) 107
5.2 Abstract.....107
5.3 Introduction.....108
5.4 Experimentations 110
5.4.1 Specimen Preparation 110
5.4.2 Low Velocity Impact Testing 112
5.4.3 Ultrasonic Imaging..... 113
5.4.4 Bending after Impact Testing..... 114
5.5 Finite Element Model 115
5.6 Results and Discussion 123
5.6.1 Impact and Bending After Impact Tests 123
5.6.2 Finite Element Modeling 128
5.7 Conclusions.....132
5.8 Acknowledgements.....135
5.9 References.....135

CONCLUSION GÉNÉRALE.....141

RECOMMANDATIONS 145

BIBLIOGRAPHIE.....147

LISTE DES TABLEAUX

Page

Tableau 1.1 Sommaire des performances obtenues avec des composites renforcés de coutures transversales, pour différents modes de chargement 17

Tableau 1.2 Différentes combinaisons de constantes de dégradation des propriétés mécaniques 29

Tableau 2.1 Failure criteria 45

Tableau 2.2 Degradation factors (T = Tensile and C = Compressive).....46

Tableau 2.3 Properties of graphite/epoxy 47

Tableau 2.4 Summary of the influence of using symmetry conditions.....60

Tableau 2.5 Properties of graphite/epoxy (T = Tension and C = Compression) 61

Tableau 3.1 Delaminated area of the impacted specimens 76

Tableau 3.2 CAI Strength 77

Tableau 3.3 Volume of the delaminated region 80

Tableau 4.1 a) Failure criteria and degradation factors; b) Mechanical properties of the carbon/epoxy material (in parentheses, properties assessed from the literature; otherwise as measured).....94

Tableau 5.1 a) Failure criteria and degradation factors; b) Mechanical properties of the carbon/epoxy material (in parentheses, properties assessed from the literature; otherwise as measured) and of the Kevlar and TiNi threads 120

Tableau 5.2 Experimental results for the volume of the delamination after impact (ultrasonic measurements) and the bending energy till failure (bending testing, zones I and II) 124

LISTE DES FIGURES

Page

Figure 1.1 Schéma d'un composite stratifié 8

Figure 1.2 Échantillon présentant plusieurs interfaces délaminées suite à un essai de compression....9

Figure 1.3 Méthodes efficaces de conception des raidisseurs 10

Figure 1.4 Structure des fibres pour le tissage 3-D (a) et le tressage 3-D (b) 11

Figure 1.5 Insertion de tiges dans un stratifié composite à l'aide d'un fusil à ultrasons 13

Figure 1.6 Poche de résine et déplacement localisé des fibres engendrés par l'insertion d'une tige (*Z-pin*) à travers l'épaisseur d'un stratifié 14

Figure 1.7 Exemple d'une couture dans un matériau composite....15

Figure 1.8 Types de points de couture utilisés pour renforcer les stratifiés 16

Figure 1.9 a) Vue de plan de la zone affectée par le fil de couture, montrant le déplacement des fibres du stratifié et la zone riche en résine; b) Vue de coupe à travers l'épaisseur du stratifié 18

Figure 1.10 Fabrication d'un composite carbone/époxy hybride incorporant des fils AMF 19

Figure 1.11 Plaque verre/époxy incorporant des coutures AMF 20

Figure 1.12 Délaminage, bris de matrice et bris de fibre induits par un impact à faible vitesse sur un stratifié graphite/époxy 21

Figure 1.13 Schéma de montage de l'essai ASTM D7137....22

Figure 1.14 Montage pour l'essai d'impact à faible vitesse ASTM D7136 23

Figure 1.15 Trois modes de propagation d'une fissure 24

Figure 1.16 Exemple typique de loi de cohésion d'interface 25

Figure 1.17 Exemple de modèle de cellule élémentaire pour l'étude d'un composite incorporant des coutures transversales....31

Figure 1.18 État de phase d'un matériau présentant une transformation martensitique.....33

Figure 1.19 Représentation schématique de la transformation martensitique à l'échelle atomique 34

Figure 1.20 Représentation schématique de l'effet mémoire de forme.....35

Figure 1.21 Représentation schématique du chemin thermomécanique nécessaire à l'observation de l'effet mémoire de forme simple sens 36

Figure 1.22 a) Représentation schématique du mécanisme de génération de contrainte sous chauffage et b) courbe contrainte-déformation. 37

Figure 1.23 Chargement thermomécanique permettant d'obtenir l'effet superélastique 38

Figure 2.1 Algorithm of the numerical model 44

Figure 2.2 Laminate under uniaxial tension 49

Figure 2.3 a) Mesh refinement near free edges of the plate and b) 1 element through thickness mesh of each layer 49

Figure 2.4 σ_z with SOLID46 and SOLID191 elements (ref. curve taken from [22]).....50

Figure 2.5 Interlaminar stress σ_{xz} for different numbers of elements through thickness for each layer, with Solid46 and Solid191 elements (ref. curve taken from [22]). The gap indicates the difference between Pagano's analytical solution and the numerical results from the present model with 2 elements through thickness of each ply 51

Figure 2.6 Interlaminar stress σ_{yz} for different numbers of elements through thickness for each layer, with Solid46 and Solid191 elements (ref. curve taken from [22]). The gap indicates the difference between Pagano's analytical solution and the numerical results from the present model with 2 elements through thickness of each ply 52

Figure 2.7 σ_z along y-axis at 90/0 interface (ref. curve taken from [22]).....55

Figure 2.8 σ_{xz} along y-axis at +45/-45 interface (ref. curve taken from [22]).....55

Figure 2.9 σ_{yz} distribution along y-axis at 90/0 interface (ref. curve taken from [22]).....56

Figure 2.10 Two different shapes of the stress distribution curve in the transition zone near the plane of symmetry.....57

Figure 2.11 Relative error between the half and complete models as a function of x-coordinate (plane of symmetry is at x = 0) 58

Figure 2.12 σ_{xz} for the quarter-model at x = 1 element length (0.5 mm) 59

Figure 2.13 State of delamination at 525 MPa (monotonic tensile test) for a $[\pm 45/0/90]_s$ layout, from a) numerical results, and b) X-ray imaging [23]....62

Figure 2.14 Areal delamination percentage at different stress states. Reference data are calculated from [23] 63

Figure 3.1 a) Modified lock stitch (after [7]); b) detail of the stitched specimen....73

Figure 3.2 Micrographs of a) Kevlar-stitched and b) TiNi-stitched laminates....74

Figure 3.3 ASTM D7137 fixture for CAI testing 75

Figure 3.4 Impacted TiNi-stitched specimen with delaminated zone at the centre (C-scan imaging) 76

Figure 3.5 Surfaces of a ruptured unstitched specimen: a) impacted face; b) opposite face 78

Figure 3.6 Surface crack path in a) Kevlar-stitched and b) TiNi-stitched specimens 78

Figure 3.7 Schematic representation of: a) C-Scan image showing circular delamination and lines for the B-Scans; b) B-Scan image....79

Figure 3.8 Example of a B-Scan image from an impacted unstitched specimen 80

Figure 4.1 a) Example of a B-Scan image from an impacted specimen; b) Schematic of a C-scan image containing a delaminated zone, along with the lines for the B-Scans 89

Figure 4.2 Schematic of: a) the three-point bending test; b) the disposition of the two video cameras....90

Figure 4.3 a) Complete mesh; b) Refined solid mesh 92

Figure 4.4 Algorithm of the numerical model 93

Figure 4.5 Typical shape and dimensions of a delaminated zone as measured by ultrasonic inspection (dimensions in mm) 95

Figure 4.6 Three-point bending response of unimpacted and impacted specimens showing the effect of the impact damage on the flexural behavior and the three zones of the force-displacement curves....96

Figure 4.7 a) Delamination cracks at the specimen's free edge and fiber breakage at the upper surface; b) Progression of the lower ply delamination; c) Final rupture of the lower ply....97

Figure 4.8 C-Scan images of the propagation of delamination at six displacement levels in three-point flexure tests 98

Figure 4.9 Progression of the delamination as obtained from the numerical model 99

Figure 4.10 Comparison between the Force-Displacement response and the accumulation of delamination damage as obtained from the numerical model 100

Figure 4.11 Force-displacement response and delamination images from numerical modeling and experimental tests 101

Figure 5.1 a) Modified lock stitch; b) Schematic of the stitched specimens 111

Figure 5.2 Tensile curves obtained for both Kevlar and superelastic TiNi stitching threads....111

Figure 5.3 Kevlar- and TiNi-stitched specimens 112

Figure 5.4 a) Example of a B-Scan image from an impacted specimen; b) Schematic of a C-Scan image containing a delaminated zone, along with the lines for the B-Scans 114

Figure 5.5 Setup for the three-point bending tests....114

Figure 5.6 a) Complete mesh; b) Refined solid mesh 116

Figure 5.7 Cut view at the mid-length of the modeled plate (left) and detail of the modeled stitching thread with the square cross-section area equal to that of two cylindrical threads (right)....117

Figure 5.8 Deformed shape of the plate loaded in three-point bending (cut view at the mid-length); the displacement is applied on a partial zone along the width of the plate……...118

Figure 5.9 Algorithm of the numerical model 120

Figure 5.10 Characteristic constants and simulated tensile curve of the superelastic material model, superimposed with experimental tensile curves....122

Figure 5.11 Typical shape and dimensions of an axisymmetric delaminated zone as measured by ultrasonic inspection (dimensions in mm) 123

Figure 5.12 Force-displacement response in three-point bending for unstitched, TiNi- and Kevlar-stitched specimens 125

Figure 5.13 Energy required to create a unit volume of impact-induced damage (left) and for bending-induced delamination propagation (right) 127

Figure 5.14 Predicted force-displacement response in bending for the three structures. The Kevlar-stitched and the TiNi-stitched models stopped at 2.5 and 3.3 mm in deflection, respectively, because of highly distorted elements (marked as 'x'); the unstitched model was intentionally stopped at 3.7 mm (marked as '//') 129

Figure 5.15 Propagation of the delamination at the mid-length of the plate, as measured by ultrasonics and as predicted by FE modeling [26].....130

Figure 5.16 Numerical prediction of the propagation of the delamination for the unstitched, TiNi- and Kevlar-stitched plates.....132

LISTE DES ABRÉVIATIONS, SIGLES ET ACRONYMES

AMF	Alliage à mémoire de forme
A_s, A_f	Températures austénitiques, début et fin de transformation (°C)
CAI	Compression résiduelle après impact (*Compression After Impact*)
FE	Éléments finis (*Finite Element*)
M_s, M_f	Températures martensitiques, début et fin de transformation (°C)
PEEK	Polyétheréthercétone
SERR	Taux de restitution de l'énergie de déformation (*Strain Energy Release Rate*)
Std. Dev.	Écart-type (*Standard Deviation*)
TiNi	Alliage Titane-Nickel

INTRODUCTION

Les matériaux composites sont formés de plusieurs couches de fibres liées par une matrice, qui est souvent une résine polymérique. Cette structure sous forme d'empilement permet de maximiser certaines propriétés mécaniques dans les directions voulues. Ainsi, le ratio rigidité vs poids de la structure peut être fortement amélioré si l'on compare aux métaux comme l'aluminium ou l'acier, ce qui fait des composites une classe de matériau de plus en plus prisée dans le domaine aéronautique.

Cependant, les stratifiés sont particulièrement sensibles aux chargements hors-plan, comme les impacts à basse vitesse, qui peuvent créer des dommages internes invisibles à l'œil nu (délaminage, rupture de matrice et de fibres). Beaucoup de travaux de recherche ont été dédiés à l'amélioration des propriétés hors-plan des composites. Une des solutions technologiques qui a démontré un potentiel intéressant est l'insertion de coutures transversales, qui se fait dans la majorité des cas à l'aide de fils de Kevlar. Ce type de renforcement permet notamment d'améliorer la ténacité au délaminage selon divers modes de chargement et la résistance résiduelle en compression longitudinale, en plus de réduire les dimensions de la zone endommagée par l'impact.

Les alliages à mémoire de forme (AMF) sont des métaux qui ont la capacité de subir de très grandes déformations récupérables (de l'ordre de 8% dans le cas de l'alliage Ni-Ti (Brailovski et al., 2003)). Cette reprise de forme peut s'effectuer par le biais de deux propriétés : la superélasticité et la mémoire de forme. La propriété de superélasticité permet le retour de forme sans apport d'énergie externe, alors que le phénomène de mémoire de forme apparaît lorsque l'on chauffe la pièce déformée. Par ailleurs, le cycle « déformation – retour de forme » sur un matériau superélastique permet d'obtenir une dissipation d'énergie. Ces propriétés particulières expliquent la présence de plus en plus grande des AMF dans divers domaines, dont l'aérospatiale, le bâtiment et le domaine médical.

Problématique

Malgré le grand nombre de publications récentes traitant du renforcement des stratifiés par couture, il n'existe toujours pas d'étude sur l'utilisation des propriétés superélastiques ou de mémoire de forme pour le fil de renfort. Par ailleurs, les modèles numériques de délaminage disponibles dans la littérature sont généralement dédiés à l'étude de cas simples standardisés, comme les cas de fissures simples en modes I, II ou mixte. De plus, l'analyse de la performance des composites après impact se limite généralement à la mesure de la résistance résiduelle en compression longitudinale, et très peu de données existent quant aux performances en flexion. Par conséquent, le comportement des stratifiés comportant une zone endommagée après un impact demande toujours à être étudié et caractérisé, particulièrement lors de chargements en flexion.

Objectifs des travaux de recherche

L'objectif principal de ce projet de recherche consiste à développer un système de renfort par couture de fils AMF superélastiques permettant d'améliorer la résistance à l'endommagement des composites carbone/époxy. Ce système doit montrer une certaine efficacité pour des structures soumises à un chargement en flexion quasi-statique, après avoir subi un impact à faible vitesse.

Par ailleurs, les objectifs spécifiques se divisent en quatre points :

1. Développer un modèle numérique permettant d'étudier la propagation de l'endommagement dans les structures composites avec ou sans couture. Le modèle doit être versatile, c'est-à-dire qu'il doit permettre la variation des paramètres suivants : modes de chargements, séquences d'empilement des couches, type de matériau pour le fil de couture, paramètres de couture (diamètre du fil, longueur de point et distance entre les lignes de couture, prétension dans le fil), état de dégradation du stratifié suite à l'impact à faible vitesse;

2. Développer la technologie de couture de fils AMF et vérifier ses performances à l'aide d'essais normalisés;

3. Mener une étude expérimentale sur le comportement en flexion après impact des stratifiés carbone/époxy. Cette partie permettra de mieux comprendre les mécanismes de propagation du délaminage lorsque la zone dégradée par l'impact est entièrement incluse dans les dimensions de l'échantillon;

4. Étudier la relation entre le renfort cousu et le matériau composite environnant lors de l'essai de flexion post-impact. Une analyse numérique permettra de cerner le rôle du fil dans le comportement localisé de la structure renforcée.

Méthodologie et organisation de la thèse

Pour mener à bien ce projet de recherche, les travaux seront divisés en quatre parties, chacune de ces parties faisant l'objet d'un chapitre.

En premier lieu, un modèle numérique sera développé à l'aide du logiciel commercial ANSYS, de façon à prédire l'initiation et la propagation de l'endommagement (rupture de matrice, de fibre et délaminage) pour un cas simple de chargement, soit une plaque en traction quasi-statique. La validation du modèle sera effectuée à l'aide d'images provenant de la littérature et présentant l'évolution de la zone délaminée durant l'essai de traction. Ce modèle sera par la suite utilisé pour l'étude des plaques renforcées, en variant numériquement certains paramètres de couture.

En second lieu, la technique de couture à l'aide de fils en alliage TiNi superélastique sera développée. Des échantillons renforcés et non renforcés seront fabriqués. Des échantillons seront découpés pour permettre l'observation des coutures au microscope optique. La performance des renforts sera ensuite évaluée à l'aide de l'essai normalisé de compression après impact (ASTM D7136 et D7137). Des échantillons incorporant des renforts de Kevlar seront également fabriqués de façon à comparer les performances des deux types de renfort.

En troisième lieu, une étude expérimentale sera menée pour caractériser le comportement en flexion trois points des plaques composites non renforcées ayant subi un chargement d'impact. La progression du délaminage durant l'essai mécanique sera suivie à l'aide de l'imagerie par ultrasons (B-Scan et C-Scan). L'essai de flexion après impact sera également modélisé, en considérant une zone endommagée au centre de la plaque. Cette zone verra ses propriétés mécaniques dégradées pour simuler les dommages induits par l'impact à faible vitesse. La prédiction de la propagation du délaminage obtenue avec le modèle numérique sera comparée avec les images expérimentales, et les mécanismes de propagation du délaminage seront étudiés.

Finalement, la performance des renforts TiNi et Kevlar sera évaluée pour un chargement en flexion trois points après impact. Le modèle numérique permettra de modifier les paramètres de couture de façon à isoler l'effet de l'utilisation d'un matériau superélastique sur les résultats obtenus.

Dans l'ensemble, le travail mené au cours de cette recherche a fait l'objet de trois articles de revue et d'un article de conférence, suivant la méthodologie décrite à la section précédente. Ces quatre publications composeront donc le corps de cette thèse, avec un chapitre pour chaque article. Ensuite, une conclusion cernera les points importants de cette recherche et apportera une ouverture pour la suite des travaux. Enfin, quelques recommandations seront proposées. Les paragraphes qui suivent donnent le détail des quatre publications issues de ce travail.

Partie 1 : Développement du modèle numérique

Cette partie est présentée dans le chapitre 2 de cette thèse. Elle fait l'objet d'un premier article scientifique intitulé « Modeling of Delamination Initiation and Propagation in Composite Laminates Under Monotonic Tensile Loading Using the Progressive Damage Modeling Technique », publié dans *Science and Engineering of Composite Materials*, vol. 16, no 2, p. 99-114. DOI : 10.1515/SECM.2009.16.2.99.

Partie 2 : Développement de la technologie de couture avec des fils TiNi

Cette partie, qui est présentée dans le chapitre 3 de cette thèse, fait l'objet d'un article de conférence intitulé « Suppression of delamination propagation in carbon/epoxy laminates by the use of superelastic stitching wires: preliminary results », présenté à la conférence *Eight Joint Canada-Japan Workshop on Composites*, Montréal, Qc, 26-29 juillet 2010.

Partie 3 : Étude expérimentale en flexion après impact sur des échantillons non renforcés

Cette partie est présentée dans le chapitre 4 de cette thèse. Elle fait l'objet d'un second article scientifique intitulé « Prediction of the Propagation of Impact-Induced Delamination in Carbon/Epoxy Laminates », publié dans *Composite Structures*, v95, p. 227-235, 2013. DOI : 10.1016/j.compstruct.2012.07.021.

Partie 4 : Étude expérimentale et numérique de la performance des plaques renforcées

Cette partie est présentée dans le chapitre 5 de cette thèse. Elle fait l'objet d'un troisième article scientifique intitulé « Impact-Induced Delamination and Delamination Propagation under Flexural Load in TiNi and Kevlar-Stitched Carbon/Epoxy Laminates », soumis à la revue *Composite Structures* en août 2012.

Contributions scientifiques

Les contributions principales de cette thèse s'énoncent en deux points. D'abord, l'étude expérimentale et numérique d'une plaque composite renforcée de coutures en AMF à l'état superélastique a été menée. La fabrication d'échantillons a été effectuée avec succès, et les résultats des essais de flexion après impact ont montré qu'il peut y avoir un certain gain de performance lorsque l'on utilise un fil AMF comme renfort transversal.

En second lieu, un modèle numérique polyvalent a été construit pour permettre l'analyse de structures composites diverses, renforcées ou non. Le modèle est bâti de façon à permettre une prédiction fiable de la propagation du délaminage à partir d'une zone pré-endommagée (e.g. impact) ou d'un concentrateur de contrainte (surfaces libres, etc.). Le modèle est entièrement paramétré, de sorte que les renforts puissent être disposés de différentes façons (distance entre les points de couture et entre les lignes). Cet outil numérique a démontré sa capacité à représenter la propagation du délaminage lors d'essais simulés de flexion après impact, pour des plaques renforcées de TiNi superélastique et de Kevlar, ainsi que pour des plaques sans renforts.

Finalement, la contribution secondaire de cette thèse consiste en l'étude du comportement en flexion après impact d'une plaque composite, dont la zone pré-endommagée est entièrement incluse dans les dimensions de la plaque. La propagation du délaminage lors de l'application du chargement a été cartographiée par la méthode des ultrasons, et prédite par éléments finis.

CHAPITRE 1

REVUE DE LA LITTÉRATURE

Cette section présente une revue de la littérature scientifique traitant de différents sujets, ce qui permet d'introduire des notions importantes et de mettre en contexte la problématique soulevée dans cette thèse. Par la suite, les objectifs de la recherche et la méthodologie utilisée seront définis, permettant ainsi de décrire l'organisation générale des différentes parties de cette thèse.

1.1 Matériaux composites

1.1.1 Généralités

L'appellation « matériau composite » désigne tout agencement de deux matériaux différents (ou plus) dont la structure combinée est à l'échelle macroscopique. La combinaison d'un renfort et d'une matrice permet d'obtenir un matériau dont les propriétés surpassent celles des constituants seuls. Les composites utilisés de façon industrielle sont généralement produits sous forme d'empilement de couches de fibres (le renfort) reliées entre elles par une résine polymérique (la matrice), formant ainsi un stratifié. Dans cet agencement, le rôle du renfort est d'assurer la rigidité de la structure et de supporter les chargements en traction. La matrice, quant à elle, supporte les chargements en compression et en cisaillement, tout en maintenant le positionnement géométrique des fibres. Les fibres de verre, de carbone, d'aramide (Kevlar) et de bore comptent parmi les types de renforts les plus utilisés. Quant aux matrices polymériques, les résines époxydes, polyesters, vinylesters et polyétheréthercétone (PEEK), pour n'en nommer que quelques-unes, sont couramment utilisées. Il est également possible de choisir une matrice céramique ou métallique pour la fabrication d'un composite lorsque les températures d'utilisation sont particulièrement élevées. La Figure 1.1 présente la structure générale d'un composite stratifié.

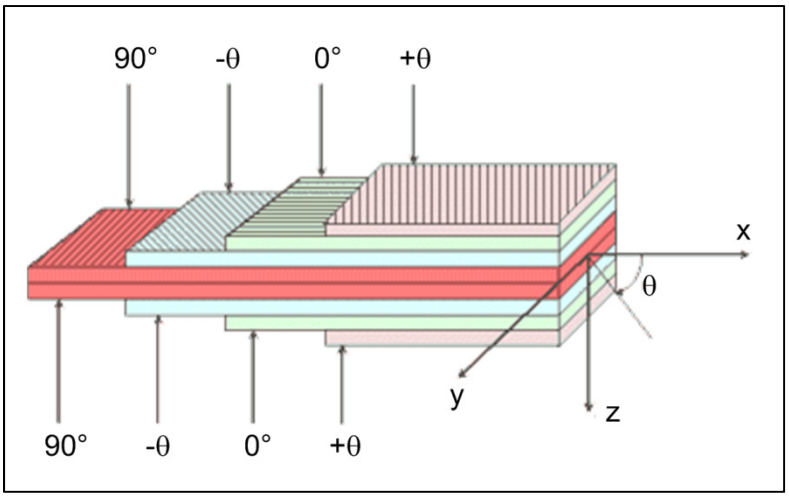

Figure 1.1 Schéma d'un composite stratifié
Tirée de University of Latvia (2012)

Le principal avantage des composites par rapport aux matériaux plus communs, comme les métaux, réside dans la possibilité de varier les propriétés mécaniques de la structure dans différentes directions, d'abord en choisissant les types de renfort et de matrice, puis en orientant les couches fibreuses de façon efficace. En jouant sur le nombre de couches, leur orientation et leur emplacement dans l'épaisseur du stratifié, il est possible de fabriquer des structures dont la rigidité et la résistance atteignent ou surpassent celles de structures métalliques équivalentes, tout en étant plus légères. Cela explique l'engouement des compagnies aéronautiques pour ces matériaux qui sont, de fait, de plus en plus présents dans les structures d'avions. Parmi les exemples récents ou futurs, citons le Learjet 85 de Bombardier, dont la structure primaire (fuselage et ailes) est entièrement faite de matériaux composites (Bombardier, 2011), ou les Boeing 787 et Airbus A350 XWB, dont environ 50% des pièces structurales sont faites de composites (Airbus, 2012; The Boeing Company, 2008). De plus, ces matériaux présentent une grande résistance à la corrosion et à la propagation des fissures en fatigue, ce qui leur confère un avantage supplémentaire sur l'aluminium, traditionnellement très présent dans les structures aéronautiques (Kaw, 2006).

La structure stratifiée des matériaux composites procure d'excellentes propriétés mécaniques dans le plan des couches de fibres (directions X et Y, Figure 1.1). Cependant, les propriétés

hors plan (dans la direction de l'épaisseur) sont généralement inférieures, puisqu'elles sont gouvernées par les propriétés de la matrice. C'est le cas notamment des propriétés interlaminaires en cisaillement (plans XZ et YZ, Figure 1.1) et en traction (direction Z, Figure 1.1). Cette faiblesse caractéristique des stratifiés est à l'origine d'un problème qu'on nomme le délaminage, qui consiste en un décollement localisé entre deux couches d'un stratifié, tel qu'illustré à la Figure 1.2.

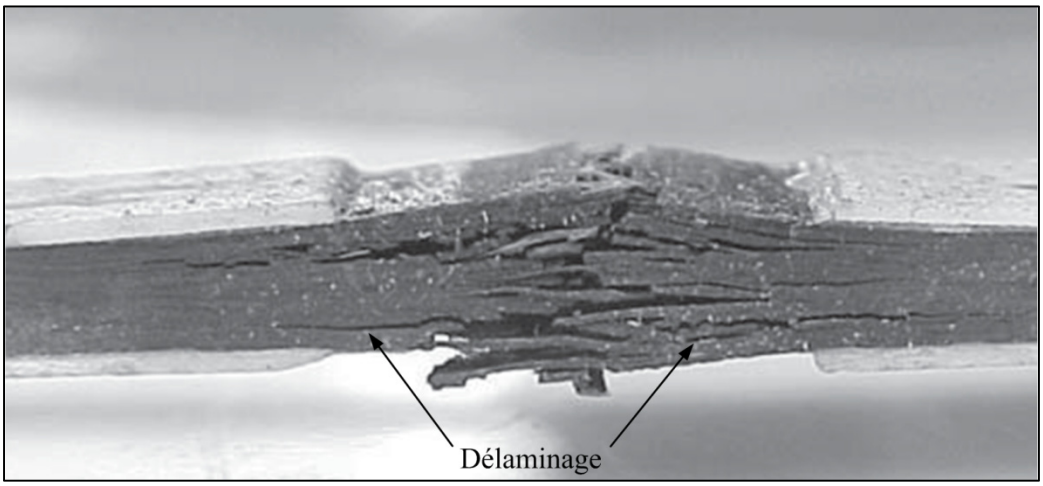

Figure 1.2 Échantillon présentant plusieurs interfaces délaminées suite à un essai de compression
Tirée de De Paiva, Mayer et Rezende (2005)

Il existe plusieurs causes pouvant expliquer l'apparition d'un délaminage : un problème lors de l'infusion ou de la cure de la matrice, la présence de corps étrangers, un impact sur la surface de la pièce, un chargement cyclique favorisant l'apparition et la propagation de fissures dans la matrice jusqu'à une interface du stratifié, etc. (Campbell, 2010). Ce type de défaut constitue un problème critique puisque sa présence et sa propagation en service peuvent affecter grandement les propriétés mécaniques de la structure, particulièrement lors de sollicitations en compression ou de chargements cycliques. De plus, le fait que le délaminage soit généralement invisible à l'œil nu le rend difficile à détecter autrement qu'à l'aide de techniques d'inspection comme les ultrasons ou les rayons X. Dans cette optique, il n'est pas surprenant de constater l'abondance des travaux visant à améliorer la résistance au délaminage dans la littérature scientifique récente. Les prochaines sections décrivent les

différentes techniques proposées par les chercheurs ainsi que l'approche préconisée dans cette thèse.

1.1.2 Amélioration des propriétés interlaminaires des matériaux composites

Il existe trois approches dans l'étude des méthodes permettant de retarder l'apparition ou la propagation du délaminage (Dransfield, Baillie et Mai, 1994; Greenhalgh et Hiley, 2003) : 1- l'amélioration des techniques de conception, de fabrication et de coupe; 2- l'amélioration des propriétés des constituants du composite; 3- l'ajout de renforts dans le stratifié.

La première approche est évidemment intéressante d'un point de vue industriel, puisqu'elle ne nécessite pas le développement et la certification de nouveaux matériaux. Un bon exemple de cette méthode est la conception des raidisseurs sur une structure composite. La Figure 1.3 présente trois méthodes qui s'avèrent efficaces pour réduire le décollement entre le raidisseur et la peau de la structure (Greenhalgh et Hiley, 2003).

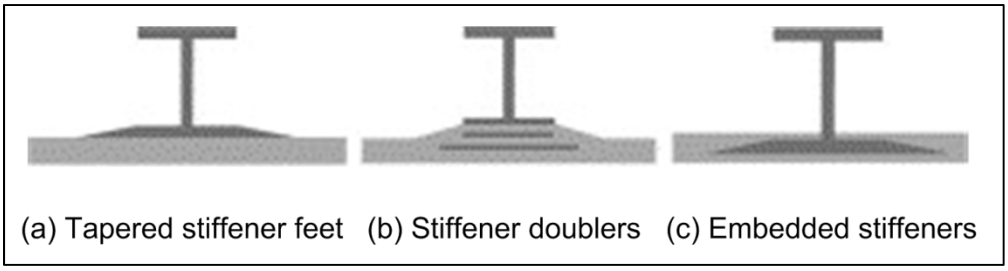

Figure 1.3 Méthodes efficaces de conception des raidisseurs
Tirée de Greenhalgh et Hiley (2003)

La deuxième approche cible les constituants du composite : amélioration des propriétés de la résine (*toughened resins*) et de l'adhérence fibre/matrice, ajout de couches adhésives aux interfaces du stratifié, développement de résines auto-réparantes (*self-healing*). Le coût élevé de ces nouvelles technologies freine leur utilisation dans les applications industrielles, et il est parfois difficile de reporter une amélioration de la résine elle-même sur le comportement de la structure composite (Partridge, 2008).

La troisième approche consiste plutôt à renforcer la structure composite dans la direction de l'épaisseur, de façon à contrebalancer la faiblesse naturelle des stratifiés dans cette direction. Pour ce faire, plusieurs techniques ont été développées, telles que le tissage et le tressage 3-D, l'insertion de tiges en Z (*Z pinning*) et la couture (*stitching*).

1.1.2.1 Tissage et tressage 3-D

Les techniques de tissage et de tressage 3-D permettent de fabriquer des pièces de différentes formes à l'aide d'une machine à tisser ou à tresser, lesquelles sont ensuite infusées avec la résine. Le composite qui en résulte possède une structure tridimensionnelle présentant une meilleure résistance à l'impact et à la propagation du délaminage qu'un stratifié équivalent (Gerlach et al., 2012). La différence entre le tissage et le tressage 3-D tient dans l'orientation des différents fils composant la structure. Comme le montre la Figure 1.4, le tissage comprend des fils placés à 90° les uns des autres, tandis que le tressage permet de placer les fils à différents angles.

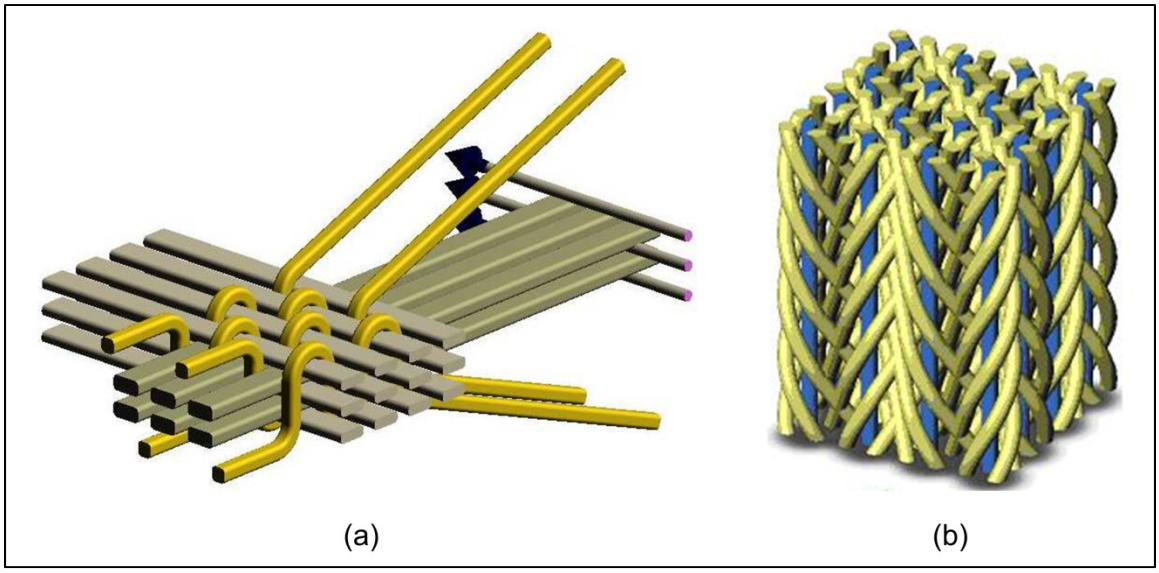

Figure 1.4 Structure des fibres pour le tissage 3-D (a) et le tressage 3-D (b)
Tirée de 3Tex (2007)

Mis à part les avantages en terme de résistance mécanique, les techniques de tissage et de tressage présentent les intérêts suivants (Bogdanovich et Mungalov, 2003; Mouritz et al., 1999) :

1. Permettent d'obtenir des pièces de forme complexe et près de la forme désirée (*near net shape*);

2. Éliminent les étapes de découpe et d'empilement nécessaires pour la fabrication de stratifiés;

3. Permettent une vaste possibilité de structures différentes en variant les types et grosseurs de fils, ainsi que les espacements entre les fils;

4. Offrent un processus de fabrication entièrement automatisé.

Par contre, plusieurs problèmes limitent toujours l'utilisation commerciale de ces techniques :

1. La comparaison des propriétés mécaniques de ces composites avec celles de composites 2-D équivalents montre parfois une dégradation de ces premières, quoiqu'aucun consensus ne ressort de la revue de littérature de Mouritz et Cox (Mouritz et Cox, 2010);

2. Les dimensions des pièces sont limitées par les dimensions des machines à tisser/tresser disponibles;

3. La complexité du montage des bobines allonge les temps de préparation avant de démarrer la production.

1.1.2.2 Insertion de tiges de renfort (*Z-pinning*)

La technique de renfort des stratifiés à l'aide de petites tiges consiste à insérer des tiges à travers l'épaisseur des couches de fibres, avant ou pendant l'infusion de résine (Baker, Dutton et Kelly, 2004). Les tiges, généralement faites de titane, de carbone/époxy ou de verre/époxy, sont d'abord maintenues perpendiculairement aux fibres dans une couche de support en polymère, avant d'être insérées dans le composite par la pression d'un autoclave, ou à l'aide d'un appareil à ultrasons. La Figure 1.5 présente le schéma de principe de l'insertion des tiges avec un fusil à ultrasons.

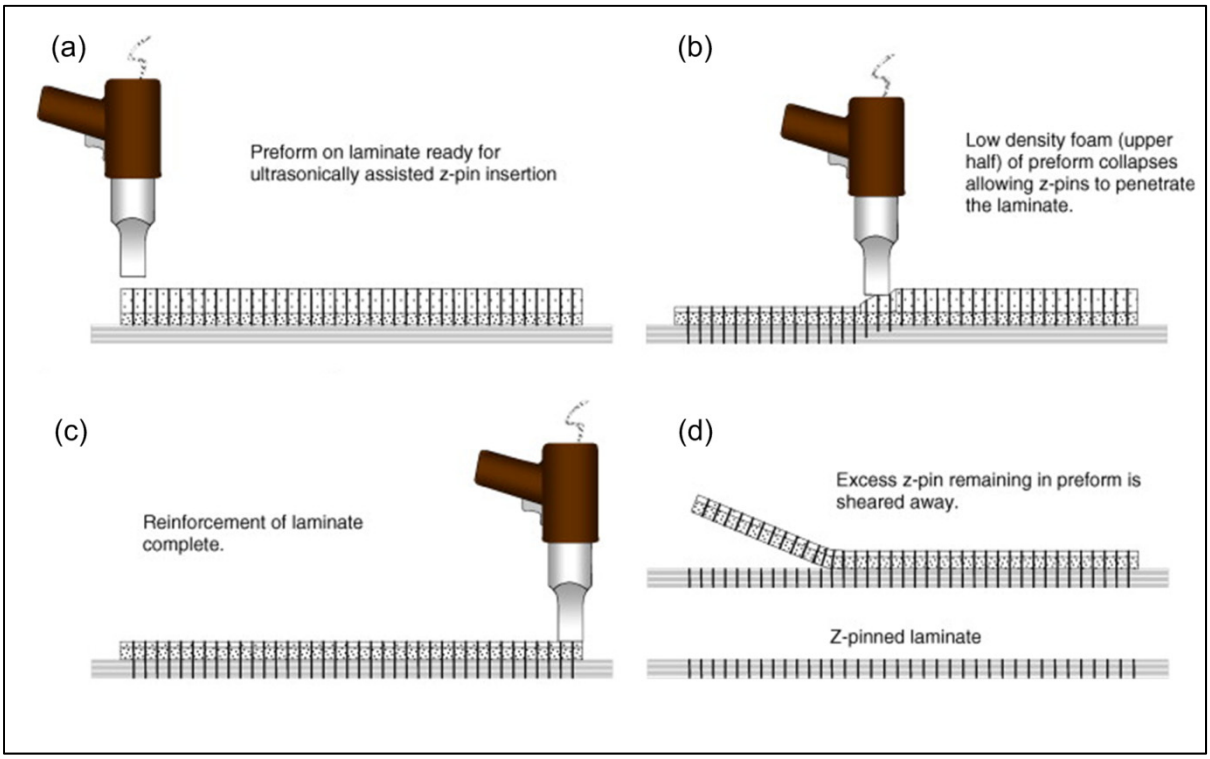

Figure 1.5 Insertion de tiges dans un stratifié composite à l'aide d'un fusil à ultrasons
Tirée de Mouritz (2007)

Cette technique de renfort permet d'améliorer grandement la ténacité au délaminage des stratifiés, surtout pour les chargements en mode I, dû à l'effet de pont qui est créé entre les couches du stratifié (Rugg, Cox et Massabò, 2002). Les tiges en Z permettent également de

transformer une propagation instable du délaminage en propagation stable, ce qui constitue une qualité appréciable du point de vue de la philosophie de tolérance au dommage. Il a été également démontré que lors d'un essai d'impact à basse vitesse, la présence de tiges en Z dans les stratifiés permet de réduire la surface délaminée ainsi que la résistance en compression après impact (Zhang, Hounslow et Grassi, 2006).

Cependant, des essais expérimentaux et de modélisation ont montré que les tiges en Z avaient un effet nuisible sur les modules en tension et en cisaillement dans le plan des stratifiés (Chang, Mouritz et Cox, 2006; Dickinson, Farley et Hinders, 1999). Les résistances en tension, en compression et en flexion sont également affectées par ces renforts (Mouritz, Chang et Cox, 2007; Steeves et Fleck, 2006). Dans tous les cas, les diminutions des propriétés mécaniques dans le plan des couches peuvent s'expliquer par les poches de résine qui sont créées autour des tiges en Z, dû au fait que l'insertion de ces tiges écarte localement les fibres du composite en plus de les abîmer (Figure 1.6).

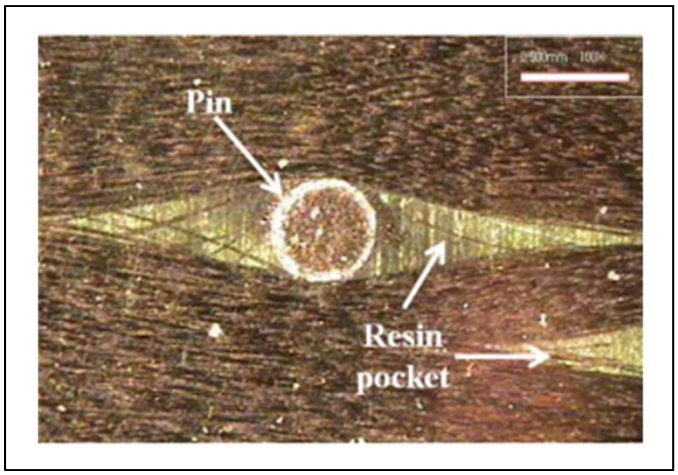

Figure 1.6 Poche de résine et déplacement localisé des fibres engendrés par l'insertion d'une tige (*Z-pin*) à travers l'épaisseur d'un stratifié
Tirée de Park et al. (2012)

1.1.2.3 Couture

L'insertion de coutures dans les stratifiés composites est une technique de renfort qui est étudiée depuis les années '80 (Mignery, Tan et Sun, 1985). Le principe consiste à coudre un empilement de couches de fibres ou de pré-imprégnés à l'aide d'une machine à coudre industrielle. L'empilement ainsi renforcé peut ensuite être infusé avec la résine ou placé en autoclave. La Figure 1.7 montre un exemple d'une couture dans un matériau composite. Différents types de points de couture peuvent être utilisés, mais le plus populaire est sans contredit le point « modified lock stitch » (Baker, Dutton et Kelly, 2004). Le détail de ce type de couture est présenté à la Figure 1.8, ainsi que deux autres types de points utilisés occasionnellement. La popularité du point « modified lock stitch » tient à sa simplicité et au fait que le croisement des deux fils s'effectue à la surface de la plaque, plutôt qu'à l'intérieur comme dans le cas du point « lock stitch ». De plus, le point « chain stitch » engendre un amoncellement de fils sur un côté de la plaque, ce qui peut créer des distorsions en surface ainsi qu'un chemin préférentiel pour le passage de la résine, lors de l'infusion (Ogale et Mitschang, 2004).

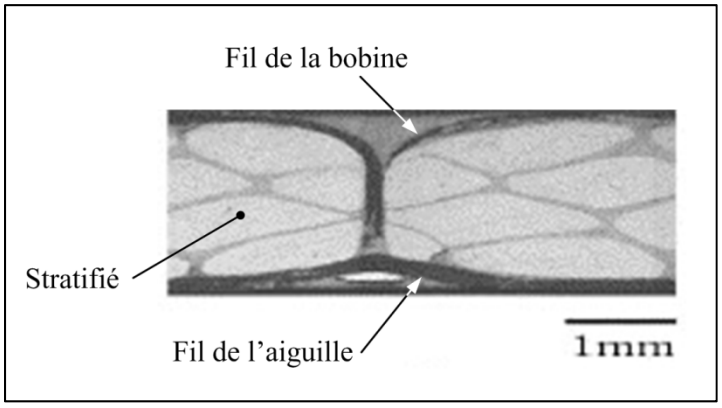

Figure 1.7 Exemple d'une couture dans un matériau composite
Tirée et adaptée de Chun, Kim et Byun (2006)

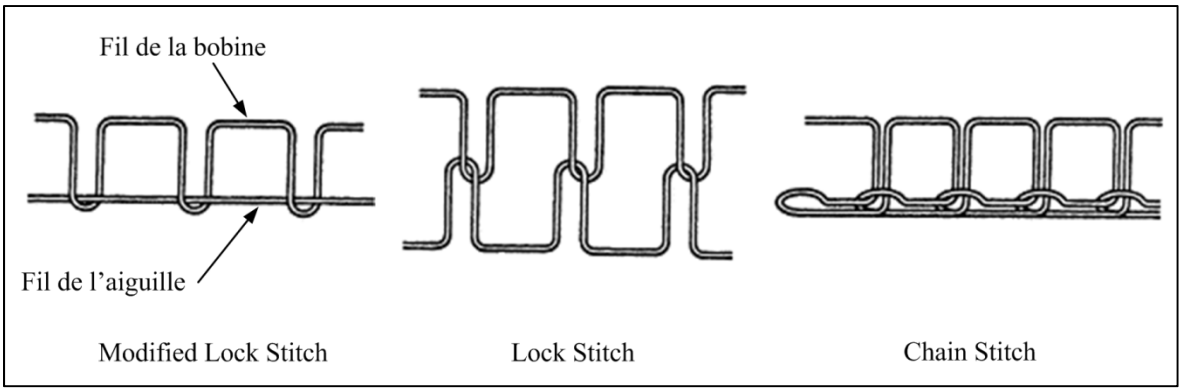

Figure 1.8 Types de points de couture utilisés pour renforcer les stratifiés
Tirée et adaptée de Mouritz et Cox (2000)

Au cours des quinze dernières années, plusieurs travaux de recherche ont été menés dans le but de caractériser les propriétés interlaminaires et la résistance au délaminage des composites incorporant des coutures. Différents modes de sollicitation ont été étudiés :

1. Modes I, II et mode mixte I-II d'ouverture de la fissure (Chen, Ifju et Sankar, 2005; Dransfield, Jain et Mai, 1998; Jain, Dransfield et Mai, 1998; Massabo, Mumm et Cox, 1998; Rys, Sankar et Ifju, 2010; Sankar et Sharma, 1997; Tsai et Chen, 2005; Wood et al., 2007a; Wood et al., 2007b);

2. Impact à basse vitesse et compression après impact (Aymerich et Priolo, 2008; Byun et al., 2006; Lopresto et al., 2006; Scarponi et al., 2007; Xiaoquan et al., 2005);

3. Joints à recouvrement (Aymerich, Onnis et Priolo, 2005; Glaessgen, Raju et Poe Jr., 2002).

De ces travaux, il ressort que l'insertion des coutures permet d'améliorer plusieurs propriétés mécaniques des composites, comme en fait foi le Tableau 1.1. Également, il a été démontré que les coutures peuvent ralentir ou même freiner la propagation du délaminage aux surfaces libres de l'échantillon, pour des plaques sollicitées en tension (Aymerich, Priolo et Sun, 2003; Yoshimura et al., 2007). La technique de couture présente aussi l'avantage d'être

versatile dans son application. Ainsi, plusieurs paramètres peuvent être modifiés de façon à optimiser la performance de la plaque renforcée : la densité de couture, la longueur des points, la distance entre les lignes de couture, de même que le matériau et le diamètre du fil utilisé (Dransfield, Baillie et Mai, 1994). La couture permet également de faciliter la manipulation d'un empilement de couches de fibres avant l'infusion, et pourrait même permettre de remplacer les éléments d'attaches (boulons, rivets) dans certaines structures composites (Mouritz, Leong et Herszberg, 1997).

Tableau 1.1 Sommaire des performances obtenues avec des composites renforcés de coutures transversales, pour différents modes de chargement

Propriété mesurée	**Augmentation de la propriété : Avec couture vs Sans couture**
Ténacité au délaminage, modes I, II et mixte I-II	Jusqu'à 50x
Durée de vie en fatigue des joints à recouvrement	3 à 5x
Aire délaminée après un essai d'impact à basse vitesse	Réduction jusqu'à 40%
Résistance en compression après impact à basse vitesse	Jusqu'à 50%

Tout comme l'insertion de tiges en Z, la technique de couture ne présente pas que des avantages. Il est maintenant établi que l'insertion d'un fil de renfort à travers les couches d'un stratifié induit généralement une dégradation des propriétés dans le plan, bien qu'aucun consensus ne ressort quant à l'intensité de cette dégradation. Cette dégradation est attribuable au déplacement et à la rupture des fibres du composite lors de la pénétration de l'aiguille dans les couches, ainsi qu'à la zone riche en résine qui apparaît autour du fil de couture (Chun, Kim et Byun, 2006; Mouritz, Leong et Herszberg, 1997). La Figure 1.9a montre un exemple de la modification localisée de la structure du composite suite à la couture. On peut constater sur cette vue en plan que les fibres du composite se sont déplacées pour laisser passer le fil de couture, créant ainsi une zone riche en résine autour du fil. À la Figure 1.9b, on peut voir le détail des fils de couture passant à travers la plaque, de même que les zones de résine formées autour des fils.

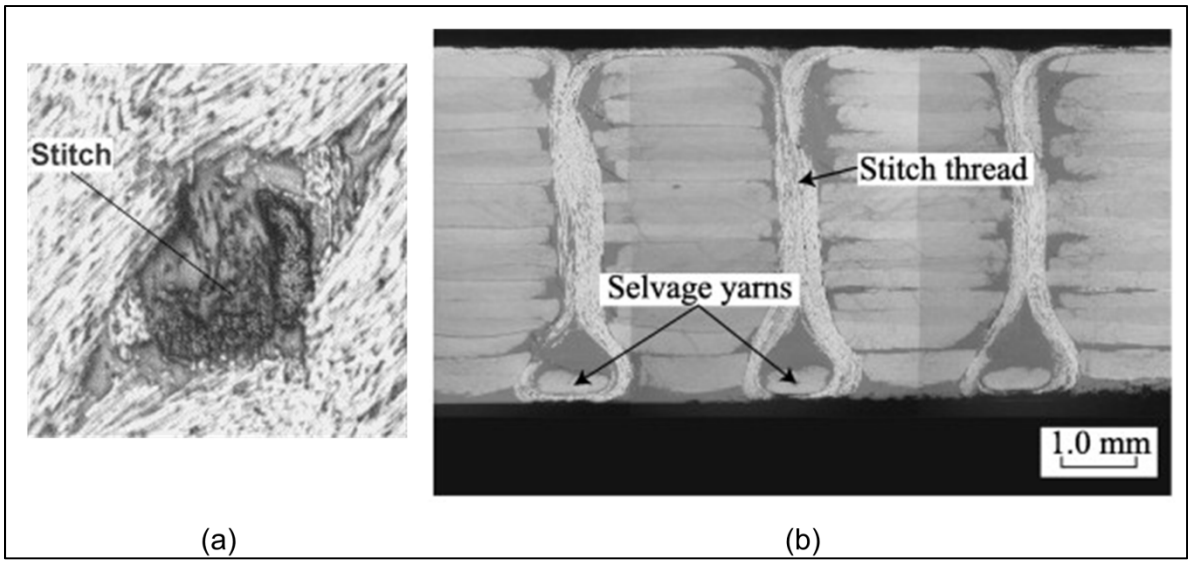

Figure 1.9 a) Vue de plan de la zone affectée par le fil de couture, montrant le déplacement des fibres du stratifié et la zone riche en résine; b) Vue de coupe à travers l'épaisseur du stratifié
Tirées de Aymerich, Priolo et Sun (2003) et Yoshimura et al. (2008)

Selon la revue de Mouritz et Cox, il est commun de retrouver dans la littérature des diminutions des propriétés dans le plan (modules et résistances) de l'ordre de 20% (Mouritz et Cox, 2000). Récemment, Hess et al. ont plutôt mesuré une diminution du module en tension jusqu'à 29% dans certains cas, pour des échantillons incorporant des coutures (Hess, Roth et Himmel, 2007). Cependant, ils notent également qu'il est possible d'annuler cette dégradation en choisissant judicieusement les paramètres de couture (fil plus petit, espacement plus grand entre les lignes de couture).

La majorité des travaux publiés sur la couture des composites porte sur l'utilisation de fils de Kevlar, mais des fils de verre, de carbone et de nylon peuvent également servir de renfort. Par ailleurs, on peut noter un certain intérêt dans la littérature récente pour l'insertion de fils métalliques en alliage à mémoire de forme (AMF). La plupart de ces travaux se concentrent sur l'ajout de fils AMF dans le plan des couches de fibres pour créer des composites hybrides (Simpson et Boller, 2008; Xu et al., 2003). Cette technique, illustrée à la Figure 1.10, permet notamment de contrôler les vibrations ou la forme de la structure, de combattre la

propagation des fissures dans le matériau composite ou d'améliorer sa performance à l'impact. Cependant, ce type de structure hybride n'est pas renforcé à travers l'épaisseur.

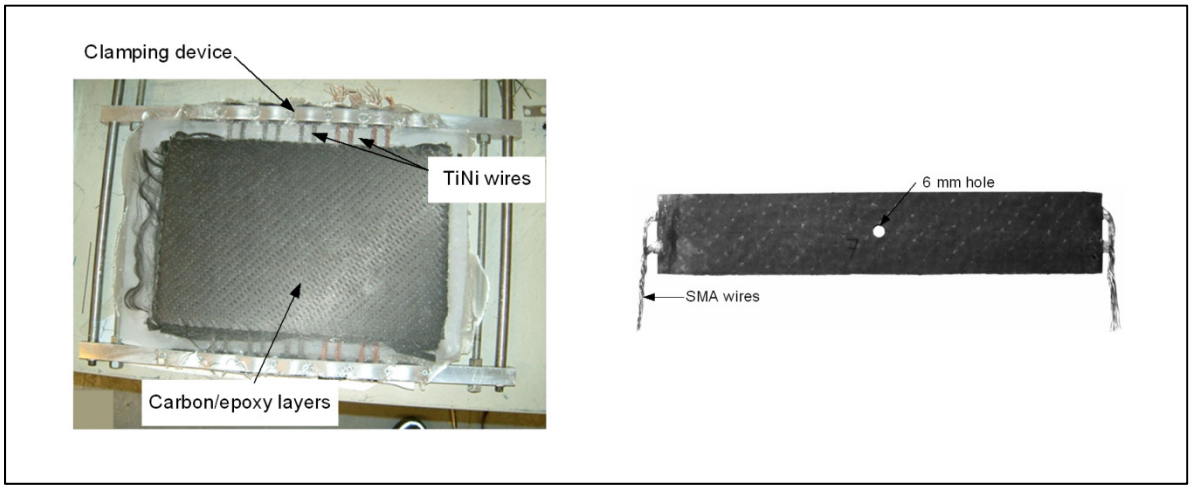

Figure 1.10 Fabrication d'un composite carbone/époxy hybride incorporant des fils AMF
Tirée et adaptée de Gauthier et al. (2006)

À la connaissance de l'auteur, il n'existe qu'une seule publication présentant une étude expérimentale sur la couture de fils AMF dans une plaque composite (Lau, Ling et Zhou, 2004). Dans cette recherche, une plaque de composite verre/époxy est renforcée de coutures faites d'un fil AMF superélastique, tel qu'illustré à la Figure 1.11. Des essais d'impact à faible vitesse sur les échantillons ont montré que l'énergie de délaminage était réduite pour les plaques renforcées, de même que la quantité de fissures interlaminaires. Cela démontre que la combinaison de la technique de renfort par couture et de l'utilisation d'un fil AMF pourrait permettre la conception de structures composites plus efficaces d'un point de vue de tolérance au dommage. Les propriétés des AMF seront traitées en détail à la section 1.3.

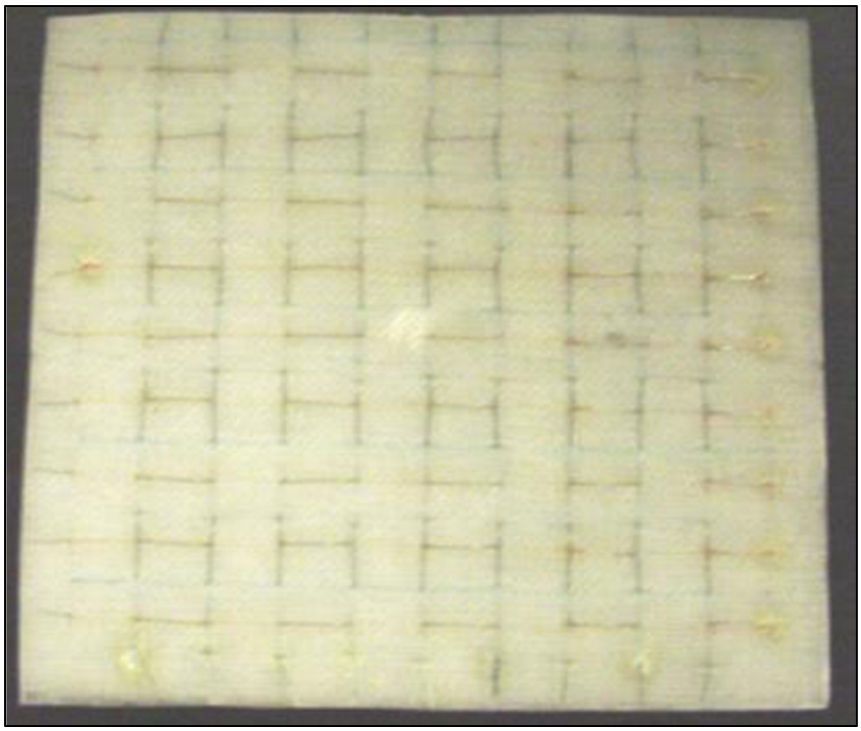

Figure 1.11 Plaque verre/époxy incorporant des coutures AMF
Tirée de Lau, Ling et Zhou (2004)

1.1.3 Impacts à basse vitesse sur les matériaux composites et propriétés résiduelles après impact

Parmi les différentes sources d'apparition du délaminage présentées à la section 1.1.1, les chargements d'impact à faible vitesse apparaissent comme étant particulièrement préoccupants (Dransfield, Baillie et Mai, 1994). Dans le domaine aéronautique, les avions sont susceptibles d'être frappés par des objets autant en situation de vol (oiseaux) que sur la piste (débris divers) ou lors de la maintenance (outils échappés) (Campbell, 2010; Mouritz, Leong et Herszberg, 1997). Les dégâts causés sur une structure composite par un impact à faible vitesse consistent principalement en un amalgame de délaminage et de rupture de la matrice. Dans une moindre mesure, des bris de fibres peuvent parfois survenir. La Figure 1.12 montre un exemple de dommages causés par un impact sur un stratifié graphite/époxy. Sur cette figure, on voit clairement que plusieurs couches du composite sont délaminées et ce, sur toute l'épaisseur de la plaque. De plus, on note une forte présence de bris de matrice,

identifiables par leur propagation en diagonale à travers l'épaisseur. Ces fissures de résine se propagent à travers l'épaisseur jusqu'aux interfaces, initiant ensuite un délaminage. Enfin, on peut remarquer une zone où la fibre est endommagée près du point d'impact. Si l'on observe la surface impactée, on constate que le point d'impact n'est que peu déformé ou endommagé. Cela illustre la nécessité de procéder à l'inspection minutieuse des structures pour s'assurer de leur intégrité.

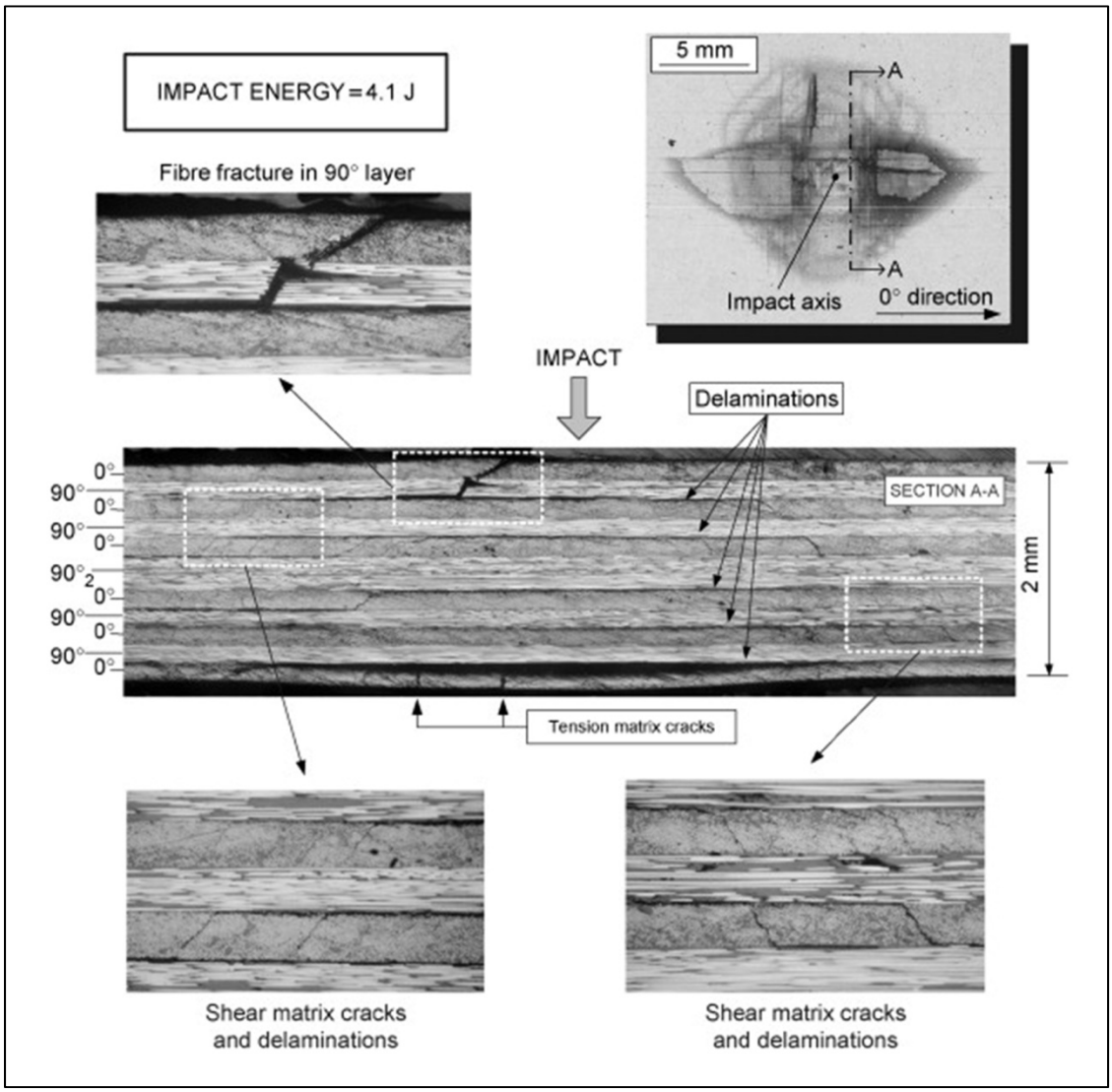

Figure 1.12 Délaminage, bris de matrice et bris de fibre induits par un impact à faible vitesse sur un stratifié graphite/époxy
Tirée de Aymerich et Priolo (2008)

Il est généralement admis que les impacts à faible vitesse peuvent causer une diminution de la rigidité et de la résistance de la structure. Dans l'optique de la tolérance au dommage, il devient important d'étudier les performances des composites après impact. La plupart des travaux sur ce sujet concernent les propriétés en compression longitudinale d'une plaque ayant subi un impact à faible vitesse. Cet essai est d'ailleurs l'objet de la norme ASTM D7137 « Compressive Residual Strength Properties of Damaged Polymer Matrix Composite Plates » (American Society for Testing and Materials, 2005a). La Figure 1.13 montre le schéma du montage nécessaire pour mener cet essai mécanique (les dimensions de l'échantillon peuvent varier).

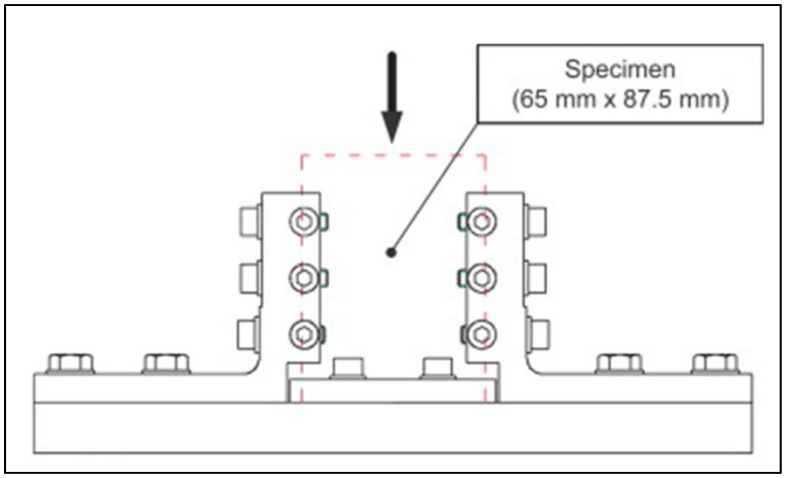

Figure 1.13 Schéma de montage de l'essai ASTM D7137
Tirée de Aymerich et Priolo (2008)

Avant d'effectuer l'essai de compression, l'échantillon est soumis à un chargement d'impact suivant la norme ASTM D7136 « Measuring the Damage Resistance of a Fiber-Reinforced Polymer Matrix Composite to a Drop-Weight Impact Event » (American Society for Testing and Materials, 2005b). Lors de cet essai mécanique, on laisse tomber une masse sur l'échantillon à partir d'une hauteur prédéterminée. L'échantillon est maintenu sur le gabarit à l'aide de brides de serrages, tel qu'illustré à la Figure 1.14. Lorsque l'impacteur frappe l'échantillon, celui-ci se déforme localement et dissipe l'énergie cinétique selon deux mécanismes (en négligeant les pertes en frottement et en déformation du montage) : 1-

déformation élastique de l'échantillon et 2- initiation et propagation de fissures. Il est à noter que la plaque de support contient une fenêtre évidée sous l'échantillon pour permettre sa déformation.

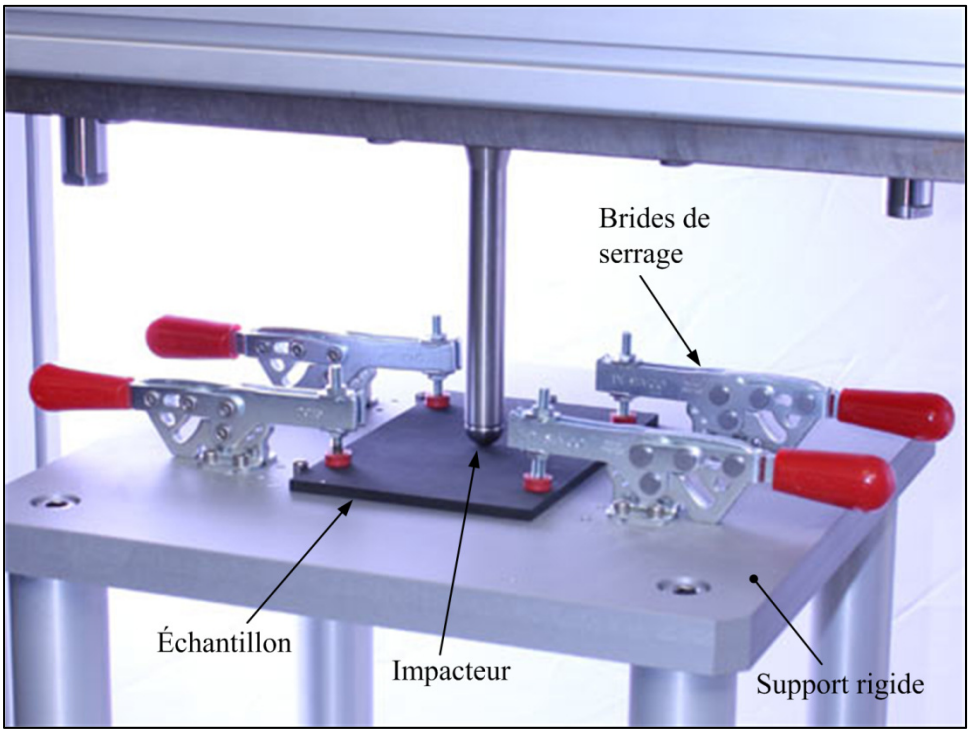

Figure 1.14 Montage pour l'essai d'impact à faible vitesse ASTM D7136
Adaptée de Instron (2012)

Bien que d'autres propriétés du matériau puissent être affectées par l'impact, la popularité de l'essai de compression s'explique par le fait que les propriétés en compression semblent être les plus endommagées par l'impact (Abrate, 1998).

1.2 Modélisation numérique

Dans cette section, les principales techniques de modélisation applicables aux composites stratifiés répertoriées dans la littérature seront brièvement présentées.

1.2.1 Modélisation du délaminage dans les matériaux composites

Globalement, les méthodes utilisées pour prédire la propagation du délaminage peuvent être classées en deux catégories : les méthodes basées sur une approche de résistance des matériaux et celles basées sur la mécanique de la rupture (Lorriot et al., 2003). L'approche de la résistance mécanique nécessite le calcul des contraintes et des déformations dans la structure, lesquelles sont ensuite comparées aux valeurs limites selon le critère approprié. Pour sa part, l'approche de la mécanique de la rupture représente la résistance à la fissuration par l'énergie qu'on doit fournir pour faire avancer la fissure (G_{Ic}, G_{IIc}), ou par l'intensité de contrainte en fond de fissure (K_{Ic}, K_{IIc}) (Mandell et al., 2003). Le paramètre G est appelé le taux de restitution de l'énergie de déformation (*Strain Energy Release Rate*, ou SERR) et il est le paramètre-clé de cette méthode de prédiction de la fissuration. L'approche de mécanique de la rupture est très utilisée pour l'étude de la fissuration en mode I, II, III et mixte, suivant le schéma de la Figure 1.15, avec le paramètre « a » représentant la longueur de fissure. Son utilisation est généralement limitée aux cas simples de chargement puisqu'elle nécessite un maillage raffiné en fond de fissure. De plus, cette théorie s'applique à la propagation d'une fissure existante, ce qui élimine l'étude de l'apparition d'un délaminage aux surfaces libres d'un échantillon ou aux abords d'un trou, par exemple (Tay, 2003).

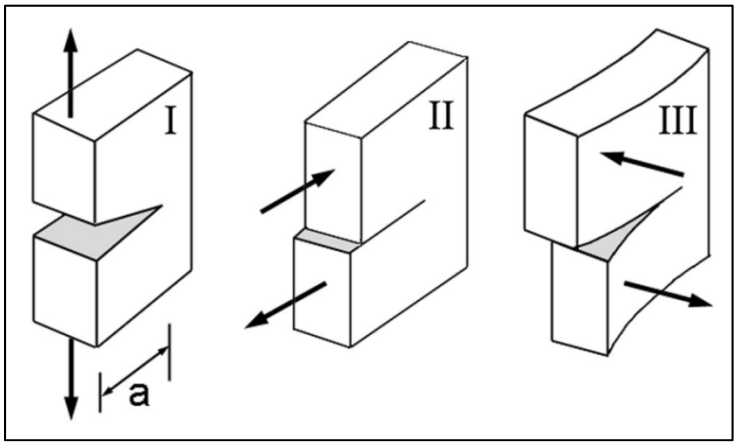

Figure 1.15 Trois modes de propagation d'une fissure
Tirée de Mandell et al. (2003)

Dans la littérature récente, on note la présence de plus en plus forte de modèles utilisant la technologie des éléments de cohésion de l'interface. Selon cette théorie, l'interface entre deux couches de fibres peut absorber une certaine quantité d'énergie avant de se rompre. Le comportement mécanique de l'interface peut se modéliser de différentes façons, dont un exemple typique est illustré à la Figure 1.16. Sur ce graphique, l'abscisse et l'ordonnée représentent respectivement le déplacement (ou séparation des couches) et la contrainte en un point de la surface, pour un mode de chargement donné (mode I, II ou III). Selon ce schéma, l'interface présente un comportement élastique lorsque $\delta < \delta_0$. Lorsque la séparation en un point dépasse δ_0, l'interface subit un endommagement progressif en restituant de l'énergie (pente descendante du graphe). Si la séparation atteint la valeur critique δ_f, l'interface se rompt et la fissure avance.

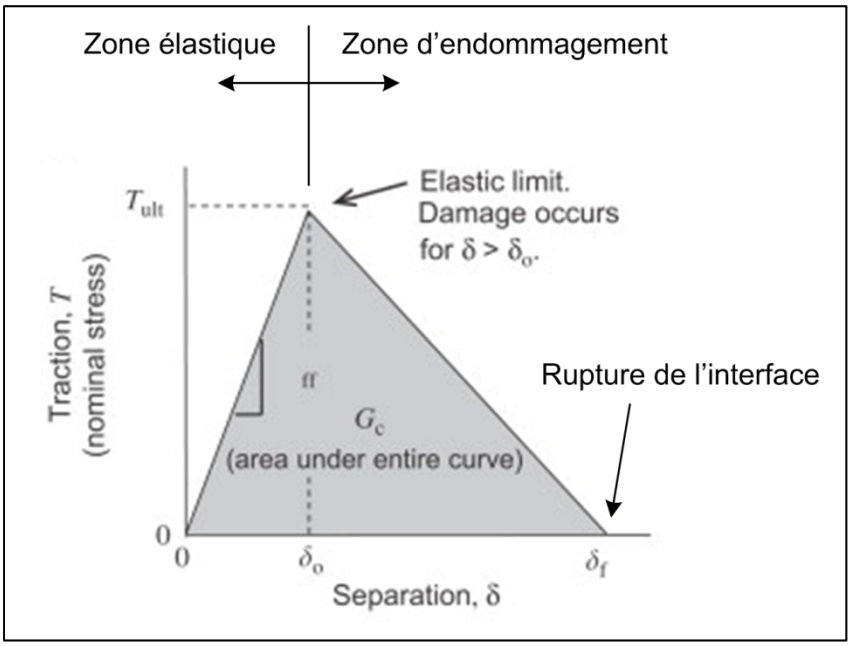

Figure 1.16 Exemple typique de loi de cohésion d'interface
Tirée de Diehl (2008)

En plus de permettre la modélisation de l'initiation et de la propagation du délaminage (Camanho, Davila et De Moura, 2003), cette théorie présente l'avantage d'être moins dépendante du maillage que la méthode de mécanique de la rupture (Tay, 2003). Par contre,

sa performance dépend directement de l'adéquation entre la loi représentée à la Figure 1.16 et le comportement réel de l'interface. Les paramètres permettant de modéliser la loi de cohésion sont difficiles à mesurer expérimentalement, ce qui peut rendre fastidieuse l'utilisation de cette théorie (Corigliano et Mariani, 2001). Il est également connu que ce type de modèle peut présenter des difficultés de convergence, limitant ainsi son utilisation à des cas relativement simples (Alfano et Crisfield, 2001).

Les modèles de propagation du délaminage sont parfois conçus en 2-D (Mandell et al., 2003; Shokrieh, 1991), mais des modèles en 3-D sont apparus à la fin des années 80 (Whitcomb, 1988) et sont maintenant très présents dans la littérature, en dépit du coût plus élevé en termes de ressources informatiques et de temps de calcul (Fleming, 2001; Pereira et de Morais, 2004; Shen, Lee et Tay, 2001; Uj, 2004; Wei et Zhao, 1991). Cela est dû au fait qu'un état de contrainte tridimensionnel peut exister dans une structure, même si le chargement appliqué est unidirectionnel (Pipes et Pagano, 1970). Cet état de contrainte en trois dimensions peut éventuellement mener à la propagation de fissures à des chargements plus faibles que les prédictions obtenues avec la théorie classique des stratifiés.

Dans une revue de littérature effectuée par Degrieck et Van Paepegem, il ressort que la technique de modélisation la plus prometteuse est celle dite d'endommagement progressif, puisqu'elle considère de façon quantitative la propagation des dommages (Degrieck et Van Paepegem, 2001). En effet, les propriétés mécaniques résiduelles peuvent être ajustées selon différents critères de rupture tout au long de la modélisation, de façon à simuler le comportement de la structure endommagée. Bien que cette revue de littérature porte sur des modèles de propagation de dommages en fatigue, cette méthodologie est fréquemment reprise pour des chargements statiques. La section suivante décrit sommairement la technique de modélisation d'endommagement progressif.

1.2.2 Modèle d'endommagement progressif

Un des premiers modèles d'endommagement progressif a été introduit par Chou et al., avec lequel l'endommagement d'une plaque composite était modélisé sans tenir compte des différents modes de rupture (Chou, Orringer et Rainey, 1976). La procédure utilisée était drastique puisque les propriétés du matériau endommagé étaient remises à zéro. La technique a par la suite été raffinée par Hashin, qui a établi des critères de rupture pour quatre modes distincts de fissuration : rupture de la fibre en tension et en compression et rupture de la matrice en tension et en compression (Hashin, 1980). Les critères proposés sont quadratiques et prennent la forme de l'équation suivante, pour une rupture de fibre en tension :

$$\left(\frac{\sigma_{11}}{\sigma_A^+}\right)^2 + \frac{\sigma_{12}^2 + \sigma_{13}^2}{\tau_A^2} = 1 \tag{1.1}$$

où σ_{11} est la contrainte dans la direction de la fibre, σ_{12} et σ_{13} sont des contraintes de cisaillement, et σ_A^+ and τ_A sont respectivement les résistances en traction et en cisaillement.

Dans la même veine, Chang et Chang ont proposé un ensemble de critères de rupture quadratiques en introduisant la non-linéarité du matériau (Chang et Chang, 1987). Le modèle consistait en la combinaison d'une analyse de contraintes et d'une analyse d'endommagement suivant les modes de rupture suivants : matrice, fibre et décollement fibre/matrice. La dégradation des propriétés des éléments pouvaient se faire de façon drastique (matrice rompue) ou proportionnelle à la dimension du dommage (fibre rompue et décollement). Ce modèle s'est avéré concluant pour la prédiction de la limite ultime en traction de stratifiés comportant un concentrateur de contrainte. Pour ce qui est du délaminage, un critère de rupture quadratique a été proposé par d'autres auteurs, prenant la forme de l'équation suivante (Brewer et Lagace, 1988) :

$$\left(\frac{\sigma_1}{Z_1}\right)^2 + \left(\frac{\sigma_2}{Z_2}\right)^2 + \left(\frac{{\sigma_z}^t}{Z^t}\right)^2 + \left(\frac{\sigma_z^c}{Z^c}\right)^2 = 1 \tag{1.2}$$

Dans cette équation, les paramètres Z_i représentent les résistances du matériau composite dans différentes directions en traction (t) ou en compression (c). Tous ces critères de rupture sont largement utilisés dans les modèles d'endommagement progressif puisqu'ils permettent de suivre la propagation de différents modes de rupture de façon distincte, contrairement à d'autres critères comme celui de Tsai-Wu, par exemple.

1.2.3 Dégradation des propriétés mécaniques

Plusieurs études utilisant des modèles d'endommagement progressif ont été publiées au cours des vingt dernières années, que ce soit dans le domaine statique ou cyclique : (Camanho et Matthews, 1999; Goyal et al., 2004; Iannucci, 2006; Papanikos et al., 2005; Papanikos, Tserpes et Pantelakis, 2003; Shokrieh et Lessard, 2000; Shokrieh et Rafiee, 2005; Tserpes, Papanikos et Kermanidis, 2001; Van Paepegem et Degrieck, 2001; Van Paepegem, Degrieck et De Baets, 2001).

Dans la plupart des cas, ces modèles utilisent une méthode de dégradation des propriétés pour prédire la propagation des fissures. Cette approche mène à une réduction localisée de la rigidité et/ou de la résistance de la structure lorsqu'une rupture est détectée. Tel qu'il a été mentionné précédemment, les premières règles de dégradation qui ont été publiées considéraient une perte complète des propriétés mécaniques de la région endommagée, dans les directions affectées par la rupture. Certaines études utilisent toujours cette hypothèse (Shokrieh et Lessard, 2000; Tserpes, Papanikos et Kermanidis, 2001), bien que la perte totale de rigidité puisse engendrer une incompatibilité mathématique dans le modèle (Tay, Tan et Tan, 2005).

Selon Zhao et al., certains modes de rupture, comme par exemple la fissuration transversale de la matrice, permettent tout de même à la structure endommagée de supporter une certaine

charge (Zhao, Warrior et Long, 2006). Dans cette optique, la dégradation partielle des propriétés mécaniques en fonction du type de bris, tel qu'énoncé à l'équation qui suit, apparaît une option intéressante :

$$E_d = f * E_0 \tag{1.3}$$

avec E_d et E_0 étant respectivement les propriétés dégradées et initiales, et f une constante définie expérimentalement pour chaque mode de rupture. Dans la littérature, aucun consensus ne ressort quant aux valeurs de la constante f. Ainsi, différentes combinaisons de paramètres de dégradation peuvent être utilisées (Camanho et Matthews, 1999; Chang et Chang, 1987; Papanikos et al., 2005; Riccio, 2005; Zhao, Warrior et Long, 2006). Par exemple, une étude de Tserpes et al. fait état de l'essai de deux combinaisons différentes de constantes de dégradation, telles que présentées au Tableau 1.2. D'après leur étude numérique et expérimentale d'un joint boulonné soumis à un chargement en tension, la seconde règle de dégradation (groupe 2) permet une représentation plus réaliste de la dégradation de la rigidité de la plaque, en plus d'une meilleure prédiction de la résistance en traction du joint.

Tableau 1.2 Différentes combinaisons de constantes de dégradation des propriétés mécaniques
Tiré de Tserpes et al. (2002)

Modes de rupture	**Règles de dégradation des propriétés**	
	Groupe 1	**Groupe 2**
Rupture de la matrice en tension	$E_{yy} = \nu_{xy} = 0$	$E_{yy} = 0.2*E_{yy}$, $G_{xy} = 0.2*G_{xy}$, $G_{yz} = 0.2*G_{yz}$
Rupture de la matrice en compression	$E_{yy}=\nu_{xy}=0$	$E_{yy} = 0.4*E_{yy}$, $G_{xy} = 0.4*G_{xy}$, $G_{yz} = 0.4*G_{yz}$
Rupture de la fibre en tension	$E_{xx,yy,zz} = G_{xy,xz,yz} = \nu_{xy,xz,yz} = 0$	$E_{xx} = 0.07*E_{xx}$
Rupture de la fibre en compression	$E_{xx,yy,zz} = G_{xy,xz,yz} = \nu_{xy,xz,yz} = 0$	$E_{xx} = 0.14*E_{xx}$

Modes de rupture	Règles de dégradation des propriétés	
	Groupe 1	**Groupe 2**
Décollement fibre/matrice	$G_{xy} = \nu_{xy} = 0$	$G_{xy} = \nu_{xy} = 0$
Délaminage en tension	$E_{zz} = G_{xz} = G_{yz} = \nu_{xz} = \nu_{yz} = 0$	$E_{zz} = G_{xz} = G_{yz} = \nu_{xz} = \nu_{yz} = 0$
Délaminage en compression	$E_{zz} = G_{xz} = G_{yz} = \nu_{xz} = \nu_{yz} = 0$	$E_{zz} = G_{xz} = G_{yz} = \nu_{xz} = \nu_{yz} = 0$

1.2.4 Modélisation de la couture dans les stratifiés

L'étude numérique des coutures dans les matériaux composites s'est beaucoup concentrée sur les propriétés dans le plan de ces matériaux renforcés, à l'aide notamment de modèles micromécaniques de cellule élémentaire (*unit-cell*). Un exemple de ce type de modèle est illustré à la Figure 1.17. L'utilisation de cellules élémentaires permet de varier plusieurs paramètres (matériau et diamètre du fil de couture, densité de couture, etc.) pour simuler le comportement du fil et du matériau composite environnant. Certains auteurs ne considèrent pas le fil dans leurs analyses numériques (Hess, Roth et Himmel, 2007; Mikhaluk et al., 2008), tandis que d'autres simulent la zone de résine entourant le fil comme si elle était vide (Steeves et Fleck, 2006). Pour justifier de telles décisions, les auteurs supposent que l'aire de section du fil est faible comparativement aux dimensions de la zone riche en résine, ou que cette zone de résine se fissure à un niveau de contrainte beaucoup plus faible que dans le cas du composite.

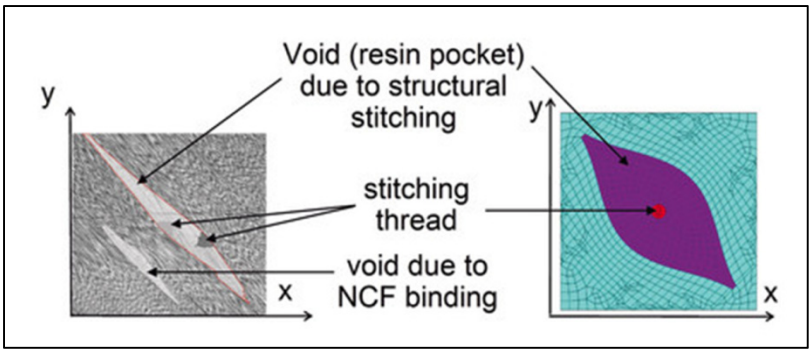

Figure 1.17 Exemple de modèle de cellule élémentaire
pour l'étude d'un composite incorporant des
coutures transversales
Tirée de Institut für Verbundwerkstoffe (2012)

Quelques travaux ont été publiés sur la modélisation à l'échelle macroscopique de composites renforcés de coutures. Par exemple, Aymerich et al. ont étudié l'effet des coutures de Kevlar et de polyéthylène sur la résistance au délaminage des joints à recouvrement (*single-lap joint*) (Aymerich, Onnis et Priolo, 2006; Aymerich, Onnis et Priolo, 2005). Le modèle 3-D utilisé dans ces travaux incorpore des éléments « Link » supportant uniquement des contraintes de tension. Par conséquent, les coutures sont considérées comme des câbles en tension. Le délaminage de l'interface du joint est simulé en libérant les nœuds adjacents lorsque le critère de rupture est atteint. La même stratégie de modélisation a été employée pour étudier la contrainte présente dans un fil de couture, lorsque la plaque de composite est soumise à un certain niveau de chargement en traction et qu'une zone délaminée est présente (Aymerich, Priolo et Sun, 2003).

Un autre modèle de plaque renforcée soumise à un chargement en traction quasi-statique a été proposé par Yoshimura et al. (Yoshimura et al., 2007). Cette simulation numérique intègre des coutures à travers l'épaisseur de la plaque, modélisées par des éléments « Beam » de section circulaire ayant des propriétés mécaniques dans la direction axiale ainsi qu'en cisaillement. Ce modèle a permis de démontrer l'efficacité des coutures pour ralentir la propagation du délaminage à partir des surfaces libres de la plaque.

La ténacité au délaminage en modes I et II de composites renforcés a aussi fait l'objet d'études expérimentales et numériques (Wood et al., 2007a; Wood et al., 2007b). Les modèles utilisés dans ces articles font appel soit à des éléments travaillant uniquement en tension, ou à des éléments tiges couplés à un matériau de type ressort-amortisseur.

1.3 Alliages à mémoire de forme

Le terme « alliages à mémoire de forme » ou AMF désigne une classe de matériau présentant des propriétés particulières dites de mémoire de forme. Dans cette section, les phénomènes microstructuraux et physiques à l'origine de ces propriétés seront présentés, de même que les propriétés fonctionnelles des AMF.

1.3.1 Transformations martensitiques thermoélastiques

Le comportement particulier des AMF tire son origine de la transformation martensitique, qui consiste en un changement de phase accompagnant une variation de température ou une contrainte mécanique. Ce phénomène permet à un échantillon préalablement déformé de retrouver sa forme initiale lorsqu'il est chauffé. Par analogie aux aciers, la phase basse température est appelée « martensite » tandis que la phase haute température est appelée « austénite ». Grâce au caractère réversible de cette transformation, cette famille d'alliage présente des propriétés de mémoire de forme et de superélasticité étonnantes. L'équation de Clausius-Clapeyron permet de relier la température de transformation de phase à la contrainte appliquée sur le matériau (Brailovski et al., 2003).

$$\frac{d\sigma}{dT} = \frac{\Delta S}{V_0 \Delta \varepsilon} \tag{1.4}$$

Dans cette équation, σ représente la contrainte mécanique, T la température, ΔS la variation d'entropie, V_0 le volume de contrôle du cristal et $\Delta\varepsilon$ la variation de la déformation. Cette

équation permet de tracer l'évolution des températures de transformation de phase en fonction de la contrainte appliquée, tel que présenté à la Figure 1.18.

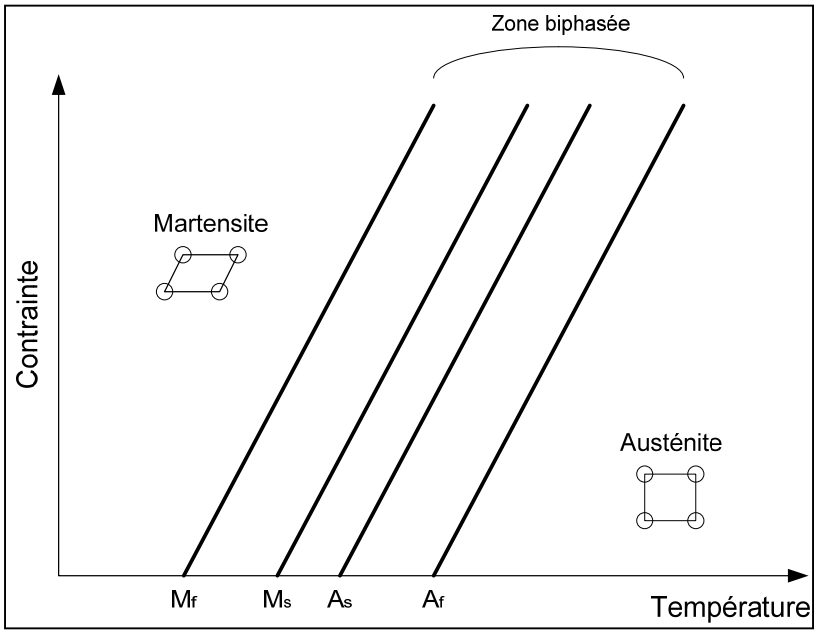

Figure 1.18 État de phase d'un matériau présentant une transformation martensitique
Tirée de Brailovski et al. (2003, p. 133)

Cette figure permet de définir les termes M_s et M_f qui sont respectivement les températures de début et de fin de transformation martensitique au refroidissement (transformation directe) sous contrainte nulle. De même, A_s et A_f sont les températures de début et de fin de transformation au chauffage (transformation inverse) dans les mêmes conditions de contrainte nulle. On remarque alors qu'à une température inférieure à M_f, le matériau est composé à 100 % de martensite alors que pour des températures supérieures à A_f, on retrouve uniquement de l'austénite. Entre les deux, le matériau est alors biphasé, avec les proportions de chaque phase dépendant de la température et de la contrainte appliquée.

1.3.2 Mécanismes de transformation et de déformation

Par définition, la transformation martensitique est dite displacive. Cela signifie que lors du changement de phase, les mouvements des atomes sont très faibles, de l'ordre d'un dixième de distance interatomique. Le passage d'une phase à l'autre se fait alors par cisaillement du réseau cristallin sous l'influence de la température ou de la contrainte appliquée. Cette transformation est donc responsable d'une déformation homogène du réseau, qui cependant ne se retrouve pas toujours à l'échelle macroscopique. En effet, lors de la transformation directe (austénite vers martensite), la déformation du réseau est compensée par la formation de macles, ce qui se traduit par une absence de déformation à l'échelle macroscopique. Ces macles vont en effet permettre à la nouvelle phase de s'accommoder de l'espace disponible pour créer des plaquettes de martensite orientées de façon totalement aléatoire. On parle alors de martensite autoaccommodante. Lors du retour en phase austénitique, sous chauffage, les macles disparaissent. La Figure 1.19 permet d'illustrer schématiquement les différentes transformations à l'échelle atomique.

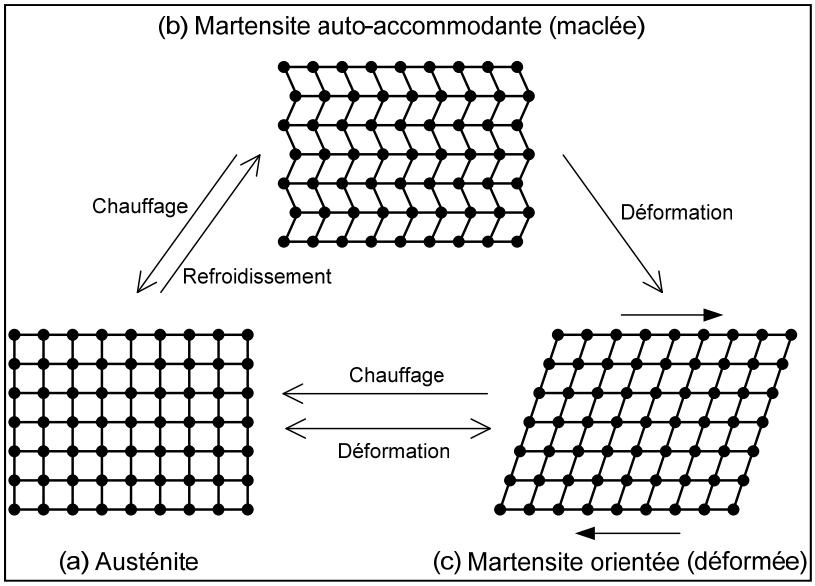

Figure 1.19 Représentation schématique de la transformation martensitique à l'échelle atomique
Tirée et adaptée de Brailovski et al. (2003, p. 13)

Partant d'un état complètement austénitique (Figure 1.19a), un refroidissement sous contrainte nulle engendre l'apparition de martensite autoaccommodante (ou maclée), ce qui n'entraîne pas de déformation à l'échelle macroscopique (Figure 1.19b). Cette transformation est totalement réversible, puisqu'un chauffage de la martensite maclée entraînera la réapparition de la phase austénitique (Figure 1.19a). Si l'on part de la martensite autoaccommodante, une déformation macroscopique de cette phase se traduira par une orientation préférentielle des aiguilles de martensite selon la direction de la contrainte (Figure 1.19c). Il est alors question de martensite orientée. Un chauffage de cette martensite orientée à une température supérieure à A_f entraînera un retour en phase austénitique, provoquant alors le retour du matériau à sa forme initiale (Figure 1.19a). Une déformation de l'austénite entraînera quant à elle la formation de martensite orientée.

1.3.3 Propriétés fonctionnelles de l'alliage Ti-Ni

Les sections qui suivent présentent trois propriétés fonctionnelles particulièrement intéressantes des alliages à mémoire de forme Ti-Ni.

1.3.3.1 Effet mémoire de forme simple sens

L'effet mémoire de forme peut être présenté graphiquement à l'aide de la Figure 1.20. Ainsi, une tige en AMF déformée de façon pseudo-plastique (étapes 1-2-3) pourra retrouver sa forme initiale si elle est chauffée à une température adéquate (étapes 4-5).

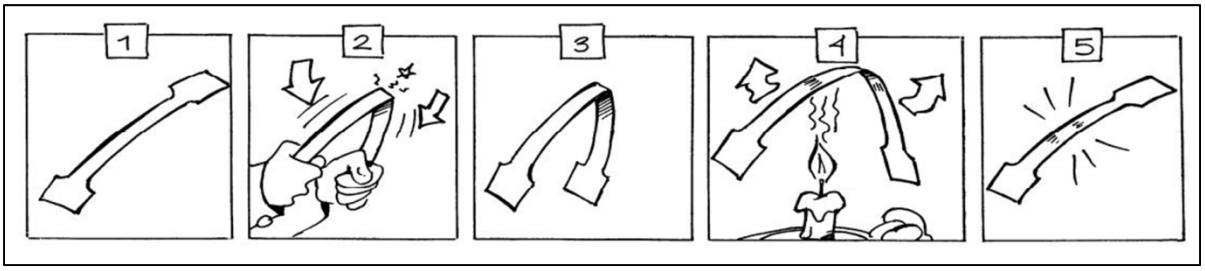

Figure 1.20 Représentation schématique de l'effet mémoire de forme
Tirée d'une réalisation interne du LAMSI

La présence de l'effet mémoire de forme simple sens dans une pièce répond cependant à certaines conditions. La Figure 1.21 présente le chargement thermomécanique permettant l'observation de cet effet particulier.

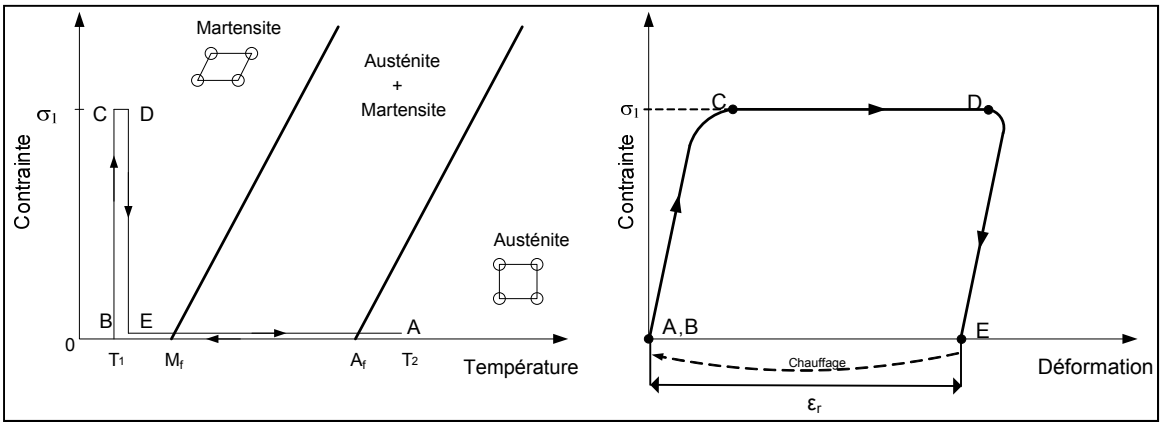

Figure 1.21 Représentation schématique du chemin thermomécanique nécessaire à l'observation de l'effet mémoire de forme simple sens
Tirée et adaptée de Brailovski et al. (2003, p. 214)

Tel que mentionné précédemment, un refroidissement d'une température T_2 (état austénitique) à une température T_1 (état martensitique) sous contrainte nulle (A-B) permet d'obtenir une structure composée de martensite autoaccommodante présentant des variantes orientées de façon aléatoire. Le chargement jusqu'à σ_1 (B-C) permet l'orientation des plaquettes de martensite selon la direction du chargement. Lors du relâchement de la contrainte, l'orientation de la martensite se traduit par une déformation résiduelle macroscopique du matériau (D-E). Le chauffage de T_1 à T_2 provoque alors une récupération de la déformation résiduelle induite précédemment. L'effet mémoire de forme représente donc la génération d'un déplacement sous contrainte nulle.

1.3.3.2 Génération de contrainte

La génération de contrainte intervient lors du chauffage d'un échantillon prédéformé et encastré, tel qu'illustré à la Figure 1.22.

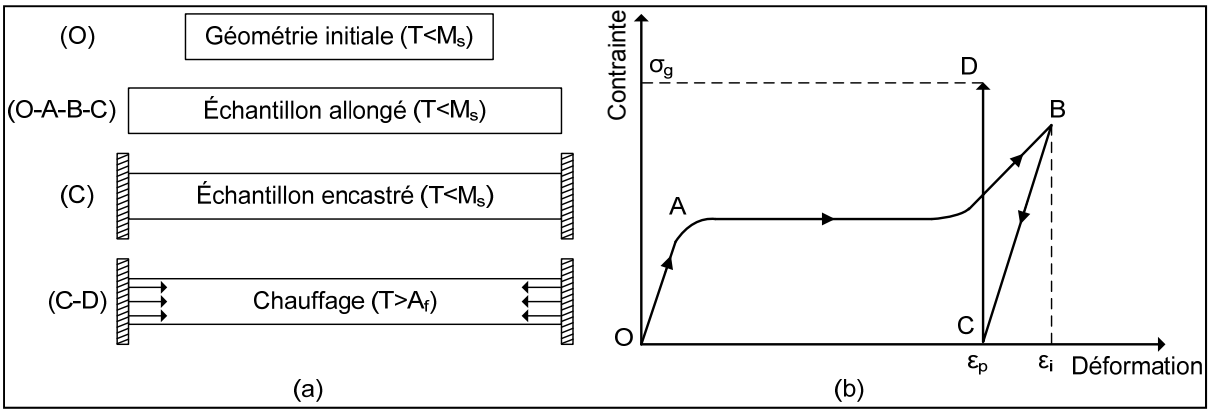

Figure 1.22 a) Représentation schématique du mécanisme de génération de contrainte sous chauffage et b) courbe contrainte-déformation.
Tirée de Facchinello (2011, p. 7)

Afin d'obtenir la génération de force au chauffage, l'échantillon doit être préalablement déformé jusqu'à une valeur donnée, alors qu'il se trouve en phase martensitique ($T < M_f$) (O-A-B). Le chargement est ensuite relâché pour permettre le retour élastique du matériau (B-C). À ce stade, l'échantillon présente une déformation résiduelle provenant de l'orientation de la martensite selon la contrainte appliquée précédemment. L'échantillon est ensuite encastré et chauffé à une température supérieure à A_f pour induire une transformation martensitique inverse complète (C-D). Le retour de forme est alors empêché par l'encastrement et l'échantillon génère une force. Au refroidissement, l'échantillon retrouve son état de martensite orientée et la contrainte chute pour atteindre une valeur nulle.

1.3.3.3 Superélasticité

La Figure 1.23 propose une représentation détaillée de l'effet superélastique, d'abord sur le diagramme d'état du matériau (gauche) et ensuite sur un diagramme contrainte-déformation (droite). Pour tirer profit de la superélasticité, l'échantillon doit d'abord se trouver en phase austénitique (A). Par la suite, une contrainte appliquée sur l'échantillon engendre la transformation de l'austénite en martensite orientée (A-C). Au relâchement de la contrainte, la martensite retourne spontanément à son état d'équilibre à cette température, qui est l'état

austénitique (C-A). Le même trajet est représenté sur le diagramme contrainte-déformation, où apparaît le plateau de transformation de l'austénite en martensite (B-C) ainsi que le retour à l'état initial après chargement (C-D-E-A). Par conséquent, l'observation de l'effet superélastique pour une application devant être utilisée à une température donnée (T) implique nécessairement l'ajustement des températures de transformation de l'alliage pour que A_f soit inférieure à T.

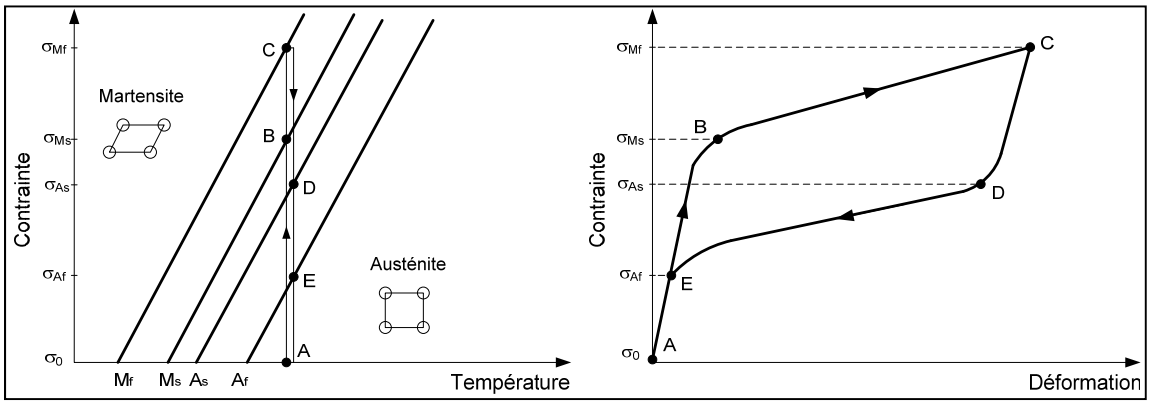

Figure 1.23 Chargement thermomécanique permettant d'obtenir l'effet superélastique
Tirée et adaptée de Brailovski et al. (2003, p. 188)

CHAPITRE 2

ARTICLE #1 : MODELING OF DELAMINATION INITIATION AND PROPAGATION IN COMPOSITE LAMINATES UNDER MONOTONIC TENSILE LOADING USING THE PROGRESSIVE DAMAGE MODELING TECHNIQUE

P.-L. Vachon, V. Brailovski, P. Terriault

École de technologie supérieure, 1100 rue Notre-Dame Ouest

Montréal (PQ), Canada, H3C 1K3

Ce chapitre a été publié dans « Science and Engineering of Composite Materials, vol. 16, Issue 2, p. 99-114, 2009 »

DOI : 10.1515/SECM.2009.16.2.99

2.1 Résumé (français)

L'article présenté dans ce chapitre a été publié dans la revue « Science and Engineering of Composite Materials ». Il introduit la validation d'un modèle numérique 3-D permettant de prédire la propagation du délaminage dans une plaque composite en traction quasi-statique. La structure du modèle fait appel à la technique d'endommagement progressif, une méthode qui a fait ses preuves dans différents cas d'analyses publiés dans la littérature scientifique. Le modèle numérique est construit dans l'environnement du logiciel commercial ANSYS en utilisant des éléments solides pour modéliser la plaque composite. La validation de ce modèle inclut une étude comparative de la performance de deux types d'éléments solides, soit les éléments Solid46 (8 nœuds) et Solid191 (20 nœuds), dont les propriétés mécaniques peuvent être orientées selon la direction des couches de fibres. Les contraintes obtenues près des surfaces libres sont comparées avec celles disponibles dans la littérature, de façon à choisir le type d'élément et le maillage appropriés pour le cas présent. L'analyse de la propagation du délaminage lors de la simulation de l'essai de traction a produit des résultats comparables à ce qu'on retrouve dans la littérature, avec le délaminage apparaissant aux surfaces libres et se propageant vers l'intérieur de la plaque.

Par ailleurs, cet article comprend également une étude sur l'utilisation des symétries lors de la modélisation 3-D d'une plaque composite en traction. Les résultats de l'analyse ont montré qu'il existe une zone de singularité près des plans de symétrie, où les contraintes interlaminaires ne peuvent être calculées avec précision.

2.2 Abstract

This paper introduces the preliminary validation of a 3-D numerical model based on the progressive damage modeling technique. Similar models have been reported in recent literature, attempting to study interlaminar stress distribution, static failure load and fatigue life of laminates, as well as delamination propagation in laminated plates under cyclic loading. The present model is intended to predict delamination initiation and propagation in laminates without stress raisers under monotonic complex loading. The validation process includes a comparative study on the performance of both SOLID46 and SOLID191 elements using the ANSYS Finite Element (FE) software, in addition to a study on the use of symmetry conditions in the FE modeling of composites. The main issues involved in the validation are: a) the ability of the model to capture interlaminar stresses near the free edge of the laminate, and b) the accuracy of progressive damage laws in representing delamination propagation in a laminate under monotonic tensile loading. A good correlation was achieved between numerical results and data in the literature for both issues. Also, the study on the use of symmetry conditions showed some singularities in interlaminar stress distribution, in the vicinity of the symmetry plane. Therefore, it was concluded that particular attention should be paid to the interlaminar stress distribution in the zone near the symmetry planes when using solid modeling.

2.3 Introduction

Today, engineers are trying to use composite materials to replace metals in the structural parts of aircrafts, a feat which requires a good understanding of the damage behavior of composites under complex loading conditions. However, much work still remains to be done

in that respect, since the damage propagation behavior of laminated composites is quite complex due to the highly anisotropic and heterogeneous nature of the materials. Moreover, delamination appears to be the most common form of damage encountered in aeronautical composites - and the most critical - since it may lead to a severe reduction in the stiffness and strength of structures [1]. Since delamination is embedded, and consequently not visible, its detection requires the use of non-destructive techniques such as C-Scans and X-rays.

A damage-tolerance philosophy is currently applied in the design of composite aircraft structures, and some concrete applications in that regard have been presented in the paper by Harris et al. [2]. In light of that, engineers are now focusing on understanding damage initiation and growth in composite materials and on the development of techniques for improving the damage-tolerance capacity of structural parts. Actually, the damage-tolerance design is based on a combination of empirical, semi-empirical and finite element models, since the damage propagation behavior in composites is still under study. The need for a highly reliable numerical model is therefore fully justified. For that reason, much effort has recently been concentrated on the development of numerical models for predicting the initiation and propagation of delamination, particularly models developed using progressive damage modeling.

Several methods have been investigated for stopping or delaying delamination propagation. Among these, the reinforcement of the laminate by through-the-thickness stitching seems to be a promising technique [3]. Although most researchers use Kevlar, carbon or glass fiber threads as stitching materials [4], there is a growing trend toward the investigation of the possibility of using shape memory alloy (SMA) stitches [5, 6]. However, integrating stitches into composite materials increases the complexity of the design process, and so modeling attempts must thus be carefully validated before they can be used with confidence in design.

2.4 Literature Review

Numerous progressive damage models, dedicated either to static or fatigue loading, have been developed in recent years. In most cases, the models use material property degradation methods for predicting damage propagation. This approach leads to a local reduction in stiffness and/or strength when a particular damage mode is predicted.

To the authors' knowledge, the first progressive damage model was introduced by Chou et al. [7], who were evaluating failure without any distinction as to failure mode. Their modeling procedure was very drastic, since they had to set all properties of the failed region to zero. Hashin [8] then proposed a set of discrete failure criteria for four different static damage modes: tensile fiber mode, compressive fiber mode, tensile matrix mode and compressive matrix mode. Similarly, Chang and Chang [9] proposed a set of quadratic criteria, introducing material nonlinearity. They performed a nonlinear analysis of notched laminated composites in order to assess damage accumulation. The Chang model consisted of two sections, stress analysis and failure analysis, which were combined with a property degradation model. The results were in agreement with experimental data, and the model was able to assess the damage accumulation and ultimate tensile strength of laminates for an arbitrary ply-orientation. Since these criteria are suitable for in-plane failure modes only, Brewer and Lagace [10] introduced a quadratic failure criterion for delamination. These criteria and their numerous variants are now widely used in progressive damage modeling since they allow the tracking of particular damage modes.

Three-dimensional models are relevant for modeling realistic delamination problems, and in recent literature, have indeed been more present than 2-D studies [11], despite the fact that 3-D modeling requires significant computer storage space and calculation time. Many analyses can be classified as quasi-3-D models because they use plate or shell elements in order to reduce computational time [12].

Among the relevant 2-D models presented in the literature, Shokrieh [13] developed a finite element code for the simulation of damage progression from initial failure to catastrophic failure, for pin-loaded composite laminates. The analysis considered both geometrical and material nonlinearities, and was restricted to net tension, shearout and bearing.

Then, Tserpes et al. [14, 15] presented a three-dimensional model for predicting residual strength, final failure mode and damage propagation in bolted composite joints under static tensile loading. The model was largely inspired by that by Shokrieh [13], except for the fact that the former assumed a linear material. Papanikos et al. [16] then used the model to study the bonded composite repairs of cracked metallic plates. They successfully assessed the stress intensity factor at the crack tip, patch debonding and damage accumulation in the composite patch, as functions of applied load.

Most investigators agree with the assumption that stress singularities exist at the free edges, and between different layers of a laminate, due to material and geometric discontinuities [17, 18]. This leads to a large but undefined magnitude of stresses in these regions. These interlaminar three-dimensional stresses can lead to delamination and failure of the laminate at lower loads than that predicted by the classical lamination theory (CLT) [19].

2.5 Problem Statement

Although many numerical models have been developed using the progressive damage modeling technique, none of them has been devoted to the study of delamination initiation and propagation for a laminated plate without stress raisers under monotonic tensile loading. Furthermore, the use of symmetry in the numerical modeling of composite laminates still deserves to be investigated since its influence on the distribution of interlaminar stresses in the vicinity of symmetries is yet to be fully reported, especially as it pertains to solid modeling. This paper therefore intends to present a finite element model, built on a commercial FE code, which allows the tracking of delamination propagation and the visualization of the delamination state at any interface of the laminate, and at any time during

the tensile test. It also presents a numerical study on the effects of commonly used symmetries on the interlaminar stress distribution in composite laminates.

2.6 Development of the Model

A numerical model is developed for predicting damage accumulation and delamination propagation in simple composite plates under quasi-static tensile loading. The model consists of two modules: 1- stress analysis, and 2- failure and degradation analysis. The algorithm is shown in Figure 2.1. Each of these modules is first described, and then validated.

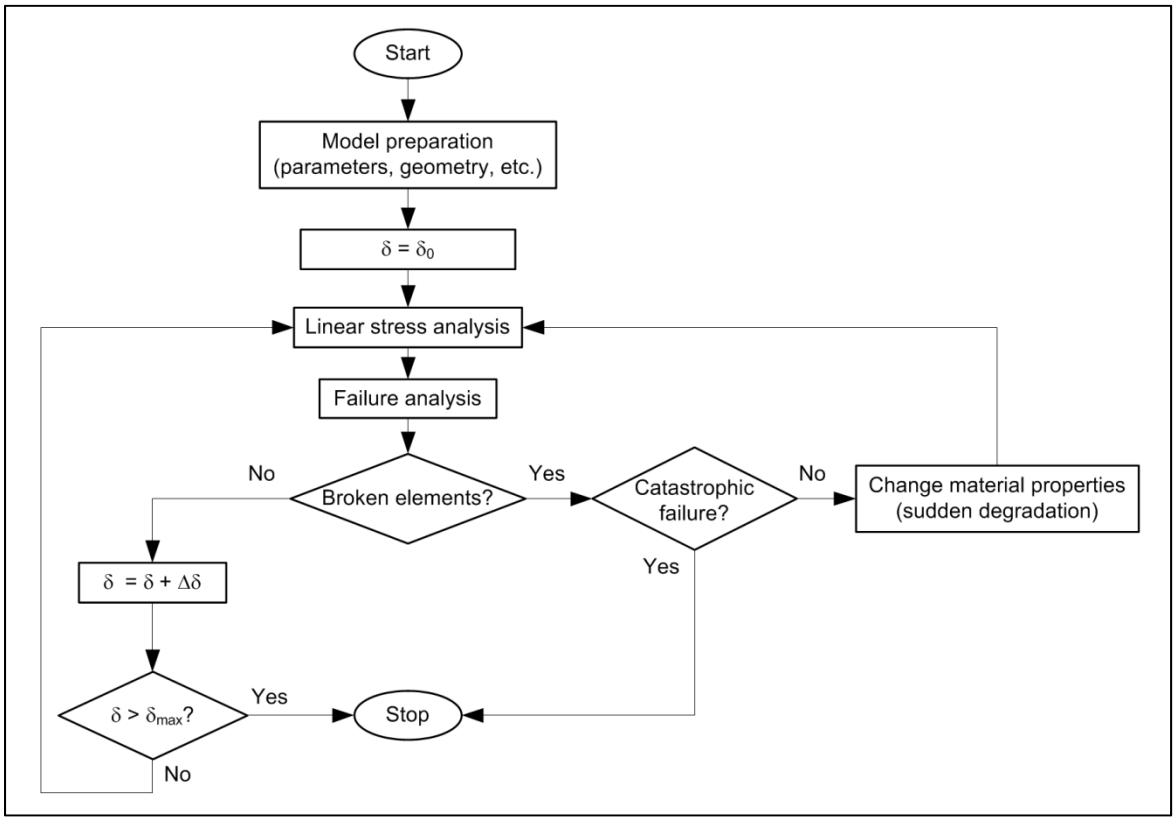

Figure 2.1 Algorithm of the numerical model

2.6.1 Stress Analysis

A 3-D numerical model is developed with Ansys V10 FE code to perform stress analysis. The composite plate is modeled using a 20-node layered SOLID191 element, with 3 displacement DOFs per node. The SOLID191 element is defined by orthotropic material properties and layer characteristics (number, thickness and orientation). Each layer can be modeled by one or more elements through thickness, in order to improve the accuracy of the calculated interlaminar stresses, if needed.

2.6.2 Static Failure Analysis and Degradation of Mechanical Properties

A set of seven failure criteria is used for detecting different failure modes. The 3-D Hashin-type criteria were chosen because they allow the prediction of different failure modes separately, hence the possibility of degrading the material properties in the appropriate directions. In this work, the criteria for each failure mode are adapted for a linear material, and are as follows [20]:

Table 2.1 Failure criteria

Matrix tensile failure	$\left(\frac{\sigma_{yy}}{S_{yy}^{T}}\right)^2+\left(\frac{\sigma_{xy}}{S_{xy}}\right)^2+\left(\frac{\sigma_{yz}}{S_{yz}}\right)^2 \geq 1$	Fibre/matrix shearout	$\left(\frac{\sigma_{xx}}{S_{xx}^{C}}\right)^2+\left(\frac{\sigma_{xy}}{S_{xy}}\right)^2+\left(\frac{\sigma_{xz}}{S_{xz}}\right)^2 \geq 1$
Matrix compressive failure	$\left(\frac{\sigma_{yy}}{S_{yy}^{C}}\right)^2+\left(\frac{\sigma_{xy}}{S_{xy}}\right)^2+\left(\frac{\sigma_{yz}}{S_{yz}}\right)^2 \geq 1$	Delamination in tension	$\left(\frac{\sigma_{zz}}{S_{zz}^{T}}\right)^2+\left(\frac{\sigma_{xz}}{S_{xz}}\right)^2+\left(\frac{\sigma_{yz}}{S_{yz}}\right)^2 \geq 1$
Fibre tensile failure	$\left(\frac{\sigma_{xx}}{S_{xx}^{T}}\right)^2+\left(\frac{\sigma_{xy}}{S_{xy}}\right)^2+\left(\frac{\sigma_{xz}}{S_{xz}}\right)^2 \geq 1$	Delamination in compression	$\left(\frac{\sigma_{zz}}{S_{zz}^{C}}\right)^2+\left(\frac{\sigma_{xz}}{S_{xz}}\right)^2+\left(\frac{\sigma_{yz}}{S_{yz}}\right)^2 \geq 1$
Fibre compressive failure	$\left(\frac{\sigma_{xx}}{S_{xx}^{C}}\right)^2 \geq 1$		

In the equations in Table 2.1, σ_{ij} and S_{ij} are the element stresses and material residual strengths in the ij directions, respectively. The directions refer to a local layer coordinate system, where x and y are respectively parallel and perpendicular to the fiber directions, while z is oriented through thickness. The subscripts T and C refer to tension and compression, respectively. The value of each criterion represents the state of damage of an

element, for a particular state of stress. Thus, each damage mode can be plotted in a scale going from 0 to 1, where 0 stands for a "healthy" material and 1 stands for a "broken" material. When damage is detected in an element through the failure criteria, the stiffnesses and strengths are altered according to Table 2.2 [21], where parameter "E" stands for stiffness as well as for strength, and then a new solution is performed. This procedure is repeated until no more damage occurs, which means that equilibrium is achieved. At that point, the displacement is incremented and the loop is repeated. Although many authors set degraded properties to zero (e.g., in [20]), it appears that the application of a degradation factor to specific stiffnesses and strengths provides more accurate results [15]. It is noted that the "0" degradation factors in Table 2.2 are replaced in FE code by a small number in order to avoid numerical instabilities.

Table 2.2 Degradation factors (T = Tensile and C = Compressive)

Matrix$_T$	**Matrix$_C$**	**Fibre$_T$**	**Fibre$_C$**	**Fibre/Matrix shearout**	**Delam.$_{TC}$**
$E^d_{yy} = 0.2*E_{yy}$	$E^d_{yy} = 0.4*E_{yy}$	$E^d_{xx} = 0.07*E_{xx}$	$E^d_{xx} = 0.14*E_{xx}$	$E^d_{xy} = 0$	$E^d_{zz} = 0$
$E^d_{xy} = 0.2*E_{xy}$	$E^d_{xy} = 0.4*E_{yy}$				$E^d_{yz} = 0$
$E^d_{yz} = 0.2*E_{yz}$	$E^d_{yz} = 0.4*E_{yy}$				$E^d_{xz} = 0$

2.7 Validation of the Model

Each of previous modules (i.e. 1- stress and 2- failure and degradation analyses) must be validated before it can be used with confidence. Such validation is performed according to the following procedure:

1. Stress analysis: the ability of the model to extract interlaminar stresses is verified using data from Pagano [22], whose paper introduces an analytical theory to define the stress field in an arbitrary composite laminate. The results of the present validation are presented in Figure 2.4-Figure 2.6;

2. Failure analysis and degradation of mechanical properties: Failure criteria and sudden degradation rules are evaluated by modeling a simple composite plate under uniaxial quasi-static tension. Delamination propagation is compared to the experimental results (X-ray images) from Aymerich et al. [23].

2.7.1 Validation of the Model: Stress Analysis

In this section, the model is verified for its ability to represent interlaminar stress distribution in the composite plate. A convergence study is first performed, and is broken down in two steps: choice of element type and study on the use of symmetry.

2.7.1.1 Choice of Element Type

In the Ansys environment, both SOLID46 and SOLID191 are layered elements with 3 displacement DOFs per node, and with 8 and 20 nodes, respectively. This characteristic allows a parabolic stress distribution along the thickness for SOLID191, providing a better representation of interlaminar stresses than that for SOLID46, while requiring more computational time. The choice between both element types must therefore involve a trade-off between accuracy of interlaminar stress representation and calculation time. Typical mechanical properties of graphite/epoxy are used in this work (Table 2.3), in conformity with reference [22]. Each element is considered as a unidirectional ply, with the x-direction corresponding to the fiber direction, the y-direction being transverse to the fiber, and the z direction corresponding to thickness.

Table 2.3 Properties of graphite/epoxy

Stiffness	
E_{xx}:	137.9 GPa
E_{yy}:	14.5 GPa
E_{zz}:	14.5 GPa

G_{xy}, G_{yz}, G_{xz}:	5.86 GPa
ν_{xy}, ν_{yz}, ν_{xz}:	0.21

Let us consider a rectangular plate under uniform axial extension, with L >> 2b, as shown in Figure 2.2. The half-width b is 8t, with t being the thickness of each ply. A displacement $\delta = 0.01*L$ is applied along direction L on nodes at x = L/2, and the boundary conditions are set as follows: x-displacements are blocked at x = -L/2, z-displacements are blocked on two nodes located at y = b and y = –b (both nodes are located at the mid-thickness of the laminate and at x = -L/2) in order to avoid the rotation of the plate due to torsional effects, and y-displacements are blocked on one of the two previous nodes. Three interlaminar stresses (σ_z, σ_{xz} and σ_{yz}) are evaluated at the interface between the 3rd and the 4th layers (z = t according to Figure 2.2) along the y direction at x = 0. Two layouts are used in this study: $[0/90]_s$ for σ_z and σ_{yz}, and $[\pm 45]_s$ for σ_{xz}. Since increasing the number of elements through the thickness of each layer is known to improve interlaminar results, each layer is meshed with 1 to 5 elements through thickness, and the mesh is refined near the free edges, as shown in Figure 2.3, in order to create a 10560-elements mesh (1 element through thickness) for the entire plate and both element types.

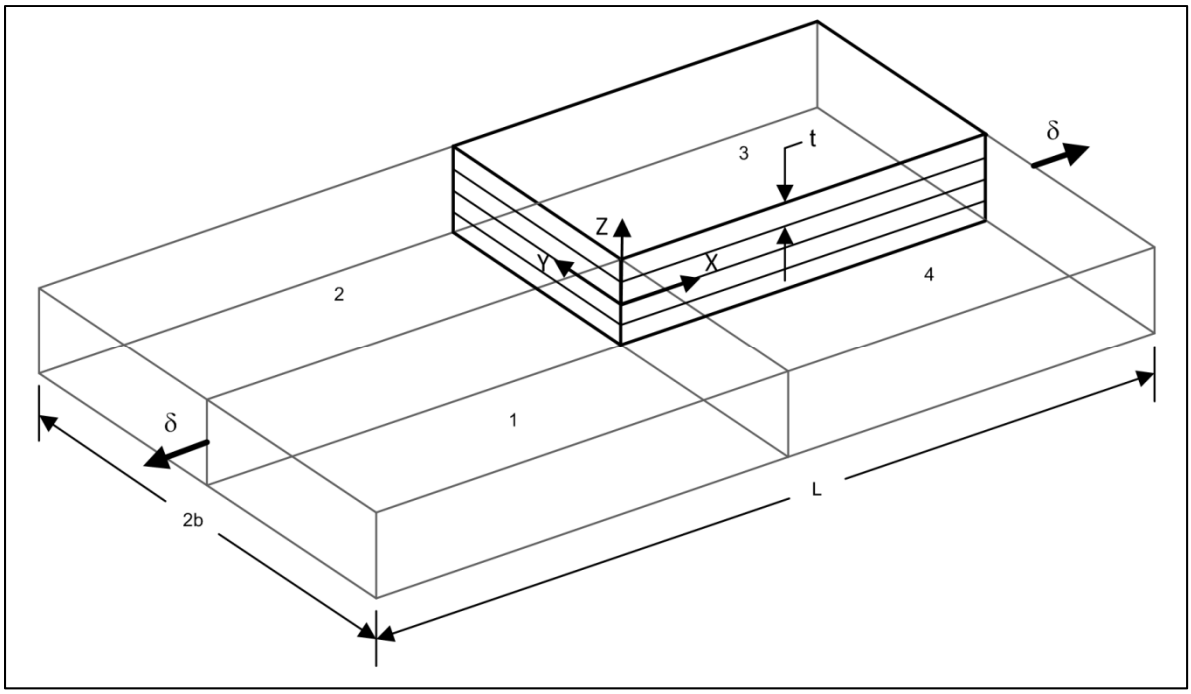

Figure 2.2 Laminate under uniaxial tension

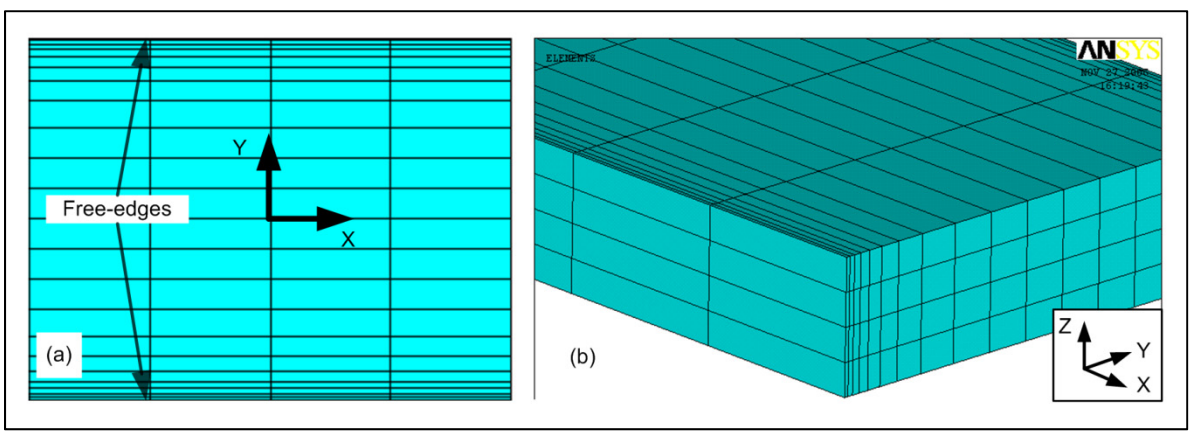

Figure 2.3 a) Mesh refinement near free edges of the plate and b) 1 element through thickness mesh of each layer

The distribution of three interlaminar stresses calculated for models using both 8- and 20-node elements is shown in Figure 2.4-Figure 2.6, plotted along with Pagano's analytical solution [22].

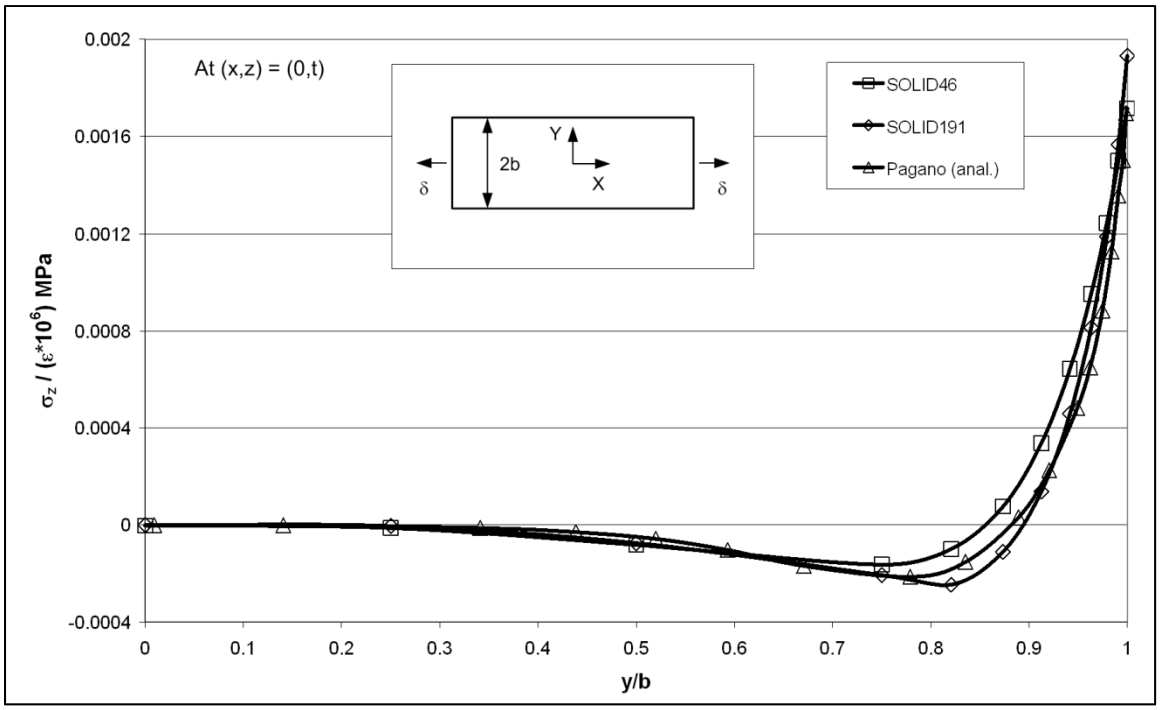

Figure 2.4 σ_z with SOLID46 and SOLID191 elements (ref. curve taken from [22])

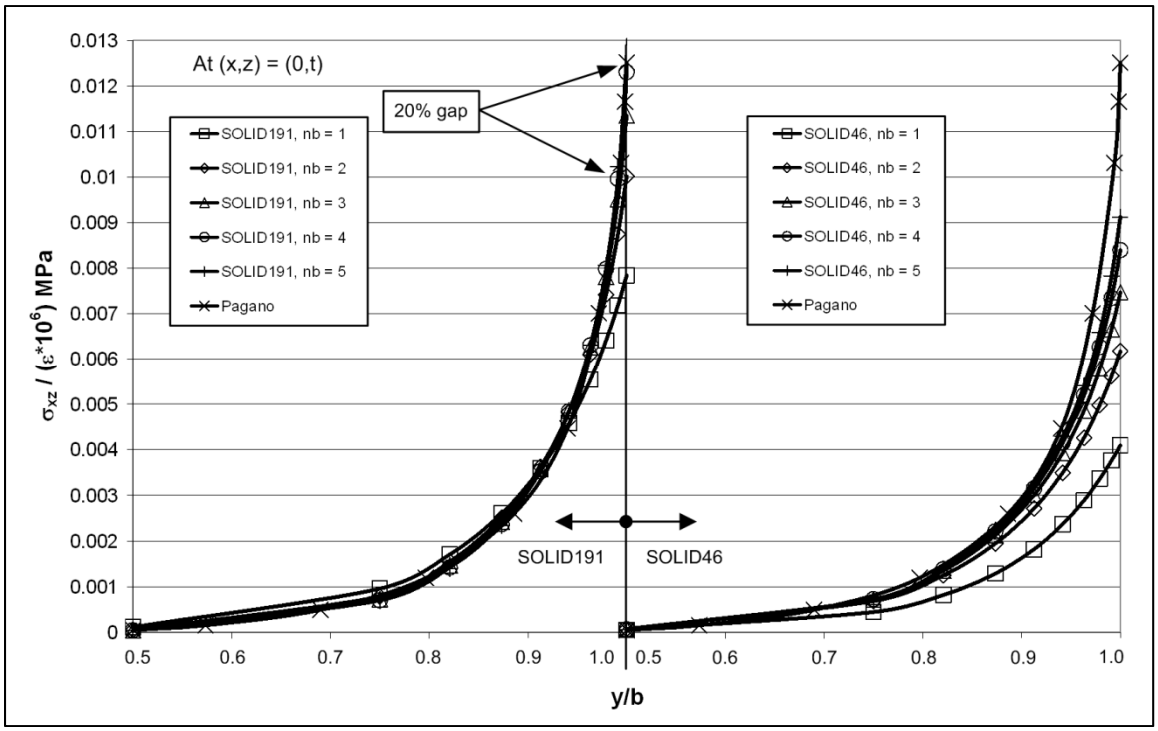

Figure 2.5 Interlaminar stress σ_{xz} for different numbers of elements through thickness for each layer, with Solid46 and Solid191 elements (ref. curve taken from [22]). The gap indicates the difference between Pagano's analytical solution and the numerical results from the present model with 2 elements through thickness of each ply

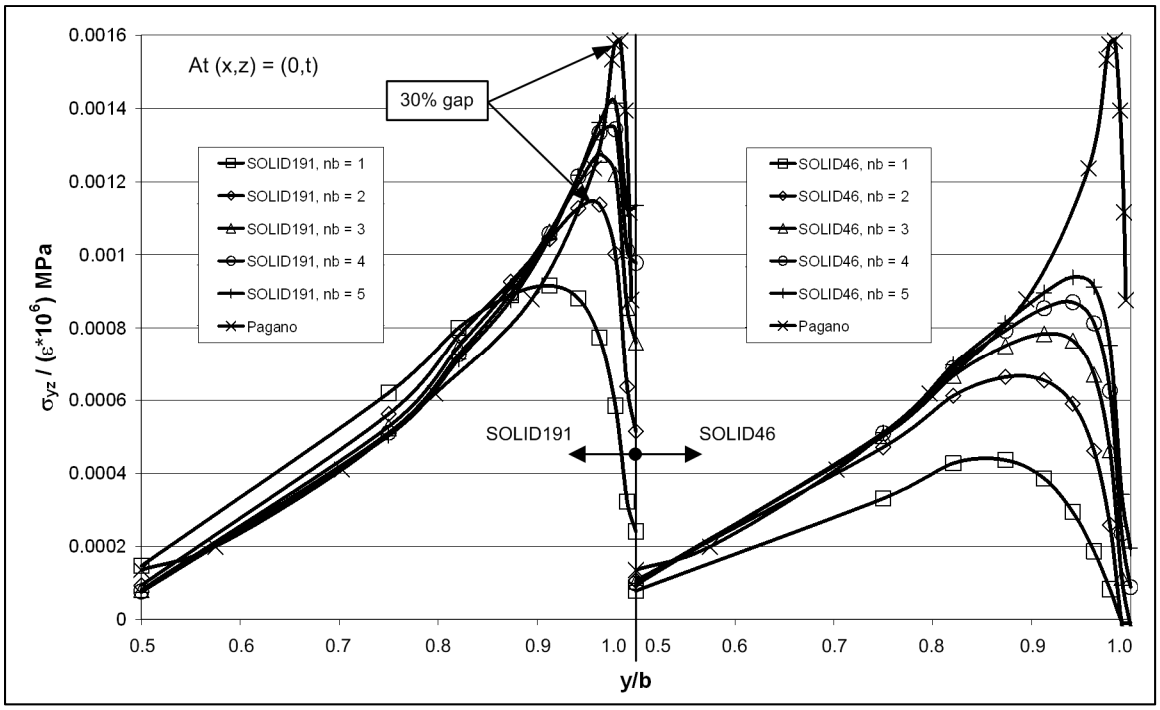

Figure 2.6 Interlaminar stress σ_{yz} for different numbers of elements through thickness for each layer, with Solid46 and Solid191 elements (ref. curve taken from [22]). The gap indicates the difference between Pagano's analytical solution and the numerical results from the present model with 2 elements through thickness of each ply

From previous figures, the curves obtained with SOLID 191 elements show a better correlation with reference data in all cases, for a similar mesh, with accuracy increasing with the number of elements through thickness. In other words, the model would require less refinement in thickness direction with 20-node elements than with 8-node elements, for the same precision. This was expected because of the parabolic distribution of stress in the thickness direction for SOLID191. Only the σ_z stress distribution is not significantly affected by the number of elements through thickness of each ply.

In addition, the authors compared the calculation time for 1, 2 and 3 SOLID191 elements through thickness: 2.5 min, 4.5 min and 10 min, respectively, on a 1.6 GHz Pentium M processor. Such differences in calculation time must absolutely be considered when using an iterative modeling technique such as the progressive damage model. Therefore, since the representation of interlaminar stresses near the free edge is an important issue, much like the

computational time, the authors chose to use 2 SOLID191 elements through thickness for each ply. From Figure 2.5 and Figure 2.6, it appears that such a choice implies, near the free edge, a 20% and a 30% difference for the value of σ_{xz} and σ_{yz} respectively, when compared to the analytical solution from Pagano. In both cases, that difference tends to vanish very rapidly as one gets towards the center of the laminate.

2.7.1.2 Numerical Study on the Use of Symmetry

Almost all researchers use symmetry boundary conditions in their numerical studies of layered composite laminates. While this allows appreciable gains in calculation time for complex models, a quick overview of the literature on that subject reveals however that there is no consensus respecting this practice. It appears that the popular use of symmetrical models may lead to erroneous results [24-27] due to the space-oriented properties of each ply of the laminate, unlike the case with an isotropic material. Therefore the accuracy of stress results in the vicinity of the symmetry boundaries becomes an important issue when a full 3-D delamination analysis is performed. For that reason, the authors investigated the influence of 2 widely used symmetry conditions in the case of a plate under uniform axial strain.

As previously discussed, delamination is known to start at free edges and to propagate towards the center of the laminate. For that reason, the ability of the model to capture a consistent distribution of interlaminar stresses in the y direction is very important. Three models have been evaluated in that respect (see Figure 2.2 for quadrants and for placement and orientation of the coordinate system):

a) Entire plate (no symmetry conditions used);

b) Two symmetry planes: longitudinal and transverse to the displacement direction (quadrant 3);

c) One symmetry plane: transverse to the displacement direction (quadrants 3 and 4).

The symmetry plane which is transverse to the displacement direction could be viewed as a "slice" along the length of the model, since the stress distribution in a plate under uniform axial extension is assumed to be constant along the length. In this paper, it will be referred to as "symmetry" since it is often used, for example, to study a plate with a circular cutout or delamination located at the center of the laminate (in the X-Y plane).

The boundary conditions have been set as follows: for model a) same as in Section 2.7.1.1; for model b) x-displacements are blocked at x = 0 and y-displacements are blocked at y = 0; for model c) x-displacements are blocked at x = 0 and z-displacements are blocked on two nodes located at (x,y) = (0,b) and (x,y) = (0,-b), both nodes being located at the mid-thickness of the laminate. Furthermore, in every case, a node is blocked in space and the displacement is applied on nodes at x = L/2. The same procedure as in Section 2.7.1.1 is then performed in order to study the stress distribution near the free edge of the laminate. The three models are built with 2 Solid191 elements through thickness for each ply, and contain around 24000, 6000 and 12000 elements, respectively.

The study of symmetry conditions is then performed using the three models described above, and with the original mesh. Figure 2.7-Figure 2.9 present the distribution of the out-of-plane interlaminar stresses σ_z, σ_{xz} and σ_{yz} for the three models, at x = 0.

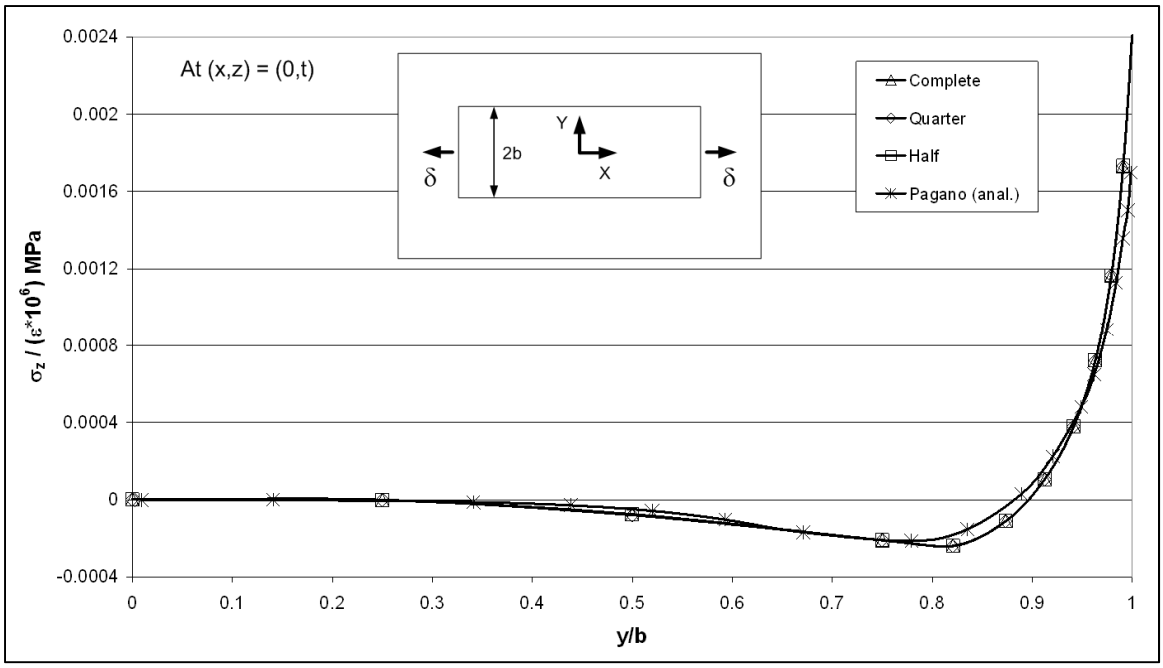

Figure 2.7 σ_z along y-axis at 90/0 interface (ref. curve taken from [22])

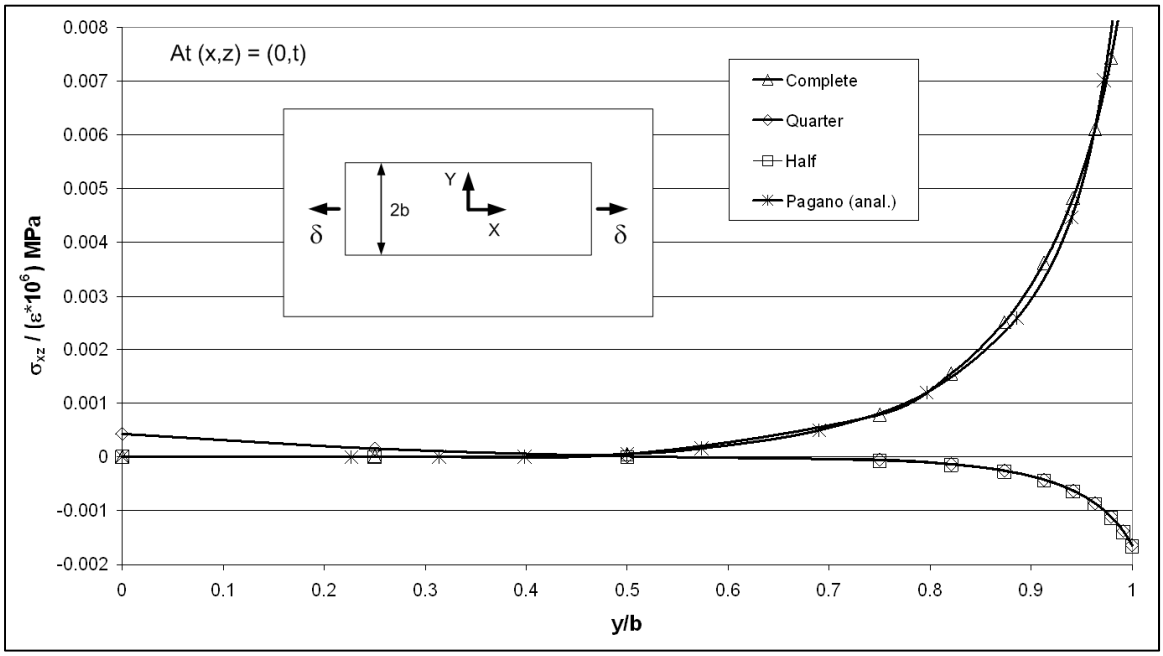

Figure 2.8 σ_{xz} along y-axis at +45/-45 interface (ref. curve taken from [22])

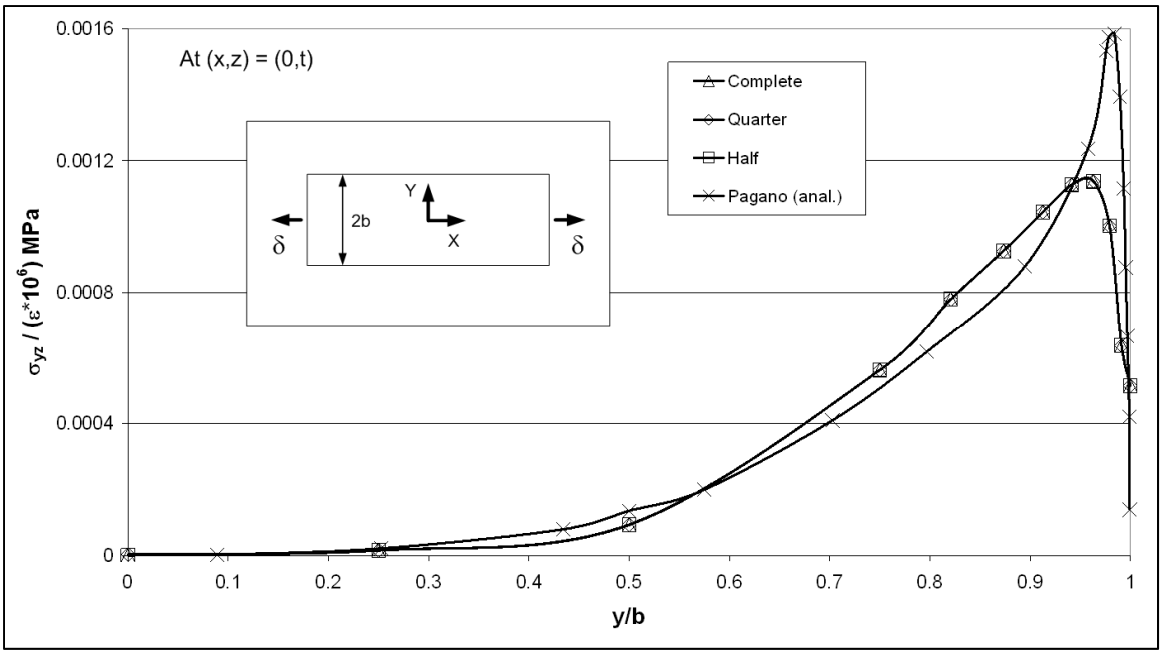

Figure 2.9 σ_{yz} distribution along y-axis at 90/0 interface (ref. curve taken from [22])

From these figures, it can be seen that the stress distribution of σ_z and σ_{yz} is not affected by symmetrical boundary conditions. However, σ_{xz} exhibits a particular behavior when using both quarter- and half-models. It would appear that the x-displacement constraints on the plane at x = 0 induce reversed shear reactions, thus creating a transition zone where stress distribution passes from a reversed shape to an expected shape, as illustrated in Figure 2.10. Similar phenomenon is observed at the plane where displacement is applied on nodes (x = L/2).

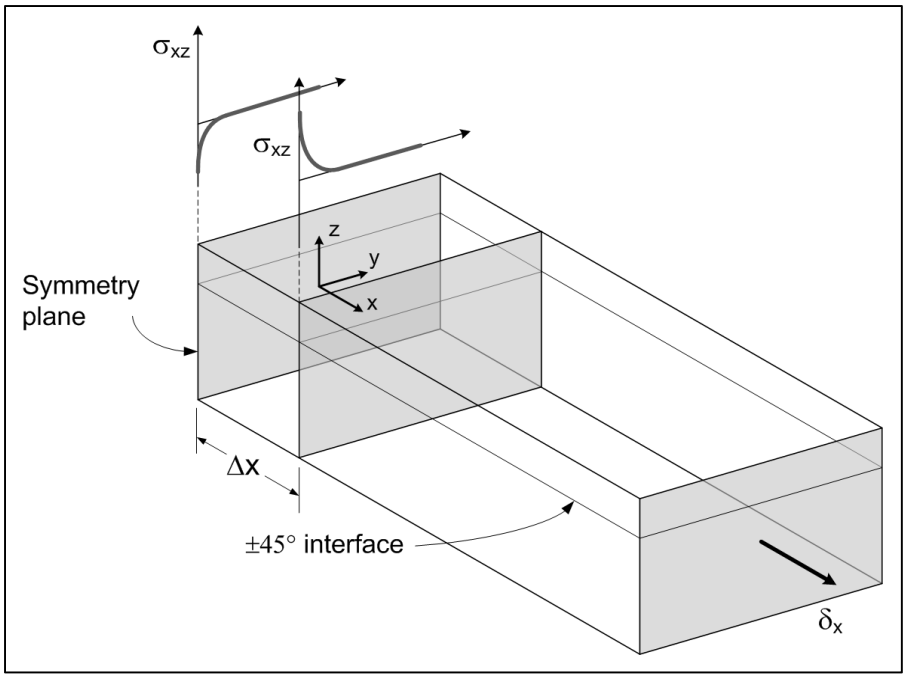

Figure 2.10 Two different shapes of the stress distribution curve in the transition zone near the plane of symmetry

The transition zone around x = 0 was investigated in detail using a refined mesh in that zone. It is important to note that convergence cannot be achieved for σ_{xz} at x = 0, even with highly refined models. Therefore, a singularity exists at the plane of symmetry. However, it is possible to converge at $x \neq 0$, with the length of the disrupted zone decreasing with mesh refinement. Results show that the relative error due to the use of the half-model, when compared to the complete model, is about 8% at 0.3 mm from the symmetry plane (with half the length of the plate being 35 mm), and decreases rapidly with increasing distance in the x direction, as shown in Figure 2.11. Consequently, even though the disrupted zone may be small in respect to the length of the model, particular attention should be paid when using the stress results in that zone.

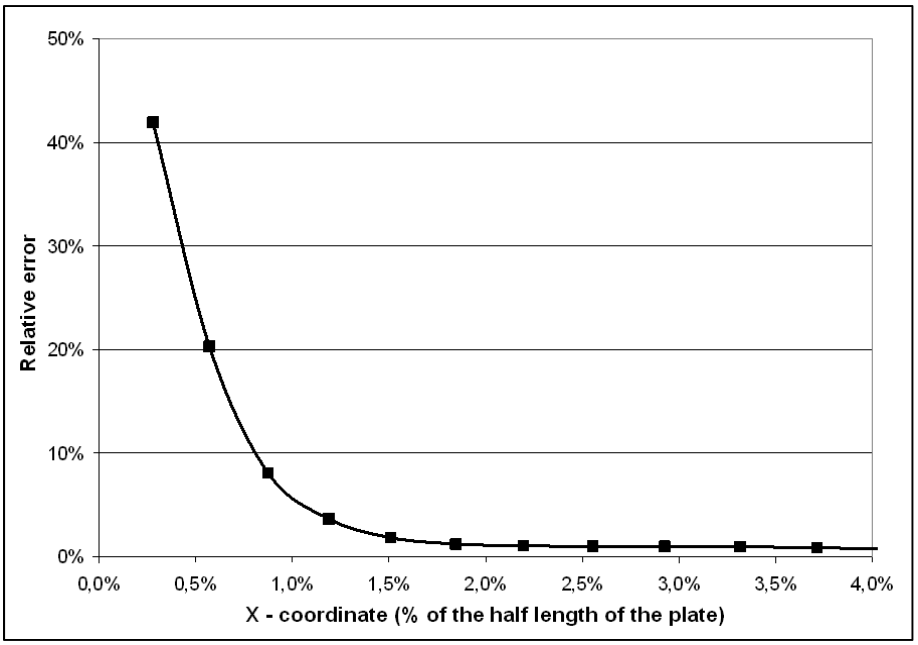

Figure 2.11 Relative error between the half and complete models as a function of x-coordinate (plane of symmetry is at x = 0)

Based on this observation, it can be stated that in every case (entire plate, partial model or slice model) the widely used technique consisting in the restriction of x-displacements (same as loading direction) on nodes located at the end of the plate or at the symmetry plane leads to an incorrect representation of interlaminar stresses in the vicinity of the boundary conditions. Further investigation is to be completed to explain this phenomenon. Therefore, the use of a slice model should be restricted to cases where the length of the slice is long enough when compared to the length of the disrupted zone.

In the case of the quarter-model, the curve presents a non-zero value at the center of the laminate (y/b = 0), which is contrary to the CLT. In fact, according to the CLT, the shear stresses σ_{xz} and σ_{yz} should vanish as one heads towards the center of the laminate. A zero shear stress assumption can therefore be implemented in a homemade FEA code when defining symmetry boundary conditions, but such a condition cannot be applied in commercial codes such as Ansys. An investigation along the length of the plate (x direction) would seem to indicate that the σ_{xz} curve still shows a stress peak in the middle of the

laminate (y/b = 0) at any x-coordinate. For example, the distribution of σ_{xz} for the quarter-model at x = 0.5 mm (1 element length) is shown in Figure 2.12. The shape of the curve is valid all along the x-axis. The stress peak at y/b = 0 and its particularly high absolute value invalidate the use of the symmetry along the y-axis, since it could favor delamination initiation in that zone.

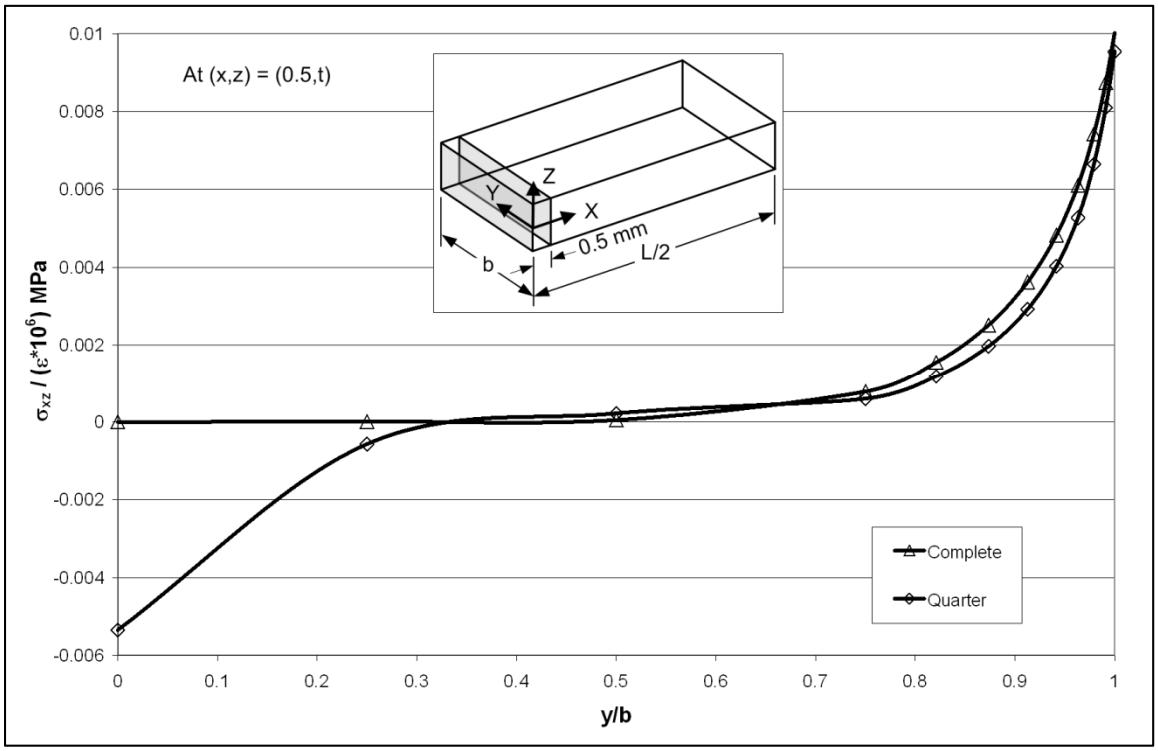

Figure 2.12 σ_{xz} for the quarter-model at x = 1 element length (0.5 mm)

In summary, given that: 1- reducing the calculation time when using progressive damage model is an issue of primary importance; 2- the disrupted zone when using the half-model is quite small when compared to the length of the plate; 3- the low-stress magnitudes in that zone prevent the erroneous initiation of delamination, and 4- the disrupted zone would be present for the entire plate as well, the boundary conditions as presented previously in the paper (for the half-model), are used in the present study. The influence of the use of symmetry on the representation of interlaminar stresses is summarized in Table 2.4.

Table 2.4 Summary of the influence of using symmetry conditions

	Quarter Model	**Half Model**
	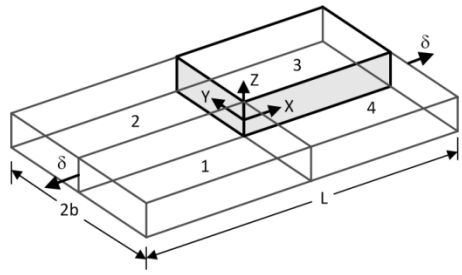	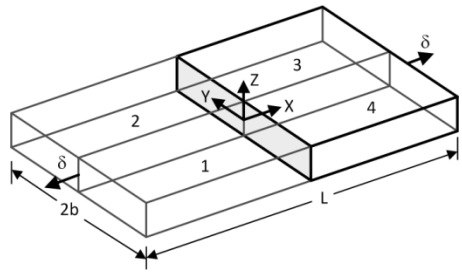
σ_z	As expected.	As expected.
σ_{xz}	A disrupted zone exists in the vicinity of the x-constrained planes (x = 0 and x = L/2), where stress results are erroneous. In the present case, the length of this zone is small with respect to the length of the model. Far from the x-constrained planes, the behavior of σ_{xz} is as expected. A stress peak is present at y/b = 0, where shear stress should vanish.	A disrupted zone exists in the vicinity of the x-constrained planes (x = 0 and x = L/2), where stress results are erroneous. In the present case, the length of this zone is small with respect to the length of the model. Far from the x-constrained planes, the behavior of σ_{xz} is as expected. Shear stress is zero at y/b = 0, as expected.
σ_{yz}	As expected.	As expected.

2.7.2 Validation of the model: Failure analysis and degradation of mechanical properties

A rectangular plate is subjected to a uniaxial tensile load, and the load is increased incrementally in order to simulate a quasi-static tensile test. At each step, the failure criteria from Table 2.1 are verified for all elements, and then, sudden degradation rules from Table 2.2 are applied. This procedure allows the tracking of 4 different failure types: fiber failure, matrix failure, fiber/matrix shearout and delamination. In this section, the delamination propagation behavior is compared to the experimental observations from Aymerich et al. [23].

The plate is 100 mm long and 20 mm wide. Two layouts are modeled: $[\pm 30/90]_s$ and $[\pm 45/0/90]_s$. SOLID191 elements are used with 2 elements through thickness for each ply,

and meshes are 16800 and 22400 elements, for 6 and 8 layers, respectively. The mechanical properties are shown in Table 2.5 [20, 23].

Table 2.5 Properties of graphite/epoxy
(T = Tension and C = Compression)

Stiffness		**Strength**			
E_{xx}:	139 GPa	S_{xT}:	2004 MPa	S_{zT}:	53 MPa
E_{yy}:	9.9 GPa	S_{xC}:	1197 MPa	S_{zC}:	204 MPa
E_{zz}:	9.9 GPa	S_{yT}:	53 MPa	S_{xy}:	137 MPa
G_{xy}, G_{yz}, G_{xz}:	5.2 GPa	S_{yC}:	204 MPa	S_{xz}:	137 MPa
ν_{xy}, ν_{yz}, ν_{xz}:	0.3			S_{yz}:	42 MPa

Only one half of the plate is modeled, as discussed in the last section, and the boundary conditions are as follows: x-displacements are blocked for all nodes at x = 0, two nodes located at (x,y,z) = (0,b,0) and (x,y,z) = (0,–b,0) are blocked in the z direction in order to avoid numerical instabilities, and one node is blocked in the y direction.

An example of the numerical results obtained is presented in Figure 2.13: the delamination state of the $[\pm 45/0/90]_s$ laminate stress state is plotted at 525 MPa, as compared to X-ray image from [23]. In this figure, the grayscale represents the delamination state of the material, going from “healthy” (0) to delaminated (1). As expected, delamination starts from the free edges and propagates towards the center of the laminate.

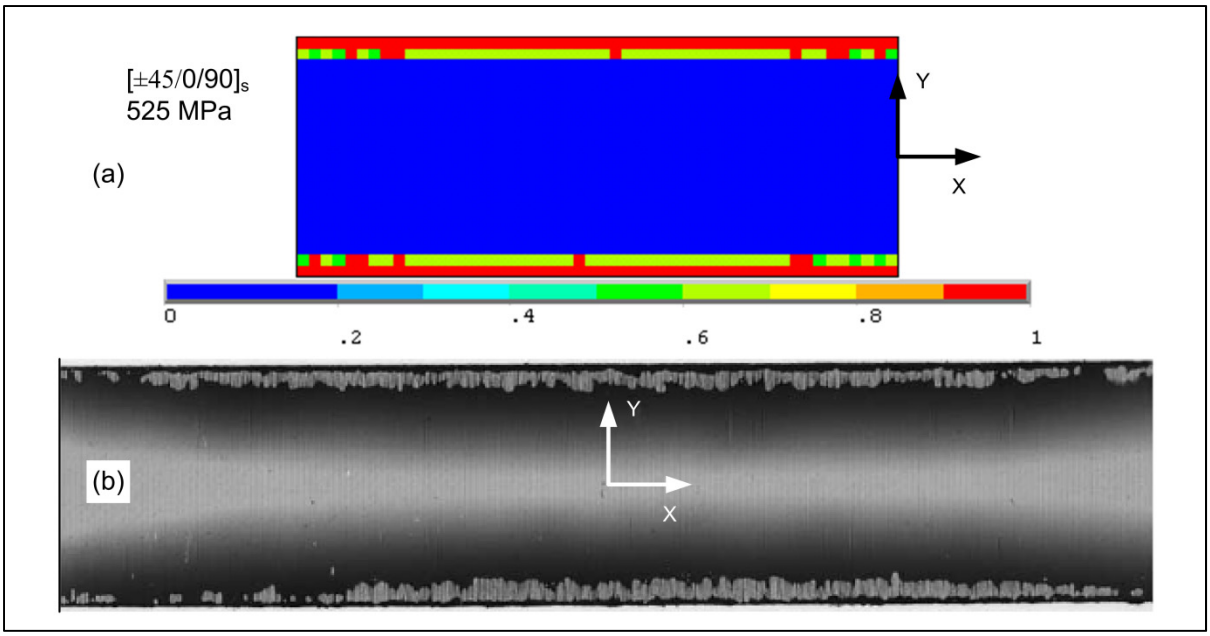

Figure 2.13 State of delamination at 525 MPa (monotonic tensile test) for a $[\pm 45/0/90]_s$ layout, from a) numerical results, and b) X-ray imaging [23]

In addition to this qualitative comparison, the progression of the delaminated area during the simulated tensile test was calculated in terms of percentage of the total area of the plate, and the results plotted in Figure 2.14 for both studied layouts. As expected, the delamination propagates more rapidly in the matrix-dominated laminate ($[\pm 30/90]_s$) than it does in the fiber-dominated laminate ($[\pm 45/0/90]_s$). Although the correlation between reference and model curves is less obvious for the $[\pm 30/90]_s$ laminate than for the $[\pm 45/0/90]_s$, the general trend showed by the curve extracted from the FE model is quite satisfying, taking into account the multitude of factors influencing delamination behavior that are not considered in the present model, such as impurities introduced during the fabrication, misaligned fibers, or free-edge delamination induced during the coupon cutting process. Although these preliminary results are encouraging, the numerical model still needs to be validated using more experimental data. Consequently, an extended experimental testing program will be used in the sequel.

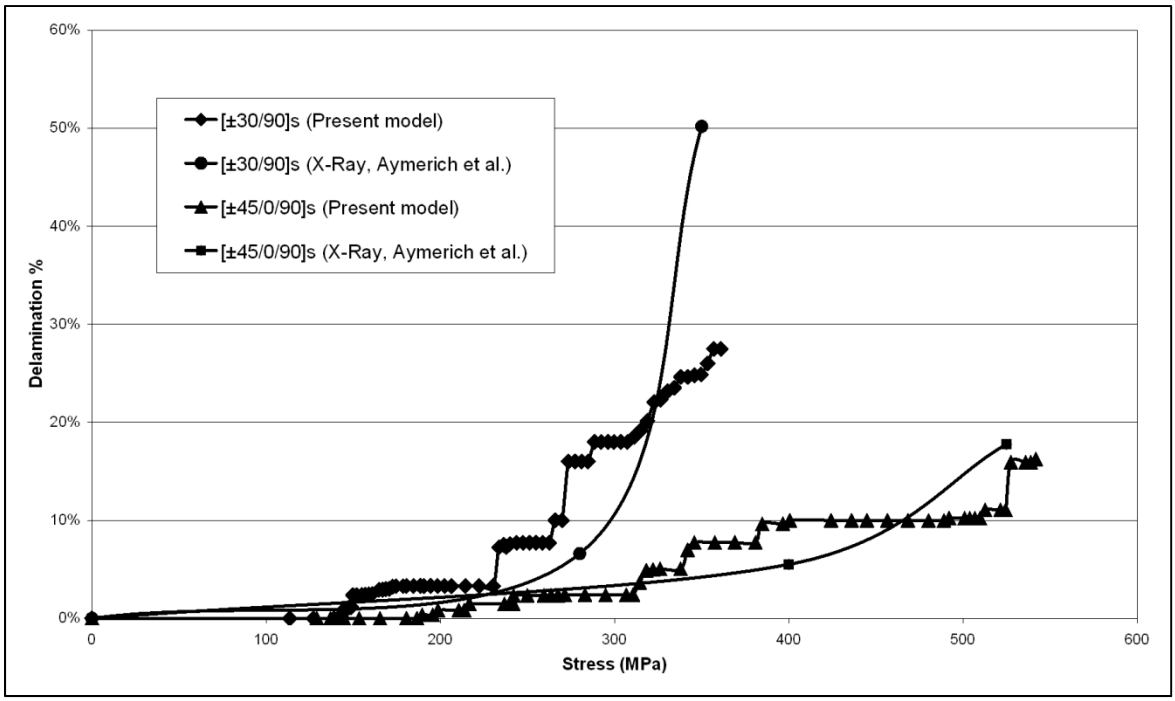

Figure 2.14 Areal delamination percentage at different stress states. Reference data are calculated from [23]

2.8 Conclusions

In this paper, a numerical model based on the progressive damage modeling technique is presented, and partially validated. The model is able to predict delamination initiation at the free edges of simple composite plates and delamination propagation under monotonic tensile loading. Preliminary results show a good correlation with results from the literature, for both interlaminar stress distribution and delamination behavior (initiation and propagation).

Furthermore, it is shown that the use of longitudinal symmetry with respect to the displacement direction should be avoided since this induces some shear stress on the symmetry plane, which is not in keeping with the CLT. On the other hand, it is observed that the use of transverse symmetry with respect to the displacement direction creates unexpected results at the symmetry plane for the σ_{xz} shear stress, but this phenomenon vanishes a short distance away from the symmetry plane. Therefore, there is a disrupted zone in the vicinity

of the symmetry plane where the σ_{xz} results are not as expected. This phenomenon is attributable to the x-displacement constraints on the nodes at the plane of symmetry, which force adjacent elements to have a straight face under shear stress, thus inducing reversed shear stress at the symmetry plane. This phenomenon is observed as well at the plane where the displacement is imposed on nodes.

However, since the numerical technique which consists in constraining the displacements on nodes is widely used because of its ease, such a disrupted zone would exist with the use of a complete model as well, or with a slice model. Thus, the use of symmetry transversally to the loading direction (or a slice model) should be restricted to cases where the length of the disrupted zone is short as compared to the length of the plate (or the slice).

The model now needs to be validated against more experimental data, hence the need to perform certain tensile tests on composite laminates. The numerical model will then be used as a design tool for developing an SMA stitched composite allowing the localized control of delamination propagation.

2.9 References

[1] Her S-C, Liang Y-C. The finite element analysis of composite laminates and shell structures subjected to low velocity impact. Composite Structures. 2004;66:277-85.

[2] Harris CE, Starnes Jr. JH, Shuart MJ. Design and manufacturing of aerospace composite structures, state-of-the-art assessment. Journal of Aircraft. 2002;39:545-60.

[3] Mouritz AP, Cox BN. Mechanistic approach to the properties of stitched laminates. Composites Part A: Applied Science and Manufacturing. 2000;31:1-27.

[4] Greenhalgh E, Hiley M. The assessment of novel materials and processes for the impact tolerant design of stiffened composite aerospace structures. Composites Part A: Applied Science and Manufacturing. 2003;34:151-61.

[5] Lau K-T, Ling H-Y, Zhou L-M. Low velocity impact on shape memory alloy stitched composite plates. Smart Materials and Structures. 2004;13:364-70.

[6] Masuda A, Ni Q-Q, Sone A, Zhang R-X, Yamamura T. Preliminary characterization and modeling of SMA-based textile composites. Smart Structures and Materials - Modeling, Signal Processing, and Control. San Diego, CA, United States: International Society for Optical Engineering, Bellingham, WA 98227-0010, United States; 2004. p. 94-102.

[7] Chou S-C, Orringer O, Rainey JH. Post-failure behavior of laminates - 2. Stress concentration. Journal of Composite Materials. 1977;11:71-8.

[8] Hashin Z. Static and fatigue failure criteria for unidirectional fiber composites. 1982. p. 213-8.

[9] Chang F-K, Chang K-Y. Progressive damage model for laminated composites containing stress concentrations. Journal of Composite Materials. 1987;21:834-55.

[10] Brewer JC, Lagace PA. Quadratic stress criterion for initiation of delamination. Journal of Composite Materials. 1988;22:1141-55.

[11] Tay TE. Characterization and analysis of delamination fracture in composites: An overview of developments from 1990 to 2001. Applied Mechanics Reviews. 2003;56:1-31.

[12] Wu H, Yan X. Interlaminar stress modeling of composite laminates with finite element method. Journal of Reinforced Plastics and Composites. 2005;24:235-58.

[13] Shokrieh MM. Failure of laminated composite pinned connections [Master Thesis]. Canada: McGill University, 1991.

[14] Tserpes KI, Papanikos P, Kermanidis T. A three-dimensional progressive damage model for bolted joints in composite laminates subjected to tensile loading. Fatigue and Fracture of Engineering Materials and Structures. 2001;24:663-75.

[15] Tserpes KI, Labeas G, Papanikos P, Kermanidis T. Strength prediction of bolted joints in graphite/epoxy composite laminates. Composites Part B: Engineering. 2002;33:521-9.

[16] Papanikos P, Tserpes KI, Labeas G, Pantelakis S. Progressive damage modelling of bonded composite repairs. Theoretical and Applied Fracture Mechanics. 2005;43:189-98.

[17] Lessard LB, Schmidt AS, Shokrieh MM. Three-dimensional stress analysis of free-edge effects in a simple composite cross-ply laminate. International Journal of Solids and Structures. 1996;33:2243-59.

[18] Tian Z, Zhao F, Yang Q. Straight free-edge effects in laminated composites. Finite Elements in Analysis and Design. 2004;41:1-14.

[19] Tahani M, Nosier A. Three-dimensional interlaminar stress analysis at free edges of general cross-ply composite laminates. Materials and Design. 2003;24:121-30.

[20] Shokrieh MM. Progressive fatigue damage modeling of composite materials [Ph.D. Thesis]. Canada: McGill University, 1996.

[21] Papanikos P, Tserpes KI, Pantelakis S. Modelling of fatigue damage progression and life of CFRP laminates. Fatigue and Fracture of Engineering Material and Structures. 2003;26:37-47.

[22] Pagano NJ. Stress fields in composite laminates. International Journal of Solids and Structures. 1978;14:385-400.

[23] Aymerich F, Priolo P, Sun CT. Static and fatigue behaviour of stitched graphite/epoxy composite laminates. Composites Science and Technology. 2003;63:907-17.

[24] Li S, Reid SR. On the symmetry conditions for laminated fibre-reinforced composite structures. International Journal of Solids and Structures. 1992;29:2867-80.

[25] Reddy JN. Note on symmetry considerations in the transient response of unsymmetrically laminated anisotropic plates. International Journal for Numerical Methods in Engineering. 1984;20:175-81.

[26] Mallikarjuna. Important note on symmetry line boundary conditions in fibre-reinforced laminated anisotropic composites. Computers and Structures. 1991;38:669-71.

[27] Shen F, Lee KH, Tay TE. Modeling delamination growth in laminated composites. Composites Science and Technology. 2001;61:1239-51.

CHAPITRE 3

ARTICLE DE CONFÉRENCE : SUPPRESSION OF DELAMINATION PROPAGATION IN CARBON/EPOXY LAMINATES BY THE USE OF SUPERELASTIC STITCHING WIRES: PRELIMINARY RESULTS

P.-L. Vachon, V. Brailovski, P. Terriault

École de technologie supérieure, 1100 rue Notre-Dame Ouest

Montréal, (Qc), Canada, H3C 1K3

Ce chapitre présente un article publié dans le compte-rendu de la conférence « Eight Joint Canada-Japan Workshop on Composites », Montréal, Qc, 26-29 juillet 2010.

3.1 Résumé (français)

Ce chapitre a fait l'objet d'une publication et d'une présentation orale à la conférence « Eight Joint Canada-Japan Workshop on Composites », tenue à Montréal en 2010. Il introduit le développement de la technologie de renfort à l'aide de couture en fil AMF. Lors de cette étude expérimentale, des plaques composites carbone/époxy comprenant 16 couches de fibres ont été fabriquées. Certaines de ces plaques ont été renforcées de fils en alliage TiNi superélastique ou en Kevlar, à l'aide d'une machine à coudre industrielle. Les échantillons renforcés (TiNi et Kevlar) et non renforcés ont été soumis à un essai d'impact à faible vitesse (ASTM D7136), de façon à induire des dommages au centre des plaques. Les dimensions et la forme de la zone endommagée ont été évaluées par la méthode des ultrasons pour caractériser l'étendue du délaminage. La résistance résiduelle en compression des plaques endommagées a été mesurée à l'aide de l'essai normalisé de compression après impact (ASTM D7137). Les résultats ont montré une certaine efficacité des renforts en TiNi pour diminuer les dimensions de la zone délaminée après impact, ainsi que pour améliorer la résistance résiduelle en compression. Par contre, les renforts en Kevlar se sont montrés plus performants dans les deux cas.

3.2 Abstract

The reinforcement of laminated composites by stitching is a promising technique, especially in the aerospace field. So far the use of Kevlar, glass and carbon yarns as stitching threads has shown great potential in preventing the delamination propagation. In this study, the authors introduced a new stitch system by the use of Shape Memory Alloys (SMA). A superelastic TiNi wire (0.1 mm dia.) was stitched through the thickness of the carbon fibre plies prior to resin infusion. The rectangular 16-layer carbon/epoxy specimens reinforced by superelastic stitches were submitted to a compression-after-impact test (CAI, ASTM D7137). Prior to the compression test, initial delamination was created by low velocity impact testing (ASTM D7136). During the compressive loading, the superelastic stitches were intended to dissipate energy that would otherwise contribute to propagate the existing delamination. The compressive strength of as-impacted SMA-stitched samples was compared to that of Kevlar-stitched and unstitched samples. The results showed that the SMA stitches were effective in reducing the area and volume of the impact-induced delamination, as well as in improving the CAI strength, but the Kevlar stitches were more effective than the TiNi stitches in both tests.

3.3 Introduction

Impact damage in aeronautical composite structures is one of the main issues considered by designers, because it may initiate invisible delamination which may lead to a severe reduction in the stiffness and strength of structures. Several methods have been investigated with the aim of improving the through-thickness properties of laminated composites, such as 3-D weaving, braiding, stitching and Z-pinning. Among them, the stitching technique was found to be the most promising, especially for aerospace applications [1].

In the recent literature, numerous studies have been devoted to the understanding of the behaviour of Kevlar-stitched composites under the low-velocity impact and post-impact loadings. This reinforcement technique has shown its capability in reducing the delaminated

area after the impact as well as in improving the Compression After Impact (CAI) strength [2-7]. The performance of the stitching system was shown to be related to the stitch material and stitching density, and the versatility of the stitching technique allows optimizing the performance of the system.

Whereas Kevlar stitching yarn has been extensively used, only one study has been published dealing with the use of shape memory alloy (SMA) wire as the stitching yarn [8]. In this paper, the authors inserted superelastic TiNi wire into a glass/epoxy plate to evaluate its response to a low-velocity impact loading. The authors found that the number of translaminar cracks was reduced by the stitching due to the damping effect of the superelastic wires. Moreover the theoretical analysis showed that the delamination energy was reduced when compared to the unstitched plates. No post-impact mechanical tests were performed.

In the present study, the authors introduce the use of superelastic TiNi stitching wire in carbon/epoxy laminates. The performance of the stitched laminates is evaluated in terms of the low-velocity impact resistance (damaged area and volume after the impact event) and the impact damage tolerance (compression after impact strength). The results are compared to those obtained with Kevlar-stitched and unstitched laminates.

3.4 Experimentations

3.4.1 Equipments

An industrial immersion ultrasonic scanner (Tecscan Systems, Canada) was used for quality control of the specimens prior to testing and for delamination measurements. The scanner is controlled by the TecView UT software and allows viewing A-Scans, B-Scans and C-Scans simultaneously. The frequency and diameter of the transducer were 5 MHz and 0.375 in, respectively.

Micrograph observations were carried out using an optical microscope (model Stereozoom 7, Bausch and Lomb, USA) equipped with a camera (Clemex DCAM-1280k B/W Firewire) and the Clemex Captiva software (Clemex Technologies, Canada).

The specimens were impacted on a custom-made impact machine equipped with a pneumatic anti-rebound system (McGill University). The impactor head was equipped with a spherical striker of 12.5 mm diameter; the total mass of the head was 8.2 kg.

The compression after impact tests were carried out on a MTS Alliance RF 200 machine equipped with a 200 kN load cell. The deformation of the specimens during compression was monitored using two video-extensometers, one being commercial (model ME-46, Messphysik Materials Testing, Austria) and the other being an in-house motion-measurement system using a GRAS-20S4M-C black-and-white camera (Point Grey Research, Canada) and the program Labview.

3.4.2 Specimen Preparation

Three different types of carbon/epoxy specimens were compared in the present study: unstitched, Kevlar- and TiNi-stitched specimens. All specimens were cut out from four large panels, with each panel including specimens from all the three types of specimens disposed randomly. The 5 mm-thick panels were made of 16 plies of uniaxial carbon fabric (JB Martin) stacked in a $[45/0/-45/90]_{2s}$ layout. Prior to the resin infusion (Ren Infusion 8604 Epoxy, Freeman Mfg. and Supply), the panels were stitched using industrial sewing machine (Juki LU-563) with either Kevlar thread (Tex 40, American & Efird) or TiNi wire (0.1 mm dia., Memry). The modified lock stitch pattern was adopted (Figure 3.1a) using Kevlar thread as the needle thread in all cases. The stitching pitch and the distance between stitch lines were both set at 5 mm since these parameters were used with satisfying results by other authors [3,5]. Note that only a square region of 50 mm x 50 mm was stitched, centered in the plane of the specimens, as shown in Figure 3.1b. Prior to stitching, the as-drawn TiNi wire

was heat treated at 350°C for 15 minutes to confer to the wire superelastic properties. The wire was then cleaned in a HF-HNO_3 solution to remove the oxide layer.

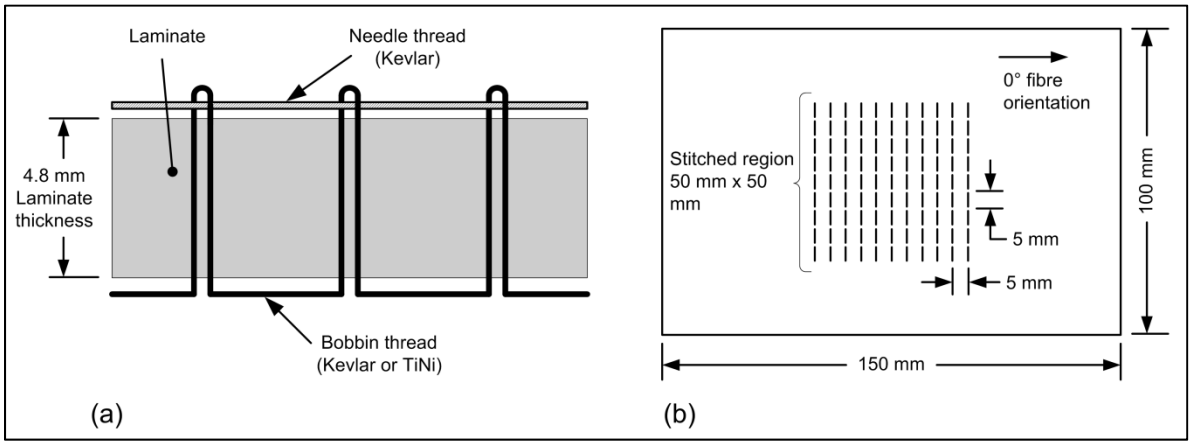

Figure 3.1 a) Modified lock stitch (after [7]); b) detail of the stitched specimen

After curing, rectangular specimens were cut from the panels with a diamond saw blade, and the specimens were then machined to the final dimensions (150 mm x 100 mm) using a diamond-coated endmill. All specimens were inspected after fabrication and the C-Scan images showed no delamination prior to testing.

It is worth noting that some tests were carried out before beginning the fabrication process, in order to set up the tensioning device of the industrial sewing machine. This device is needed to keep a certain tension force on the needle thread during the stitching, to be capable of pulling the bobbin thread through the 16 carbon plies. For these tests, the tension force was varied between 200 and 500 cN and the resulting stitches were observed by optical microscopy.

For both Kevlar- and TiNi-stitched plates, it appeared that a minimum tension force of around 400 cN was necessary to pull the bobbin thread completely through the laminate. Under this value, the thread loop was located inside the laminate, which is undesirable. Figure 3.2 shows the micrographs of a Kevlar-stitched and a TiNi-stitched specimen with a needle thread tension of 400 cN.

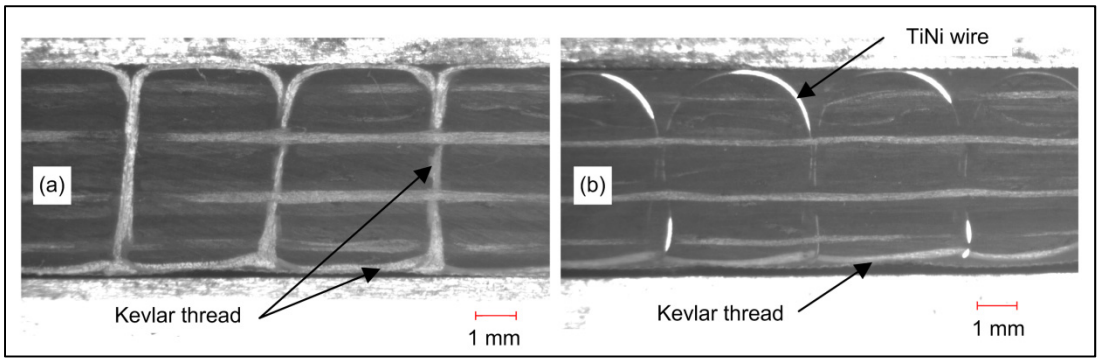

Figure 3.2 Micrographs of a) Kevlar-stitched and b) TiNi-stitched laminates

3.4.3 Impact Testing

All specimens were impacted at their center with an energy level of 1 J/mm (normalized with the thickness). The specimens were maintained on the base plate by rubber clamps at each corner according to ASTM D7136. Machined in the base plate was a 125 mm x 75 mm rectangular window allowing deformation of the specimens during the impact. The speed of the impactor head just prior to the impact was measured using a high speed camera (Fastec Troubleshooter HRMS, Fastec Imaging, California). The delaminated area was then observed by C-Scan imaging.

3.4.4 Compression After Impact (CAI) Testing

The compression strength of the impacted specimens was measured according to ASTM D7137. The specimens were placed in an anti-buckling fixture as shown in Figure 3.3, and loaded up to failure with the displacement rate of 1 mm/min. The deformation on both sides of the plates was monitored during the test by two video-extensometers. Six specimens of each type were tested.

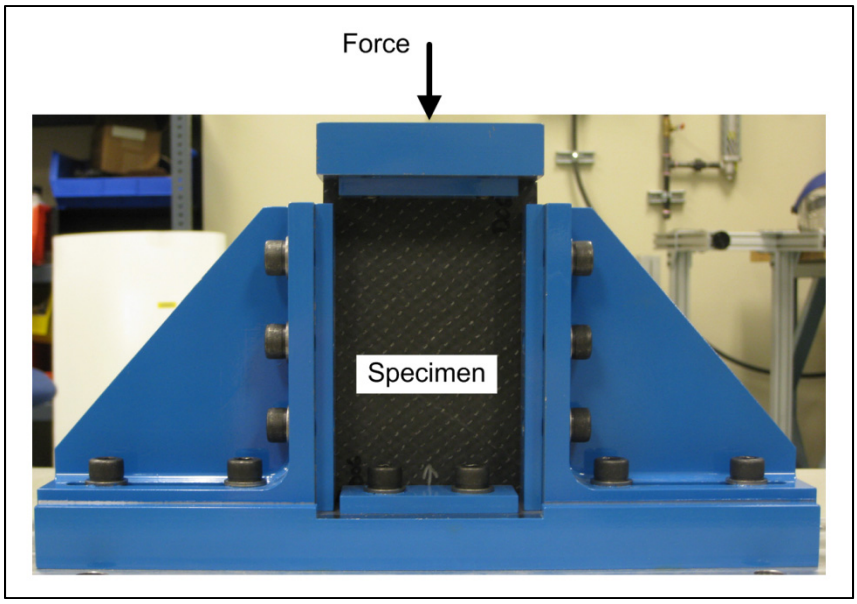

Figure 3.3 ASTM D7137 fixture for CAI testing

3.5 Results and Discussion

3.5.1 Impact Testing

After the impact, no visible damage was noticed on the surface of the plates. The impacted specimens were inspected using C-Scan imaging technique. All the plates exhibited an in-plane circular-shaped delamination at the impact location. An example of the C-Scan image is shown in Figure 3.4. C-Scan imaging allowed the delaminated area to be measured for all specimens prior to carry out the CAI tests. The results are presented in Table 3.1.

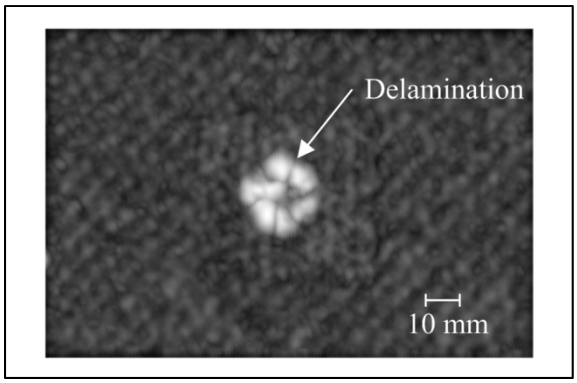

Figure 3.4 Impacted TiNi-stitched specimen with delaminated zone at the centre (C-scan imaging)

Table 3.1 Delaminated area of the impacted specimens

	Delaminated Area (mm^2)		**Deviation**
	Mean	**Std. Dev.**	**(ref: Unstitched)**
Unstitched	556	56	0%
Kevlar-stitched	449	31	-19%
TiNi-stitched	518	38	-7%

It can be observed in Table 3.1 that both the Kevlar and the TiNi stitch threads acted as energy dissipaters during the impact, with the Kevlar thread being strongly efficient with a reduction of the area of 19% when compared to the unstitched specimens. For the case of TiNi, the dissipating effect appears to be smaller than that of Kevlar. However, the 7% reduction of the delaminated area, combined with the good bonding between the TiNi stitch and the epoxy matrix revealed by the optical micrographs, are considered as a potentially promising output.

3.5.2 CAI Testing

Table 3.2 presents the ultimate compression strength of all impacted specimens. From this table, one can observe that the insertion of Kevlar stitches in laminates resulted in an

improvement of the compressive strength (8%) when compared to the unstitched specimens, a phenomenon which is directly linked to the results from the previous section. Regarding the TiNi stitches, the slight CAI strength improvement of 1% indicates that the present stitching configuration does not offer a significant contribution to the overall performance of the structure. Obviously the CAI strength of the TiNi-stitched plates would definitely benefit from an optimization of the stitch pitch, spacing and the TiNi wire diameter.

Table 3.2 CAI Strength

	CAI Strength (MPa)		**Deviation**
	Mean	**Std. Dev.**	**(ref: Unstitched)**
Unstitched	222	10	0%
Kevlar-stitched	240	12	8%
TiNi-stitched	224	15	1%

In all cases, the final rupture of the plates was brutal and localized at the mid-length (i.e. at the impact location). The observation of the broken specimens demonstrated that the rupture mode was different on each side of the plates, due to the asymmetrical distribution of the delamination across the thickness of the laminates (to be discussed later). On the surface that received the impactor striker, the outer plies delaminated on a line along the width of the plates and localized buckling appeared along this line, as shown in Figure 3.5a. On the opposite surface, the rupture mode appeared as a ply crack which covered the entire width of the plate as seen on Figure 3.5b.

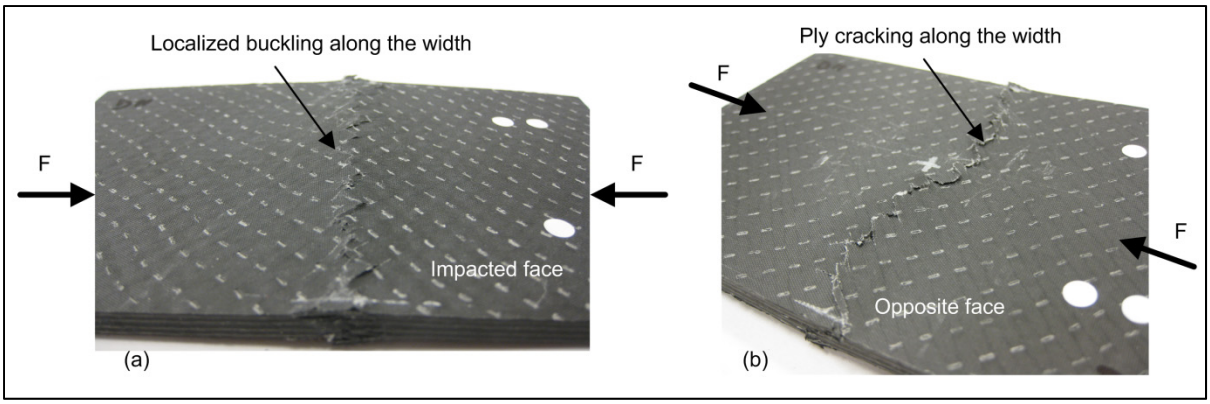

Figure 3.5 Surfaces of a ruptured unstitched specimen: a) impacted face; b) opposite face

The behaviour of the plates during the CAI tests was captured with a video camera from the opposite side to the impact. According to the images, in all cases (unstitched and stitched), the crack initiated roughly in the centre of the specimens, before propagating towards both sides of the plates. The crack always appeared a few seconds prior to the final rupture. In the case of stitched specimens, it was observed that the path of the crack on the non-impacted face followed a stitch line, jumping from one stitch line to another, as illustrated in Figure 3.6.

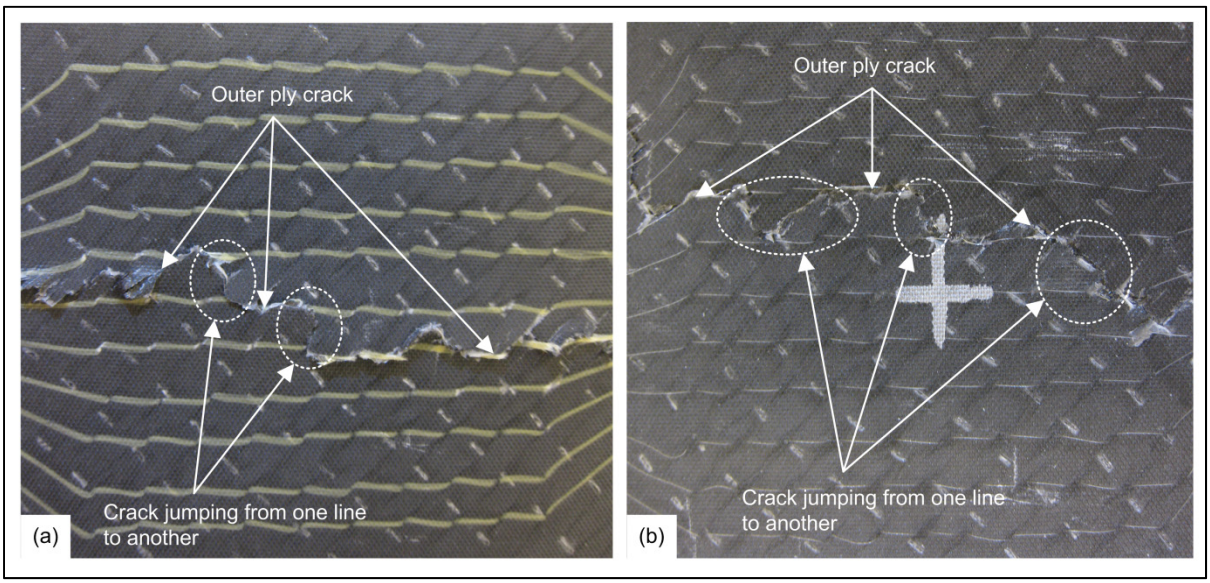

Figure 3.6 Surface crack path in a) Kevlar-stitched, and b) TiNi-stitched specimens

Another series of CAI tests was also conducted in which the maximum force applied was either 70%, 80% or 90% of the ultimate compressive force. The specimens were then inspected using C-Scan imaging to track the propagation of the delamination in the in-plane direction, as well as through the thickness of the plates. The distribution of the delamination through the thickness of the specimens was investigated by the use of B-Scan images. To do so, for each C-Scan data file, several B-Scan images were taken along different lines across the specimen width. Having several B-Scans at every 2 mm along the length of the specimens allowed assessing the volume of the delaminated zone. A schematic representation of a C-Scan image with the B-Scan lines crossing the damaged zone is shown in Figure 3.7a, while Figure 3.7b is a schematic of a B-Scan image.

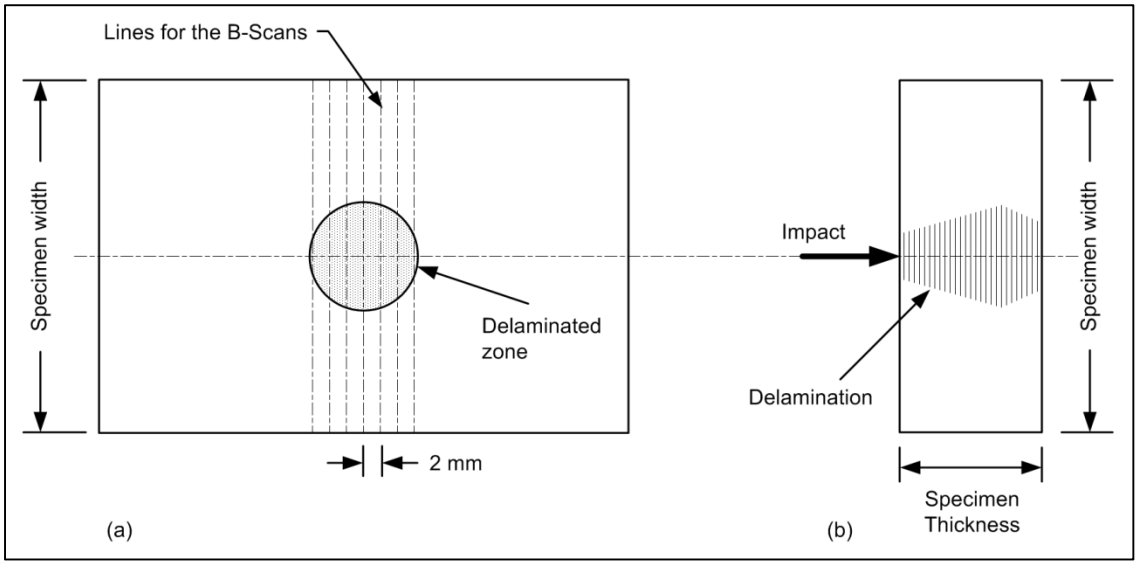

Figure 3.7 Schematic representation of: a) C-Scan image showing circular delamination and lines for the B-Scans; b) B-Scan image

In Figure 3.8 is presented a B-Scan image taken from an impacted unstitched specimen. The shape of the delaminated region as shown in this figure is typical of what could be observed from all the specimens (unstitched, Kevlar- and TiNi-stitched). In all cases, the largest delamination was located at an interface near the unimpacted face of the specimen.

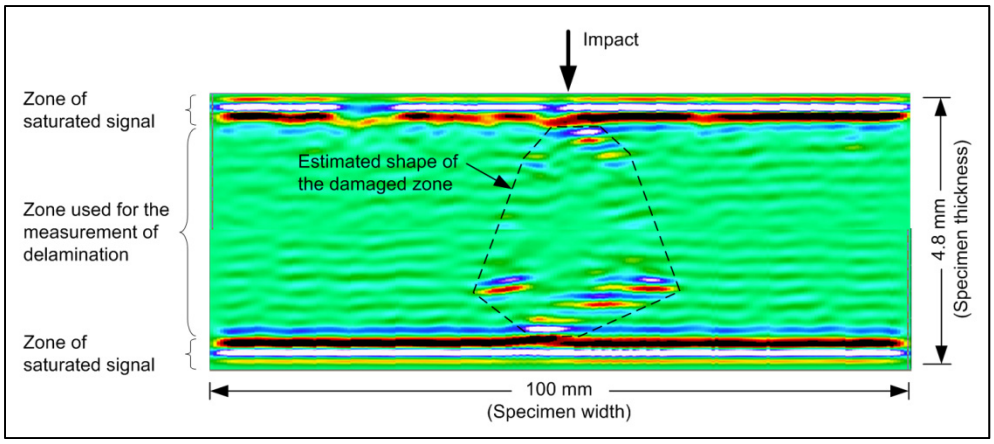

Figure 3.8 Example of a B-Scan image from an impacted unstitched specimen

In Table 3.3 is presented the average volume of the damaged zone for the three different types of specimens. No noticeable increase of the delaminated volume was observed with the increase of the applied force, which indicates that the CAI tests are not well suited for gradual delamination growth observation. Consequently, these results could not be used to validate the numerical model as it was expected. However, it is clear from Table 3.3 that the Kevlar yarn acted strongly against the delamination spreading, with a volume reduction of 27% in average when compared to the unstitched plates. The TiNi-stitched specimens also exhibited significant performance with a 10% reduction of the damaged volume. These results were in accordance with the measurements of the delaminated area presented in Table 3.1.

Table 3.3 Volume of the delaminated region

	Mean mm^3	**Std. Dev.** mm^3	**Deviation (ref: Unstitched)**
Unstitched	1306	169	0%
Kevlar-stitched	949	100	-27%
TiNi-stitched	1169	55	-10%

3.6 Conclusions

In this work, a new material was used as a through-thickness reinforcement with the goal of improving the impact resistance as well as the compression after impact strength. The carbon/epoxy laminates were stitched with a TiNi wire prior to the resin infusion. The performance of the SMA-stitched specimens was compared to that of the Kevlar-stitched and unstitched specimens. The results showed that the TiNi reinforcement, as compared to the unstitched laminates, was capable of reducing the after-impact delaminated area (-7%) and increasing the CAI strength (+1%). The performance of the SMA stitch was not as good as the Kevlar stitch (-19% and +8% respectively), but can be considered satisfying providing future optimization of the stitching design and technology. Moreover, it can be noticed that standard deviations of the experimental results are relatively small for all the laminates tested, which means that the stitching and infusing processes were well-controlled: a paramount condition for any technology improvement. Optical microscopy of the impacted stitched specimens showed good adherence between the TiNi wire and the epoxy matrix. The results from the CAI tests did not allow validating the numerical model since no gradual delamination growth could be observed. For this reason, three-point bending tests will be carried out on impacted stitched laminates, since it is known that the stitching can provide stable delamination growth under bending load [9]. Once the model is validated for stitched laminates, the next step of this work is the optimization of the SMA stitching system (wire diameter, stitch pitch and line spacing).

3.7 Acknowledgements

The authors would like to thank CREPEC (Centre de Recherche en Plasturgie et Composites) for providing logistical support for this project. We are also thankful to Prof. Larry Lessard from McGill University (Montreal, Qc) for giving an access to the drop-weight impact machine, to Mr Harold Hébert from the Industrial Materials Institute (Boucherville, Qc) for allowing the use of the ultrasonic scanner and for providing the technical support, as well as

to Mr Yannick Baril from École de technologie supérieure (Montréal, Qc) for allowing the use of an in-house motion-measurement system.

3.8 References

[1] Greenhalgh, E., & Hiley, M. (2003). The assessment of novel materials and processes for the impact tolerant design of stiffened composite aerospace structures. Composites Part A: Applied Science and Manufacturing, 34(2), 151-161.

[2] Yoshimura, A., Nakao, T., Yashiro, S., et al. (2008). Improvement on out-of-plane impact resistance of CFRP laminates due to through-the-thickness stitching. Composites Part A: Applied Science and Manufacturing, 39(9), 1370-1379.

[3] Aymerich, F., & Priolo, P. (2008). Characterization of fracture modes in stitched and unstitched cross-ply laminates subjected to low-velocity impact and compression after impact loading. International Journal of Impact Engineering, 35(7), 591-608.

[4] Scarponi, C., Perillo, A. M., Cutillo, L., et al. (2007). Advanced TTT composite materials for aeronautical purposes: Compression after impact (CAI) behaviour. Composites Part B: Engineering, 38(2), 258-264.

[5] Byun, J.-H., Song, S.-W., Lee, C.-H., et al. (2006). Impact properties of laminated composites with stitching fibers. Composite Structures, Fifteenth International Conference on Composite Materials - ICCM-15, 76(1-2), 21-27.

[6] Xiaoquan, C., Al-Mansour, A. M., Zhengneng, L., et al. (2005). Compression strength of stitched laminates after low-velocity impact. Journal of Reinforced Plastics and Composites, 24(9), 935-947.

[7] Aymerich, F., Pani, C., & Priolo, P. (2007). Effect of stitching on the low-velocity impact response of $[03/903]_s$ graphite/epoxy laminates. Composites Part A: Applied Science and Manufacturing, 38(4), 1174-1182.

[8] Lau, K.-T., Ling, H.-Y., & Zhou, L.-M. (2004). Low velocity impact on shape memory alloy stitched composite plates. Smart Materials and Structures, 13(2), 364-370.

[9] Jain, L. K., Dransfield, K. A., & Mai, Y.-W. (1998). On the effects of stitching in CFRPs - II. Mode II delamination toughness. Composites Science and Technology, 58(6), 829-837.

CHAPITRE 4

ARTICLE #2 : PREDICTION OF THE PROPAGATION OF IMPACT-INDUCED DELAMINATION IN CARBON/EPOXY LAMINATES

P.-L. Vachon, V. Brailovski, P Terriault

École de technologie supérieure, 1100 rue Notre-Dame Ouest

Montréal (PQ), Canada, H3C 1K3

Ce chapitre a été publié dans « Composite Structures, v95, p. 227-235, 2013 ». DOI : 10.1016/j.compstruct.2012.07.021

4.1 Résumé (français)

L'article présenté dans ce chapitre a été publié dans la revue « Composite Structures ». Il présente l'étude de la propagation du délaminage durant un essai de flexion trois-points quasi-statique. Le modèle numérique développé précédemment est utilisé pour simuler le cas de flexion avec un échantillon pré-endommagé. La validation du modèle se fait par la comparaison des images de propagation du délaminage prédites numériquement, avec celles obtenues à l'aide de l'inspection par ultrasons. Les résultats démontrent la capacité du modèle à représenter de façon fiable le comportement du délaminage engendré par l'impact, lors d'un chargement de flexion.

4.2 Abstract

In this study, a numerical model is developed especially for tracking the propagation of the impact-induced delamination under subsequent flexural loading. The progressive damage modeling technique is used to simulate the quasi-static three-point bending test. The numerical model is validated with experimental bending tests on impacted carbon/epoxy specimens. The specimens contain embedded delamination caused by low velocity impact prior to applying the flexural load. The impact-induced delaminated zone and the

delamination propagation during the bending test are assessed using ultrasonic inspection. The force-displacement response and the delamination propagation obtained from the model and the experiments are compared for validation, with satisfactory results.

Keywords: Polymer-matrix composites, flexural behavior, delamination, low-velocity impact, finite element analysis.

4.3 Introduction

Composite materials are used extensively in aerospace structures because of their high stiffness-to-weight ratio. Among the main issues considered by designers is the possibility of impact by foreign objects during manufacture and maintenance. Indeed, such low-velocity impact loads may initiate invisible damage such as delamination, matrix cracks and fiber breakage, which could lead to a reduction in the stiffness and strength of a structure. It is therefore of primary importance to understand and model the post-impact behavior of composite laminates, especially in terms of the propagation of delamination and the residual mechanical properties.

Traditionally, the study of the residual properties after impact has been strongly oriented towards compression load, perhaps because the properties in compression have been found to be those most affected by impact-related damage [1]. However some recent papers have shown that the flexural modulus and strength are also affected by low velocity impact damage [2-6], in some cases with a linear relation between the relative loss and the impact energy, provided a critical energy threshold was reached. Similar results were reported by Rotem [7], except for graphite/epoxy laminates, which did not experience any loss in their properties until complete failure was induced by the impact. It has also been demonstrated that the distribution of the delamination through the thickness of a specimen can influence the modes of delamination propagation upon flexural loading [6, 8].

In a paper from Amaro et al. [5], the propagation of the delamination during the bending test was noticeable on the force-displacement curves, in the form of a zigzag path, as soon as the delamination started to grow. Similar behavior was reported by Nilsson et al. [8]. In another paper, Amaro et al. [9] simulated experimentally the presence of impact-induced delamination by inserting a Teflon sheet into specimens, to study the effect of the position of the crack through the thickness. The results showed that the worst case (in terms of the maximum load at rupture) was for the delamination located at the mid-thickness of the specimen. The experimental results were verified with a numerical model involving the use of interface elements and a cohesive mixed-mode damage law.

From this review, it appears that the study of the flexural post-impact response has been mainly experimental. Although the numerical results presented in [9] are of great interest, they are restricted to a single delamination in the laminate, one which passes over the complex shape of the real impact-induced delamination. Therefore, the need for a versatile numerical tool allowing realistic representation of the delamination distribution in a laminate is still present. The goal of this work is to present a numerical model that allows predicting the post-impact delamination propagation under flexural loading. The overall shape and distribution of the impact-induced delamination, as measured by ultrasonic inspection, is modeled. Three damage modes are considered in the model: matrix cracking, fiber rupture and delamination. The model was validated with experimental testing and ultrasonic inspection for tracking the delamination propagation under the bending load. The carbon/epoxy specimens were submitted to low-velocity impact tests to generate embedded delamination. The comparison between the delamination propagations obtained experimentally and numerically is presented and discussed.

4.4 Experimentations

4.4.1 Specimen Preparation

Large rectangular panels were made of 16 plies of uniaxial carbon fabric (JB Martin) stacked in a $[45/0/-45/90]_{2s}$ layout. The panels were vacuum infused with epoxy resin (Ren Infusion 8604 Epoxy, Freeman Mfg. and Supply). After curing, rectangular specimens were cut from the panels with a diamond saw blade, and the specimens were then machined to the final dimensions (150 mm x 100 mm) using a diamond-coated endmill. The thickness of the specimens after curing was 4.8 mm and the fiber content was 62%. An industrial immersion ultrasonic scanner (Tecscan Systems, Canada) was used in pulse-echo mode for quality control of the specimens prior to testing and for delamination measurements. The scanner is controlled by the TecView UT software and allows viewing B-Scans and C-Scans simultaneously. The frequency and diameter of the transducer were 5 MHz and 0.375 in, respectively. No delamination was detected prior to impact testing.

4.4.2 Low-Velocity Impact Testing

All specimens were impacted at their center with an energy level of 1 J/mm (normalized with the thickness). The specimens were impacted on a custom-made impact machine equipped with a pneumatic anti-rebound system (McGill University). The impactor head was equipped with a spherical striker of 12.5 mm diameter; the total mass of the head was 8.2 kg. The specimens were maintained on the base plate by rubber clamps at each corner, in accordance with ASTM D7136. Machined in the base plate was a 125 mm x 75 mm rectangular window to allow deformation of the specimens during impact. The velocity of the impactor head just prior to impact was measured using a high speed camera (Fastec Troubleshooter HRMS, Fastec Imaging, California). In all cases, the measured impact velocity was around 1 m/s. The specimens were then inspected by ultrasonic imaging.

4.4.3 Ultrasonic Imaging

The delamination state of the specimens in the in-plane and through-thickness directions was assessed using respectively the C-scan and the B-scan capabilities of TecView UT software. The B-Scan images were reconstructed from two C-scan data files, one for each side of the impacted specimens. Figure 4.1a shows an example of a typical reconstructed B-scan image. The parameters used for the ultrasonic inspection induced a small zone of saturated signal at each surface, in which no measurement could be performed.

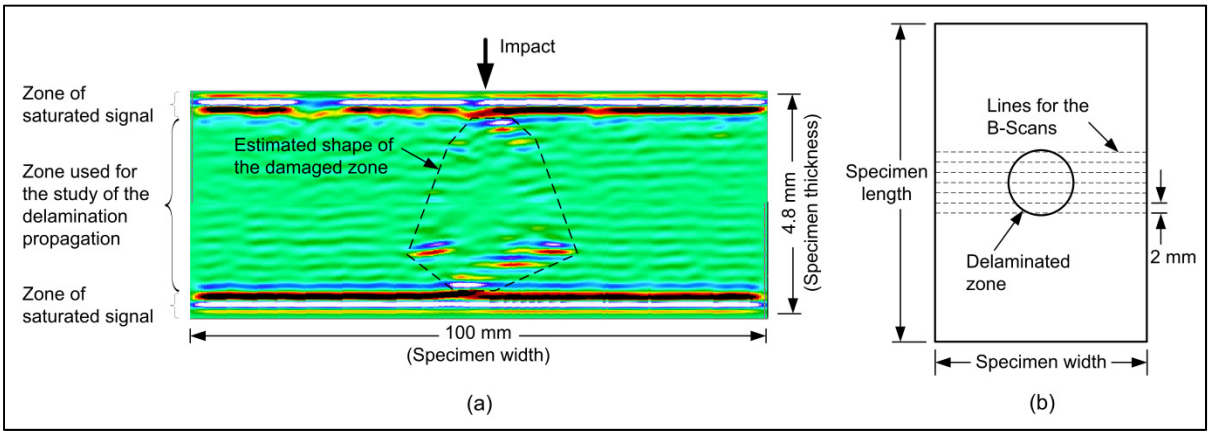

Figure 4.1 a) Example of a B-Scan image from an impacted specimen; b) Schematic of a C-scan image containing a delaminated zone, along with the lines for the B-Scans

The total volume of the damaged zone was reconstructed by taking B-Scan images at every 2 mm along the length of each specimen. A schematic representation of a C-Scan image is shown in Figure 4.1b, along with the B-Scan lines crossing the damaged zone.

4.4.4 Bending after Impact Testing

The bending after impact tests were carried out on an MTS Alliance RF 200 machine equipped with a 200 kN load cell. A three-point bending fixture was used, as shown schematically in Figure 4.2a. The ASTM D7264 standard was followed, except for the span-to-thickness ratio (20 instead of 32) and the specimen width (100 mm instead of 13 mm). The

cylindrical supports and loading nose were 6.35 mm in diameter and the support span was 100 mm. The displacement rate was 1 mm/min. To measure the progression of the delamination with the ultrasonic inspection, some specimens were loaded up to failure and others were loaded up to a certain displacement. A different specimen was used for each of these interrupted bending tests. The impacted face was placed on the tension side, in order to promote the progression of delamination and buckling of the delaminated plies, as observed in [8]. The behavior of the specimens during bending was captured using two video cameras (GRAS-20S4M-C black-and-white cameras, Point Grey Research, Canada) and the Labview program (Figure 4.2b). The apparition and propagation of the delamination cracks at the free edges could thus be monitored.

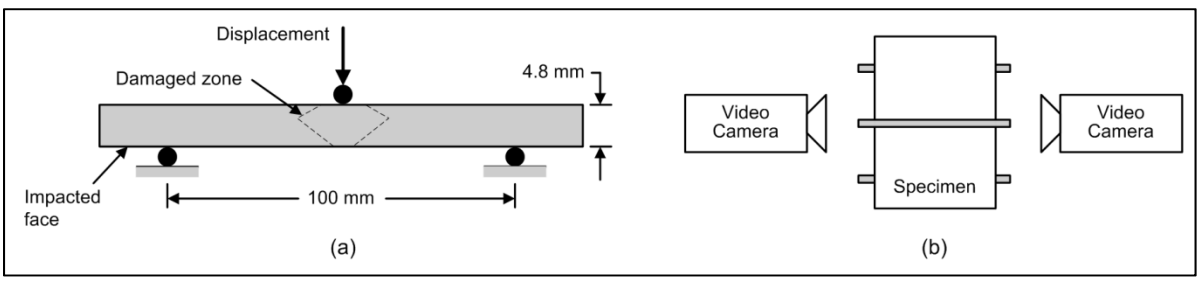

Figure 4.2 Schematic of: a) the three-point bending test; b) the disposition of the two video cameras

4.5 Finite Element Model

The numerical model was developed on the ANSYS 13 commercial finite element software. It was adapted from [10] to simulate the case of a plate under three-point bending loads. To reduce the computational time, only the central zone of the plate was meshed with solid elements, while shell elements were used for the ends, as shown in Figure 4.3a. The refined zone was modeled using 20-node Solid186 layered elements, and each ply was modeled with two elements in the thickness direction. Both ends of the plate were meshed with 8-node Shell281 layered elements. The dimensions of the plate were 150 mm x 100 mm x 4.8 mm and the 16-ply layout was $[45/0/-45/90]_{2s}$. About 360000 solid elements and 5000 shell elements were used in this model. The mesh of the refined zone is shown in Figure 4.3b. The

three-point bending load was simulated by applying the following boundary conditions: the z-displacements were blocked on the two lines representing the supports, and the x- and y-displacements as well as the z-rotation were blocked on one node of one support line to prevent rigid body motion. The z-displacement was applied at the top surface, mid-length of the plate, on two parallel lines of nodes in the central zone inside the grid mesh, and on one line of nodes outside the grid mesh, as shown in Figure 4.3. The two parallel lines were distanced by 0.25 mm. This allowed sharing the load and avoiding stress concentration in the region of higher interest (the impacted region, enclosed into the grid mesh), while lightening the mesh outside this zone. The maximum face length of the solid elements was fixed at 10 times the thickness of the elements. As it can be seen in Figure 4.3b, the grid mesh was refined in the vicinity of each grid corners, where the element face length was fixed at 0.25 mm. The automatic tool for mesh checking was enabled during the mesh generation and before each nonlinear solution. The warning limits for the mesh check were kept at the default values of the software: aspect ratio: 20; parallel deviation of opposite edges: 100°; maximum corner angle: 165°; Jacobian ratio: 30; Warping factor: 0.4.

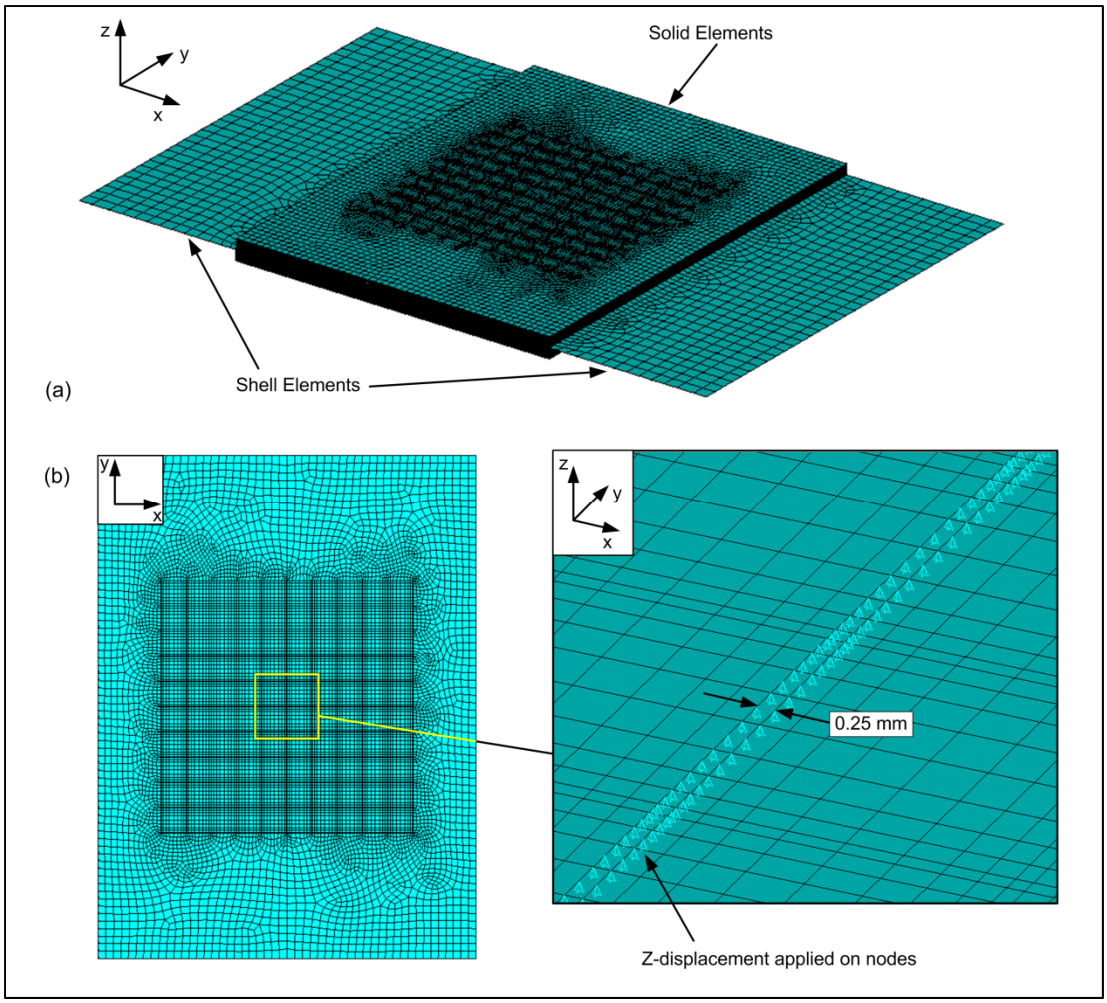

Figure 4.3 a) Complete mesh; b) Refined solid mesh

The calculation algorithm was based on the progressive damage modeling technique developed by Shokrieh et al. [11]. It is presented in Figure 4.4. The strength of this algorithm lies in its capacity of predicting the delamination progression with acceptable level of accuracy, using only some basic engineering parameters as inputs (Young's moduli and strengths of the composite material in tension, compression and shear). In addition, the exclusive presence of solid and shell elements in the present model eliminates some source of convergence issues that may arise when cohesive elements are used for the modeling of the delamination progression [12]. The algorithm was previously validated using a simple plate in tension and the results are presented in [10]. The displacement applied at the mid-length of the plate was increased by small increments, solving at each step and verifying the rupture

criteria for all the solid elements. Three failure criteria were considered in the present study: matrix failure, fiber failure and delamination. These are presented in Table 4.1a, along with their respective degradation factors [13]; σ, S, T and C stand for Stress, Strength, Tension and Compression, respectively, while E represents both modulus and strength. Following these rules, the appropriate mechanical properties of the broken elements were degraded. It is noted that the degradation factors for both matrix and fiber cracking depend on the sign of the stress (tensile or compressive), following the principle that the cracked material under compressive loading can still carry some load, unlike that under tensile loading [14]. This rule was used successfully by Camanho and Matthews [15] and Tserpes et al. [13]. This procedure allowed the delamination propagation to be tracked throughout the simulation of the bending test. Large displacements were considered in the geometrically nonlinear analysis.

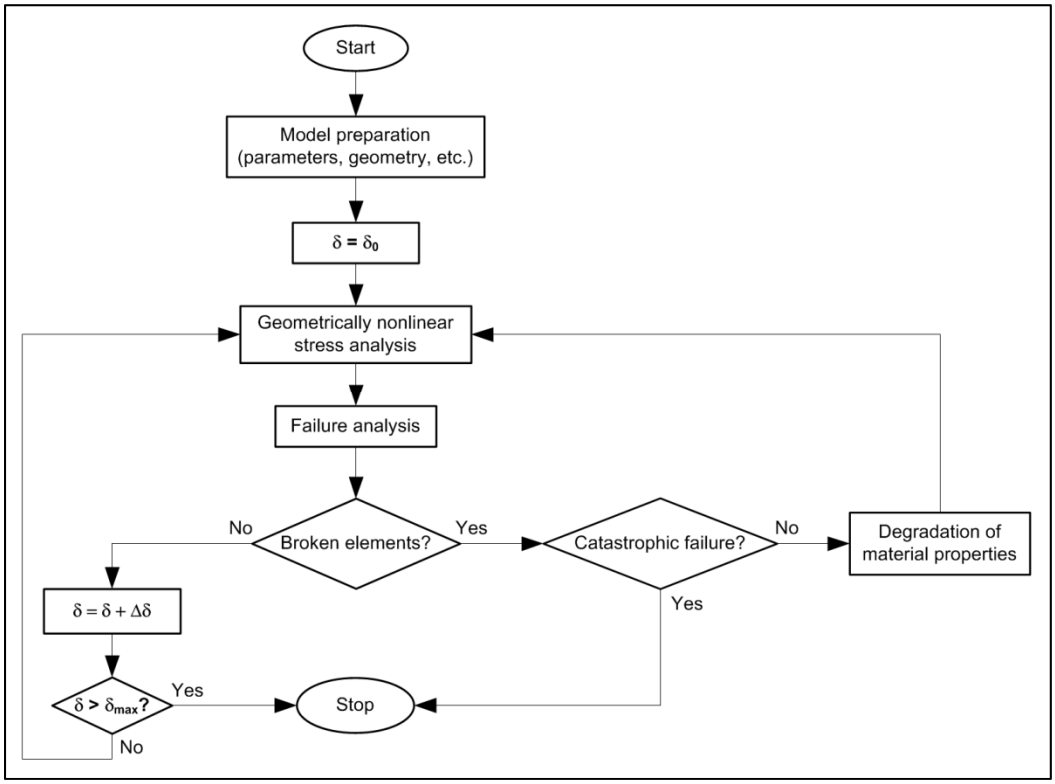

Figure 4.4 Algorithm of the numerical model

Table 4.1 a) Failure criteria and degradation factors; b) Mechanical properties of the carbon/epoxy material (in parentheses, properties assessed from the literature; otherwise as measured)

(a)	Failure Criteria		Degradation Factors
Matrix Tensile Failure	$\left(\frac{\sigma_{yy}^{T}}{S_{yy}^{T}}\right)^2+\left(\frac{\sigma_{xy}}{S_{xy}}\right)^2+\left(\frac{\sigma_{yz}}{S_{yz}}\right)^2 \geq 1$	$\rightarrow$	$E^d_{yy} = 0.2*E_{yy}$ $E^d_{xy} = 0.2*E_{xy}$ $E^d_{yz} = 0.2*E_{yz}$
Matrix Compr. Failure	$\left(\frac{\sigma_{yy}^{C}}{S_{yy}^{C}}\right)^2+\left(\frac{\sigma_{xy}}{S_{xy}}\right)^2+\left(\frac{\sigma_{yz}}{S_{yz}}\right)^2 \geq 1$	$\rightarrow$	$E^d_{yy} = 0.4*E_{yy}$ $E^d_{xy} = 0.4*E_{xy}$ $E^d_{yz} = 0.4*E_{yz}$
Fibre Failure	$\left(\frac{\sigma_{xx}^{T,C}}{S_{xx}^{T,C}}\right) \geq 1$	$\rightarrow$	$E^d_{xx} = 0.07*E_{xx}$ (T) $E^d_{xx} = 0.14*E_{xx}$ (C)
Delamination Failure	$\left(\frac{\sigma_{zz}^{T,C}}{S_{zz}^{T,C}}\right)^2+\left(\frac{\sigma_{xz}}{S_{xz}}\right)^2+\left(\frac{\sigma_{yz}}{S_{yz}}\right)^2 \geq 1$	$\rightarrow$	$E^d_{zz} = 0.1*E_{zz}$ $E^d_{xz} = 0.1*E_{xz}$ $E^d_{yz} = 0.1*E_{yz}$

(b)	Modulus
E_{xx}:	128.3 GPa
E_{yy}, E_{zz}:	6.95 GPa
G_{xy}, G_{xz} (G_{yz}):	2.88 (2.44) GPa
ν_{xy}, ν_{xz} (ν_{yz}):	0.3 (0.42)

Strength	
S_{xT} (S_{xC}):	2000 (1200) MPa
S_{yT}, S_{zT}:	14 MPa
S_{yC}, S_{zC}:	56 MPa
S_{xy}, S_{xz}, S_{yz}:	34 MPa

The mechanical properties of the unidirectional carbon/epoxy laminate are reported in Table 4.1b, with "x" being the fiber direction. The in-plane tensile and shear properties were determined experimentally in the composite laboratory at the Ecole de technologie superieure (Montreal, Canada), according to the appropriate ASTM standards: D3039 (tensile) and D3518 (shear). The compressive strengths were assumed to be in accordance with what could be found in the literature (e.g. [16]). The Young's modulus and Poisson's coefficient in the "yz" direction were fixed following the assumption of transverse isotropy. All the mechanical properties in the model were assumed to be linear up to the rupture.

In all the modeling cases, a schematized pre-damaged zone was considered in order to simulate the effect of low-velocity impact. The shape of this zone was in accordance with the B-scan observations and the dimensions were as shown in Figure 4.5. The mechanical properties of the solid elements confined in this zone were degraded according to the factors in Table 4.1a, prior to launching the numerical algorithm simulating three-point bending.

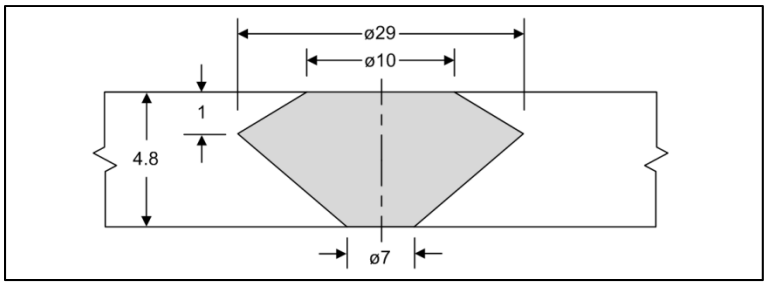

Figure 4.5 Typical shape and dimensions of a delaminated zone as measured by ultrasonic inspection (dimensions in mm)

4.6 Results and Discussion

4.6.1 Bending after Impact Testing

The effect of low velocity impact on the mechanical properties of a laminate was verified by submitting two specimens to three-point bending tests: one specimen impacted and one unimpacted. The two force-displacement curves obtained are shown in Figure 4.6, along with a C-Scan image of the impact-induced delamination. The C-Scan image represents a picture of the in-plane delaminated region, through-the-thickness of the specimen. From this figure, it is possible to identify three distinct zones in the bending response of the specimens: Zone I- a linear response with no noticeable loss of rigidity; Zone II- a gradual loss of stiffness (change in the curves' slope) until a "plateau" is reached; and Zone III- a brutal drop of the force applied to the specimens and finally, a gradual decrease of the force until the final rupture of the specimen.

It is clear from Figure 4.6 that the selected impact energy (1J/mm of thickness) affected the performance of the laminate, since the energy that was necessary to induce the final rupture of the specimen was lower for the impacted specimen. Although the Young's modulus did not appear to be affected by the impact damage, the onset of the plateau in the impacted specimen's curve appeared at a slightly lower force than it did for the undamaged specimen. Therefore, it can be stated that the selected impact energy did not have a large detrimental

effect on the laminate's mechanical properties, perhaps because of the small dimension of the damaged zone in comparison to the width of the specimen. Nevertheless, the impact-induced delamination played a role in the change of the flexural behavior of the plate, probably by promoting some damage modes that were not present in the undamaged specimen. The present study is thus devoted to the investigation and modeling of the impact damage under flexural load, especially in zones I and II.

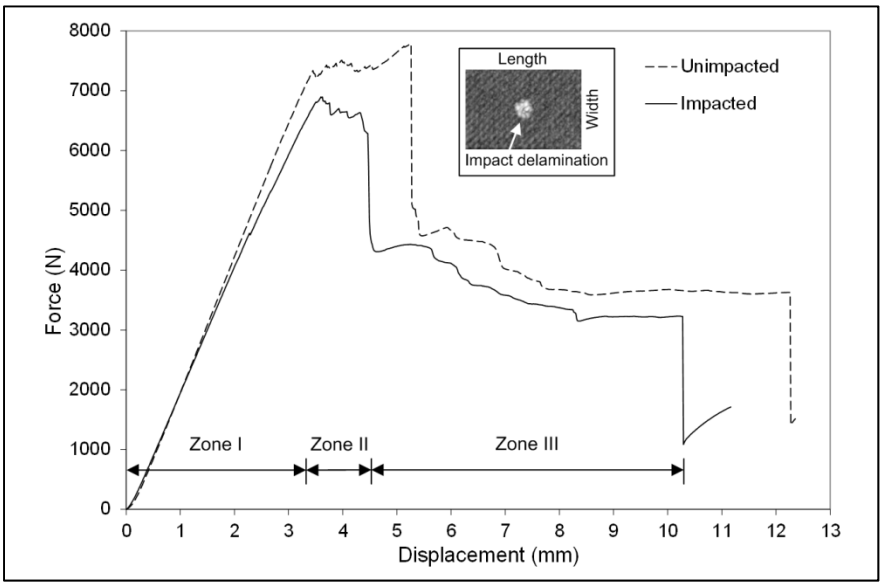

Figure 4.6 Three-point bending response of unimpacted and impacted specimens showing the effect of the impact damage on the flexural behavior and the three zones of the force-displacement curves

Study of the videos recorded during the tests showed that the drastic drop in the force-displacement curves (end of zone II) was coincident with the sudden apparition of delamination cracks at the free edge of the specimens in the vicinity of the loading nose, accompanied by fiber breakage at the upper ply. An example of these cracks is shown in Figure 4.7a. The delamination cracks appeared at the upper interfaces, which are under compression load. Next, the lower interfaces were delaminated in the mid-length section and this delamination extended longitudinally towards either one or both supports, as illustrated

in Figure 4.7b. The final rupture of the specimens consisted of the complete delamination of the lowest interface, beyond one of the supports (Figure 4.7c).

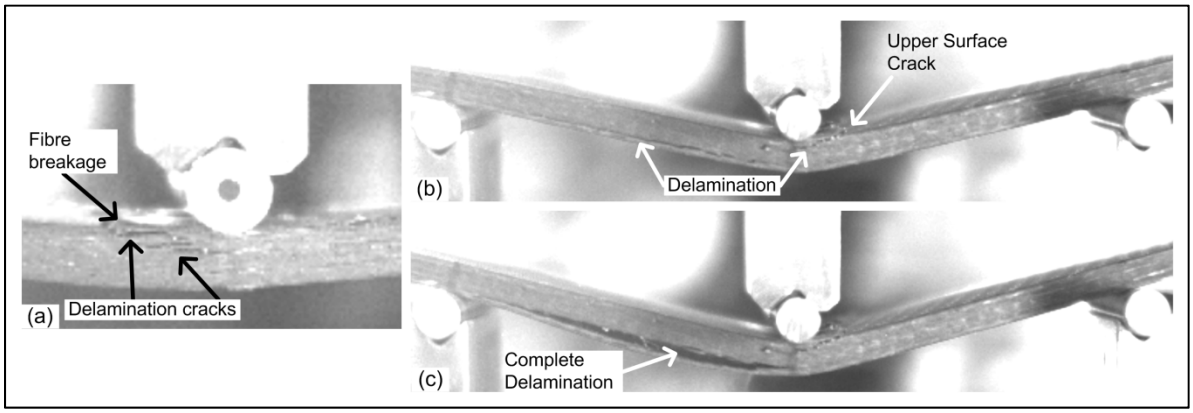

Figure 4.7 a) Delamination cracks at the specimen's free edge and fiber breakage at the upper surface; b) Progression of the lower ply delamination; c) Final rupture of the lower ply

C-Scan imaging was used to characterize the delamination progression during the bending tests. Six specimens were tested up to a particular displacement and then ultrasonically inspected to detect the progression of delamination. The C-Scan results are presented in Figure 4.8. In each C-Scan image, a delaminated zone is represented by a blue-colored area. Propagation through the specimen's width will be referred to as lateral propagation while propagation through the specimen's length will be referred to as longitudinal propagation.

In the two first C-Scan images (a and b), which correspond to zone I of the force-displacement curves in Figure 4.6, no noticeable progression of the delamination could be measured. The comparison of the before- and after-bending B-Scan images for those two specimens confirmed this observation. In image c, the delamination starts to spread laterally under the loading nose, from the impact-induced delamination towards the free edges of the specimen. This delamination state corresponds to the end of the linear part of the force-displacement curve, and thus the specimen enters zone II of the curve. Image d shows that delamination has progressed towards the free edges and seems to have reached them, while not being damaging enough to move on to zone III of the force-displacement curve. In image e, the force applied on the specimen has dropped drastically, thus indicating a loss of

integrity in the structure. The delamination at that point is equally distributed all over the specimen's width, entirely covering the circular-shaped impact-induced delamination. This introduces the specimen to zone III. The last image (f) shows the longitudinal propagation of the delamination while the applied force decreases gradually. The propagation seems to be promoted at the free edge rather than in the middle of the plate. From a structural point of view, the sudden drop in the measured force at the end of zone II can be considered as a failure of the specimen, since its integrity has been strongly corrupted. For this reason, only zones I and II will be investigated in detail. Note that in addition to C-Scan images, B-Scan images were also taken to investigate the propagation of the delamination through the thickness. They will be presented in Figure 4.11.

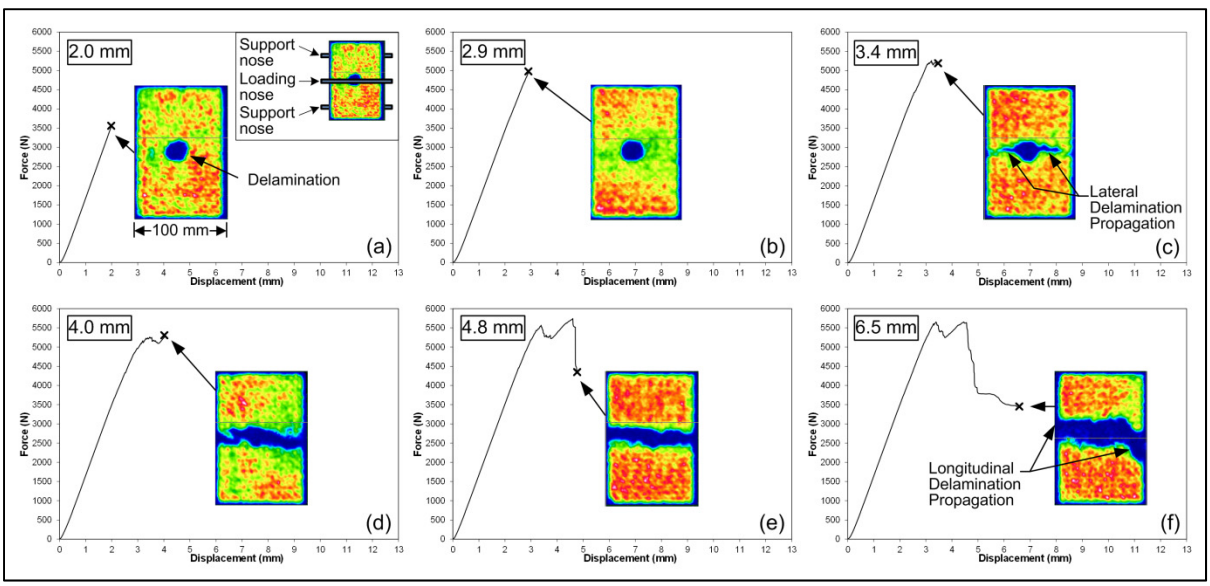

Figure 4.8 C-Scan images of the propagation of delamination at six displacement levels in three-point flexure tests

4.6.2 Finite Element Modeling

The bending response of the impacted plate was simulated, and the progression of the delamination was calculated incrementally for each 0.1 mm step in deflection. Figure 4.9 shows the state of delamination (in red) from 0 mm to 3.3 mm of displacement, at the mid-

length of the plate. The color scale represents the value of the delamination failure criterion as presented in Table 4.1a, running from blue (low stress level) to red (delamination failure). Only the elements whose failure criteria are greater or equal to 1 have their mechanical properties degraded (in red in Figure 4.9). From this figure, it is clear that the delamination extends initially in the upper interfaces from the pre-damaged zone towards the free edges. From 2.0 mm onwards, the delamination propagates also to the adjacent interfaces (i.e. through the thickness) and appears at the lower interfaces.

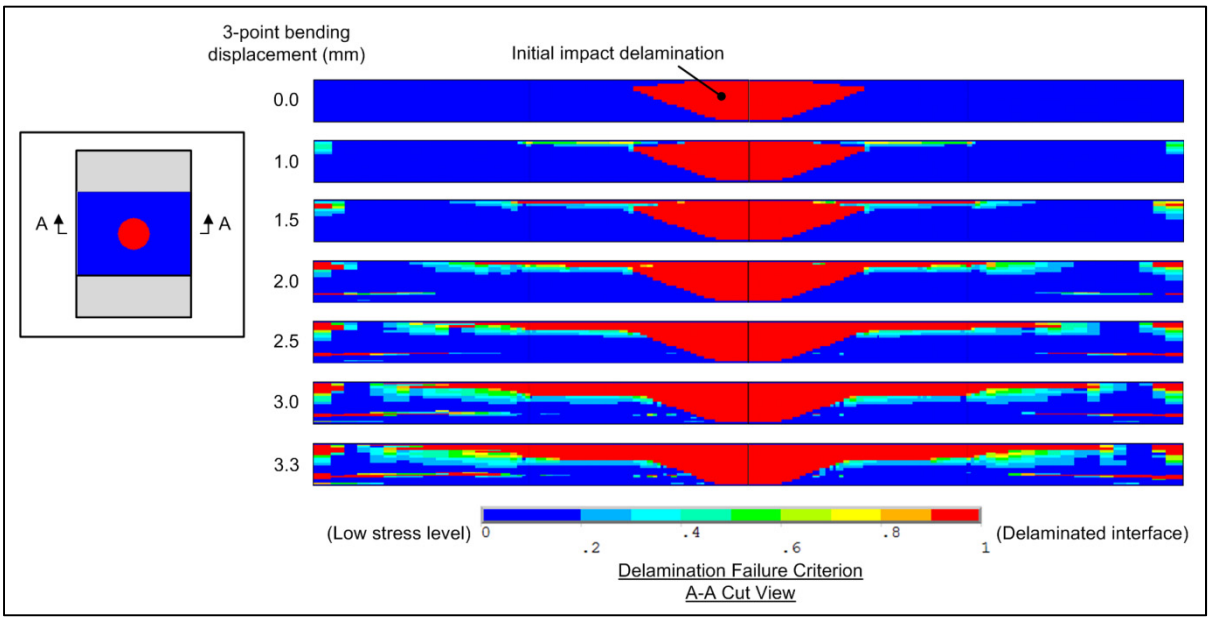

Figure 4.9 Progression of the delamination as obtained from the numerical model

It can be noted that in the model, the first appearance of delamination propagation occurs at 1 mm of displacement, which is much lower than what could be observed from the ultrasonic observations (Figure 4.8). Indeed, according to Figure 4.8, no propagation was noticeable until a displacement of around 3 mm. This numerical result suggests that damage propagation may effectively exist in real specimens at low displacement level, while remaining undetectable with the present ultrasonic settings. The graph of Figure 4.10 illustrates this point. In this figure, there is a noticeable increase of the propagation rate of the delamination at a displacement level of around 2 mm, which is not clearly reflected in the force-

displacement response of the laminate. This knee in the delamination curve corresponds to the apparition of the delamination at the free edges and at the lower interfaces, as it was noticed in the experiments. Therefore the force-displacement response might not be a reliable indicator of the state of damage in the laminate, in the case of three-point bending load.

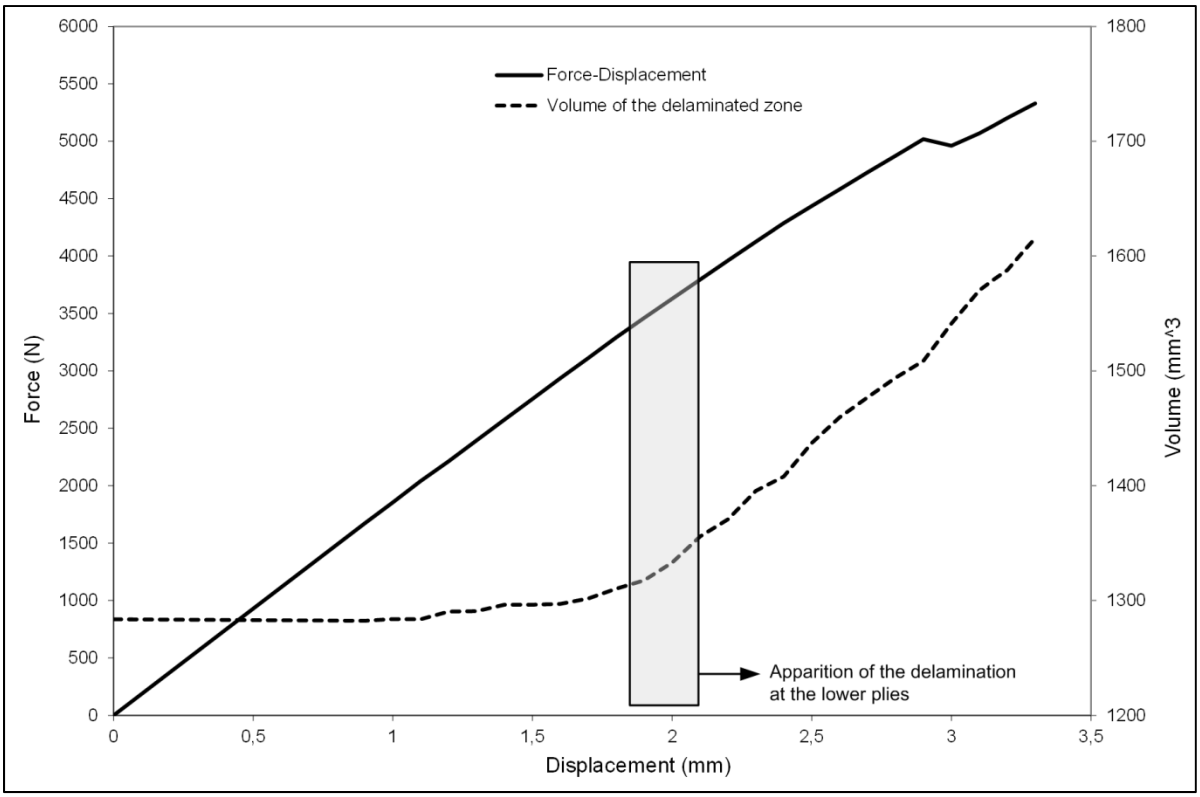

Figure 4.10 Comparison between the Force-Displacement response and the accumulation of delamination damage as obtained from the numerical model

The numerical results for the delamination propagation are compared to the experimental results in Figure 4.11, at four displacement levels. Each image in this figure shows a top view of the plate (left) as well as a cut view at the mid-length of the plate (right), from both the ultrasonic images and the FE model. The predicted by the model contour of the delaminated region (dashed line) is superimposed on the ultrasonic images. Even though, according to this figure, the model predicts a more advanced state of delamination than could be measured with the ultrasonics (Figure 4.11a, b and c), both the simulated delamination propagation and its through-thickness distribution are quite realistic. In Figure 4.11d, the B-Scan image

indicates that the delamination propagates through the thickness to the adjacent interfaces, just as predicted by the model. The force-displacement response from the model presents a slight gradual degradation of the stiffness due to the propagation of matrix cracks and delamination, even though the experimentally observed zigzag path, normally attributed to fiber breakage, could not be completely represented. All along the simulation, the dimension of the delaminated region remains relatively small in comparison to the cross section of the plate. This can explain why the delamination propagation does not have a drastic effect on the predicted force-displacement curve, until a certain level of damage is reached.

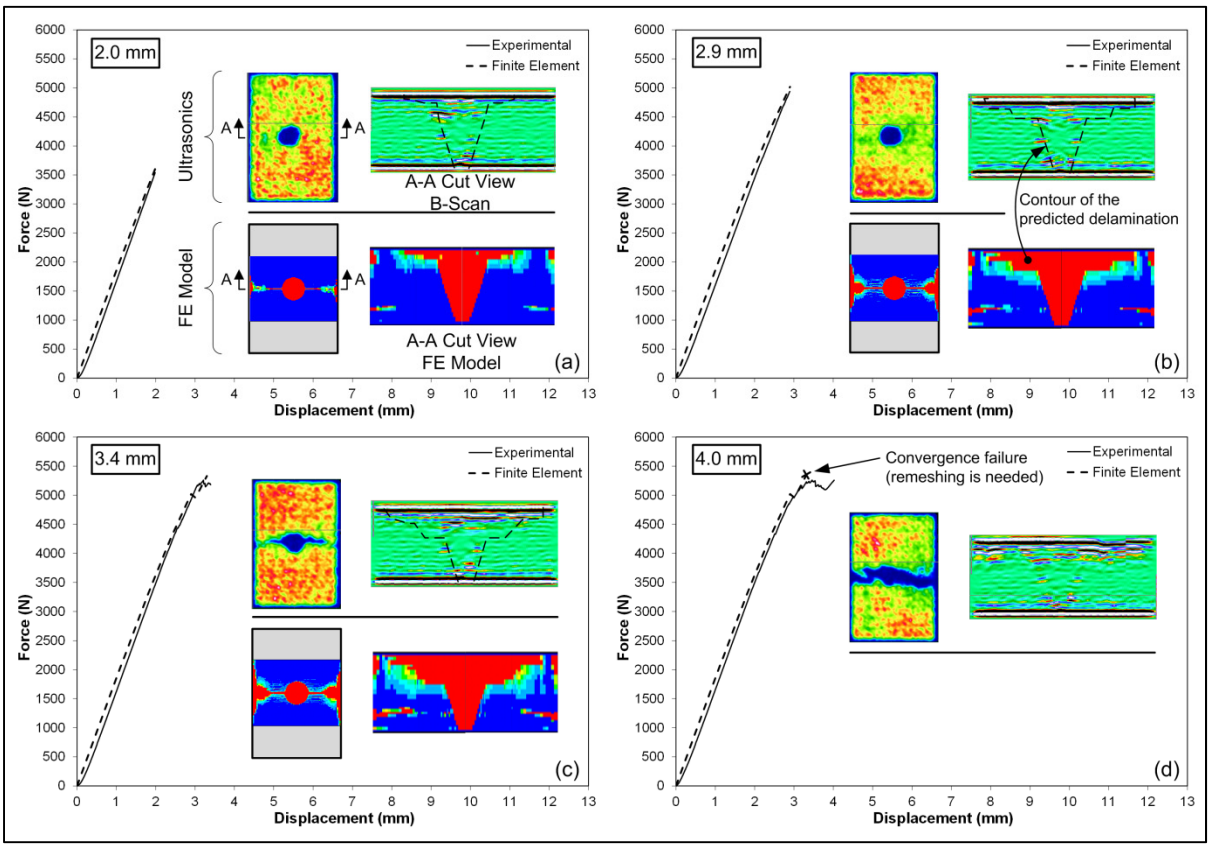

Figure 4.11 Force-displacement response and delamination images from numerical modeling and experimental tests

The model's convergence stopped at 3.3 mm as some solid elements became highly distorted due to their degraded mechanical properties, thus explaining why there is no image from the model in Figure 4.11d. To overcome this limitation, the mesh should be refined, but the

computer and time resources would then become huge and impractical. Since the scope of the present study is oriented towards the modeling of the delamination propagation before the structure collapses (zones I and II, Figure 4.6), the results presented herein are considered quite satisfactory. Therefore it can be stated that the progressive damage algorithm used in this study allows a good representation of the mechanical response of impacted laminates under a three-point bending load, as well as a realistic prediction of the in-plane delamination propagation.

4.7 Conclusions

In this work a numerical model was used for predicting the post-impact behavior and the propagation of delamination in composite laminates under a three-point bending load. The complex shape of the impact-induced delamination was modeled accordingly to the B-Scan measurements, thus allowing realistic representation of the behavior of the impacted laminate. The distribution of the delamination was captured throughout the simulated bending test. The numerical results were compared to ultrasonic images taken at different displacement levels during experimental bending tests. The experimental results showed that the bending behavior of impacted laminates can be broken down into three zones, based on the force-displacement response. The onset of the delamination propagation was detected at the transition between zones I and II with the present ultrasonic settings.

Although no delamination propagation could be detected with ultrasonic imaging during the almost-linear zone I of the tests, the model clearly showed that propagation may occur even at low displacement level, with only a slight influence on the force-displacement curves. This observation demonstrates the usefulness of a numerical approach for understanding the propagation modes of delamination under flexural load. Moreover, the model allowed realistic prediction of the overall propagation path of the delamination for the zones I and II of the bending tests, with the images of the state of delamination being similar to the ultrasonic images.

Considering that the overall delamination behavior was satisfactorily predicted, it can be confirmed that the present model is capable of simulating the propagation and through-thickness distribution of delamination during three-point bending tests. The model is thus confirmed as a useful tool for assessing the post-impact flexural behavior of composite laminates.

Because of its versatility, this model might be helpful for studying the propagation mechanisms for complex delamination geometries and various stacking sequences or laminate dimensions, for instance. It might serve as well as a useful tool for developing manufacturing techniques to improve the performance of impacted composite laminates. The authors will use this model in a subsequent study on the effect of stitching on the propagation of delamination in impacted composite laminates under flexural loading.

4.8 Acknowledgements

The authors would like to thank CREPEC (Centre de Recherche en Plasturgie et Composites) for providing logistical support for this project. We are also thankful to Prof. Larry Lessard from McGill University (Montreal, Qc) for access to McGill's drop-weight impact machine and to Mr Harold Hébert from the Industrial Materials Institute (Boucherville, Qc) for allowing the use of their ultrasonic scanner and for providing technical support.

4.9 References

[1] Abrate S. Impact on composite structures. Cambridge, UK: Cambridge University Press, 1998.

[2] Santiuste C, Sanchez-Saez S, Barbero E. Residual flexural strength after low-velocity impact in glass/polyester composite beams. Composite Structures. 2010;92:25-30.

[3] He C, Li Y, Zhang Z, Sun Z. Impact damage modes and residual flexural properties of composites beam. Journal of Reinforced Plastics and Composites. 2008;27:1163-75.

[4] Zhang ZY, Richardson MOW. Low velocity impact induced damage evaluation and its effect on the residual flexural properties of pultruded GRP composites. Composite Structures. 2007;81:195-201.

[5] Amaro AM, Reis PNB, Moura MFSF. Residual strength after low velocity impact in carbon-epoxy laminates. Materials Science Forum. 2006;514-516:624-8.

[6] Im K-H, Sim J-K, Yang I-Y. Impact damages and residual bending strength of CFRP composite laminates subjected to impact loading. Journal of Mechanical Science and Technology. 1996;10:423-34.

[7] Rotem A. Residual Flexural Strength of FRP Composite Specimens Subjected to Transverse Impact Loading. SAMPE Journal. 1988;24:19-25.

[8] Nilsson S, Bredberg A, Asp LE. Effects of CFRP laminate thickness on bending after impact strength. Plastics, Rubber and Composites. 2009;38:61-6.

[9] Amaro AM, Reis PNB, De Moura MFSF. Delamination effect on bending behaviour in carbon-epoxy composites. Strain. 2011;47:203-8.

[10] Vachon P-L, Brailovski V, Terriault P. Modeling of Delamination Initiation and Propagation in Composite Laminates Under Monotonic Tensile Loading Using the Progressive Damage Modeling Technique. Science and Engineering of Composite Materials. 2009;16:99-114.

[11] Shokrieh MM, Lessard LB. Progressive fatigue damage modeling of composite materials, Part I: Modeling. Journal of Composite Materials. 2000;34:1056-80.

[12] Alfano G, Crisfield MA. Finite element interface models for the delamination analysis of laminated composites: Mechanical and computational issues. International Journal for Numerical Methods in Engineering. 2001;50:1701-36.

[13] Tserpes KI, Labeas G, Papanikos P, Kermanidis T. Strength prediction of bolted joints in graphite/epoxy composite laminates. Composites Part B: Engineering. 2002;33:521-9.

[14] Tan SC, Perez J. Progressive failure of laminated composites with a hole under compressive loading. Journal of Reinforced Plastics and Composites. 1993;12:1043-57.

[15] Camanho PP, Matthews FL. Progressive damage model for mechanically fastened joints in composite laminates. Journal of Composite Materials. 1999;33:2248-80.

[16] Shokrieh MM, Lessard LB. Progressive fatigue damage modeling of composite materials, Part II: Material characterization and model verification. Journal of Composite Materials. 2000;34:1081-116.

CHAPITRE 5

ARTICLE #3 : IMPACT-INDUCED DAMAGE AND DAMAGE PROPAGATION UNDER FLEXURAL LOAD IN TINI AND KEVLAR-STITCHED CARBON/EPOXY LAMINATES

P.-L. Vachon, V. Brailovski, P. Terriault

École de technologie supérieure, 1100 rue Notre-Dame Ouest

Montréal (PQ), Canada, H3C 1K3

Ce chapitre présente un article soumis à « Composite Structures » en août 2012. Numéro de la soumission : COST-D-12-00837R1

5.1 Résumé (français)

L'article présenté dans ce chapitre a été soumis pour publication dans la revue « Composite Structures ». Il présente une étude des performances des composites renforcés de TiNi et de Kevlar lors du chargement d'impact, suivi d'un chargement en flexion trois-points. Les résultats sont comparés à ceux obtenus pour des échantillons non renforcés. La performance est mesurée en termes de la quantité d'énergie de déformation qui est nécessaire pour créer un volume unitaire de matériau endommagé (G_v, J/mm^3). Les résultats expérimentaux ont montré que les renforts de Kevlar offraient une meilleure performance lors de l'impact que ceux en TiNi, alors que l'inverse se produit lors de l'essai de flexion, où les mécanismes de propagation graduelle de l'endommagement sont actifs. De plus, l'étude numérique du comportement interne de la structure lors du chargement de flexion a montré qu'il existe des différences entre les deux types de renforts, pour ce qui est des schémas de propagation interlaminaire de l'endommagement.

5.2 Abstract

This paper presents a study of the effect of stitched reinforcements on impact-induced damage and damage propagation under flexural load. TiNi and Kevlar threads were used as

the superelastic element and the reference thread, respectively. Unstitched carbon/epoxy laminates were also produced. Embedded damage (matrix cracks, fiber rupture and delamination) was induced by low velocity impact testing. The performance of the unstitched and stitched specimens was assessed in terms of the energy per unit volume of damage created during impact testing, and the energy to failure of the impacted specimens during their three-point bending testing. A finite element model was used for simulating the propagation of damage, and particularly delamination, in stitched and unstitched structures during the bending test, and, depending on the mechanical properties of the stitching threads, different propagation schemes were predicted with this model.

Keywords: Polymer-matrix composites, stitching, flexural behavior, delamination, low velocity impact, finite element analysis.

5.3 Introduction

Laminated composite materials are used extensively in aerospace structures because of their high stiffness-to-weight ratio. Such materials were shown to be sensitive to low velocity impact damage, since the resulting delamination may significantly alter the stiffness and strength of the structures [1]. Since the resistance to the delamination onset and propagation is closely related to the out-of-plane properties of the laminates, several technological solutions have been proposed with the aim of improving the through-thickness properties of laminated composites, such as 3D weaving, braiding, stitching and Z-pinning. Among those, the stitching technique was found to be especially promising for future aerospace structures [2].

In recent literature, numerous studies have been devoted to understanding the behaviour of stitched composite laminates under low-velocity impact and post-impact loading. This reinforcement technique has proven its capability in reducing impact-induced delamination as well as in improving the Compression After Impact (CAI) strength [3-7]. Moreover, the presence of stitched reinforcement allows the delamination toughness of modes I and II to be

improved, as well as providing stable crack propagation [8-10]. In general the performance of the stitching system was found to be proportional to the stiffness of the stitch material and the stitching density [6, 8]. The stitching pattern also played a significant role in the delamination toughness. Indeed it was observed that the higher the stitch density at the crack front, the higher the delamination toughness in mode I. Even though no such influence was detected in mode II [11, 12], the versatility of the stitching technique may become an interesting tool for optimizing the overall performance of the system. It was also demonstrated that stitching delays or even stops the free-edge delamination propagation in laminates under tensile loading [13, 14].

Whereas Kevlar stitching thread has been used extensively in research, only a few papers have been published dealing with the use of shape memory alloy (SMA) wire as the stitching thread. In [15], superelastic TiNi wire was inserted into a glass/epoxy plate to evaluate its response to low-velocity impact loading. The authors found that the number of translaminar cracks was reduced by the stitching due to the damping effect of the superelastic wires. Moreover, theoretical analysis showed that the delamination energy was reduced when compared to the unstitched plates. The impact-induced delaminated area and the CAI strength were evaluated for unstitched, Kevlar- and superelastic TiNi-stitched carbon/epoxy laminates in [16]. That study showed that the Kevlar thread allowed a 19% reduction whereas TiNi thread allowed a 7% reduction of the delaminated area compared to the unstitched laminates, while the CAI strength remained relatively unchanged. According to these observations, it can be supposed that the use of stitching combined with a superelastic thread would be beneficial during the service life of impacted composite structures, provided a broader knowledge-base is obtained.

In the present study, the authors investigate the level of the impact-induced delamination and post-impact flexural behavior of TiNi-stitched carbon/epoxy laminates. Unstitched and Kevlar-stitched specimens are also used for comparison. The specimens are subjected to low velocity impact loading prior to being tested under a three-point bending load. The performance of the different structures is assessed in terms of: 1) the delaminated area after

impact, 2) the propagation of the impact-induced delamination under the flexural load, and 3) the bending energy up to the rupture of the specimens. The ultrasonic inspection method is used for evaluating the dimensions and shape of the post-impact damaged zone to be represented in the model. A 3-D finite element model is used for predicting the propagation of the delamination around the stitched reinforcements during post-impact bending. Experimental and numerical results are presented and discussed.

5.4 Experimentations

5.4.1 Specimen Preparation

Three different types of carbon/epoxy specimens were compared: unstitched, Kevlar- and TiNi-stitched specimens. All of the specimens were cut from large panels, with each panel including specimens from all three types, disposed randomly. The dimensions of the specimens and the stacking sequence were chosen in accordance with the ASTM D7136 standard covering the testing of polymer-matrix composites under drop-weight impact loading. The 4.8 mm-thick panels were made of 16 plies of uniaxial carbon fabric (JB Martin) stacked in a $[45/0/-45/90]_{2s}$ layout. Prior to the resin infusion, the panels were stitched using an industrial sewing machine (Juki LU-563) with either Kevlar thread (Tex 40, 0.2 mm dia., American & Efird) or TiNi thread (0.1 mm dia., Memry). The modified lock stitch pattern was adopted (Fig. 5.1a) using Kevlar thread as the needle thread in all cases. The tensioning device of the sewing machine was set at about 4 N. The stitching pitch and the distance between stitch lines were both set at 5 mm. Note that only a square region of 50 mm x 50 mm was stitched, centered in the plane of the 150 mm x 100 mm specimens, as shown in Fig. 5.1b. Prior to stitching, the as-drawn TiNi thread was heat treated at 350°C for 15 minutes to confer the superelastic properties. The thread was then cleaned in a $HF-HNO_3$ solution to remove the oxide layer. Fig. 5.2 shows the tensile curves obtained for both the Kevlar and the TiNi threads. The tensile tests were carried out on an Enduratec ELF 3200 tensile machine (Bose) at 0.05 mm/s (Kevlar) and 0.1 mm/s (TiNi) displacement rates.

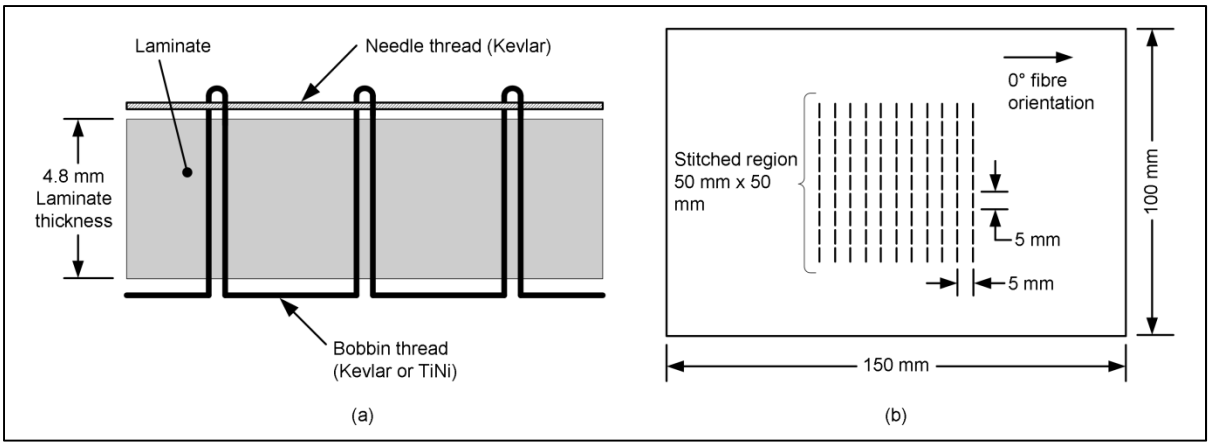

Figure 5.1 a) Modified lock stitch; b) Schematic of the stitched specimens

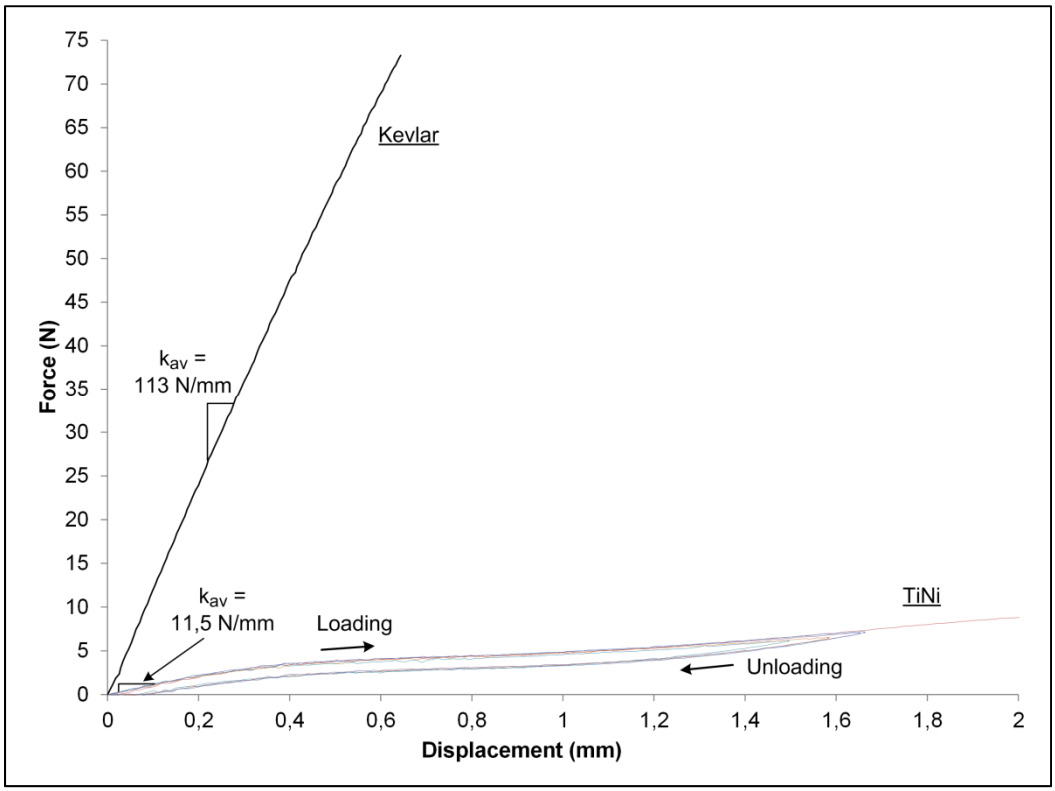

Figure 5.2 Tensile curves obtained for both Kevlar and superelastic TiNi stitching threads

After stitching, the panels were vacuum infused with epoxy resin (Ren Infusion 8604 Epoxy, Freeman Mfg. and Supply). The rectangular specimens were cut from the cured panels with a

diamond saw blade, and then machined to the final dimensions (150 mm x 100 mm) using a diamond-coated end mill. The thickness of the specimens after curing was 4.8 mm and the fiber content was 62%. An example of Kevlar- and TiNi-stitched specimens is presented in Fig. 5.3. An industrial immersion ultrasonic scanner (Tecscan Systems, Canada) was used for quality control of the specimens prior to testing and for delamination measurements. The scanner is controlled by TecView UT software and allows the simultaneous viewing of A-Scans, B-Scans and C-Scans. The frequency and diameter of the transducer were 5 MHz and 0.375 in, respectively. No delamination was detected in any specimens prior to impact testing.

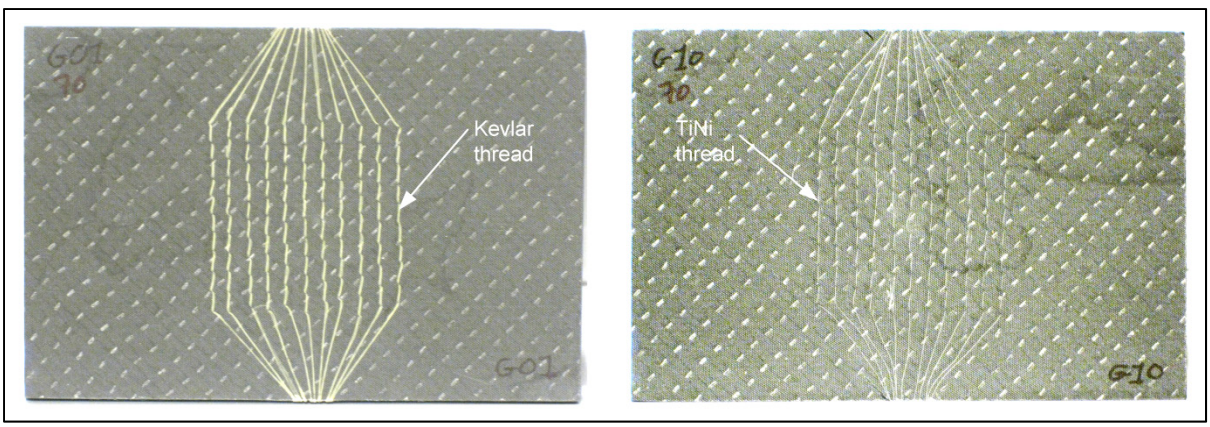

Figure 5.3 Kevlar- and TiNi-stitched specimens

5.4.2 Low Velocity Impact Testing

Five (5) specimens of each type were impacted at their center with an energy level of 1 J/mm (normalized with the thickness), in accordance with other publications (e.g. [3, 4]). The specimens were impacted on a custom-made impact machine equipped with a pneumatic anti-rebound system (McGill University). The impactor head was equipped with a spherical striker of 12.5 mm diameter; the total mass of the head was 8.2 kg. The specimens were maintained on the base plate by rubber clamps at each corner, in accordance with ASTM D7136. Machined in the base plate was a 125 mm x 75 mm rectangular window to allow deformation of the specimens during impact. The velocity of the impactor head just prior to

impact was measured using a high speed camera (Fastec Troubleshooter HRMS, Fastec Imaging, California). In every case, the measured impact velocity was around 1 m/s. The specimens were then inspected by ultrasonic imaging.

5.4.3 Ultrasonic Imaging

The delamination state of the specimens in the in-plane and through-thickness directions was assessed using the C-scan and the B-scan capabilities of TecView UT software. The B-Scan images were reconstructed from two C-scan data files, one for each side of the impacted specimens. Fig. 5.4a shows an example of a typical reconstructed B-scan image. The parameters used for the ultrasonic inspection induced a small zone of saturated signal at each surface (approximately 10% of the total thickness), in which no measurement could be performed. The total volume of the damaged zone was reconstructed by taking B-Scan images at every 2 mm along the length of each specimen. Despite the known fact that the impact-induced delamination usually appears as an oblong shape with the main axis oriented with the adjacent fiber layers, the entire damaged zone of the multiple-layer balanced laminate used in this work was assumed to be axisymmetric. This damaged zone includes not only delamination but also interlaminar matrix cracks and fiber damage. A schematic representation of a C-Scan image is shown in Fig. 5.4b, along with the B-Scan lines crossing the damaged zone.

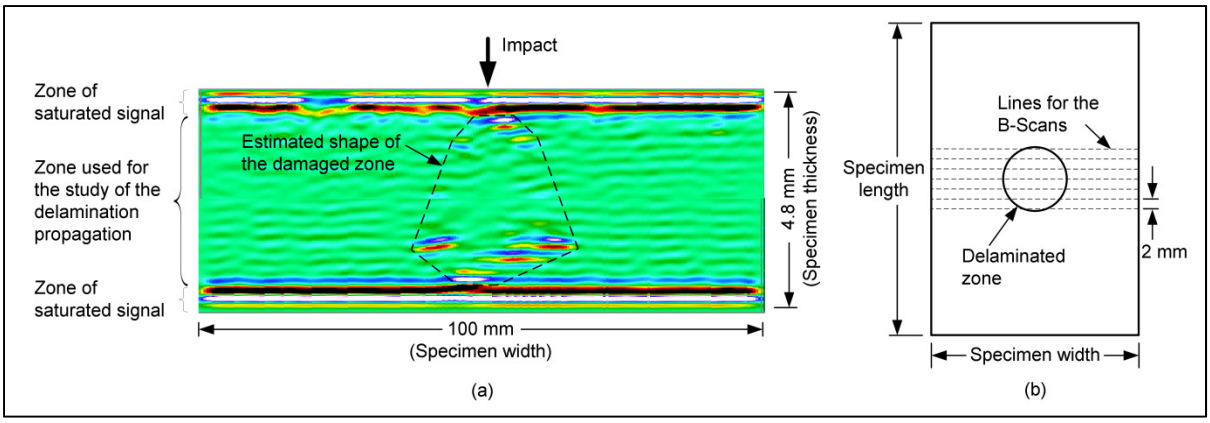

Figure 5.4 a) Example of a B-Scan image from an impacted specimen; b) Schematic of a C-Scan image containing a delaminated zone, along with the lines for the B-Scans

5.4.4 Bending after Impact Testing

The bending after impact tests were carried out on an MTS Alliance RF 200 machine equipped with a 200 kN load cell. A three-point bending fixture was used, as shown schematically in Fig. 5.5. The ASTM D7264 standard was followed, except for the span-to-thickness ratio (20 instead of 32) and the specimen width (100 mm instead of 13 mm). The cylindrical supports and loading nose were 6.35 mm in diameter and the support span was 100 mm. The displacement rate was 1 mm/min. The impacted face was placed on the tension side, in order to promote the progression of delamination and buckling of the delaminated plies, as observed in [17]. Four specimens were tested in bending for both the TiNi- and Kevlar-stitched plates, and three were used for the unstitched plate.

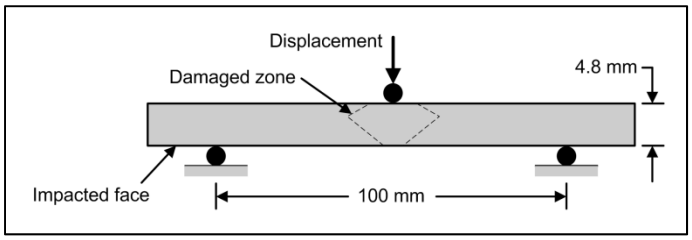

Figure 5.5 Setup for the three-point bending tests

5.5 Finite Element Model

The numerical model was developed on the ANSYS 13 commercial finite element software. To reduce computing time, the plate was divided into three parts: one central and two end-plates. The central portion of the plate was meshed with solid elements, while shell elements were used for the end-plates, as shown in Fig. 5.6a. The refined zone was modeled using 20-node Solid186 layered elements, and each ply was modeled with two elements in the thickness direction. The mesh of the refined zone is shown in Fig. 5.6b. Both end-plates were meshed with 8-node Shell281 layered elements. The dimensions of the plate were 150 mm x 100 mm x 4.8 mm and the 16-ply layout was $[45/0/-45/90]_{2s}$. About 360000 solid elements and 5000 shell elements were used in this model. The entire plate was modeled in this study since the use of symmetry with layered solid elements may induce erroneous results in the vicinity of the symmetry planes [18]. The stitched reinforcement was modeled using Solid186 elements with isotropic mechanical properties. To simulate the modified lock stitch arrangement used in this study, the cross section of an individual thread was meshed as a square with the same section area as two parallel round threads (Fig. 5.1 and Fig. 5.7). Perfect bonding was assumed between the stitch and the surrounding composite material.

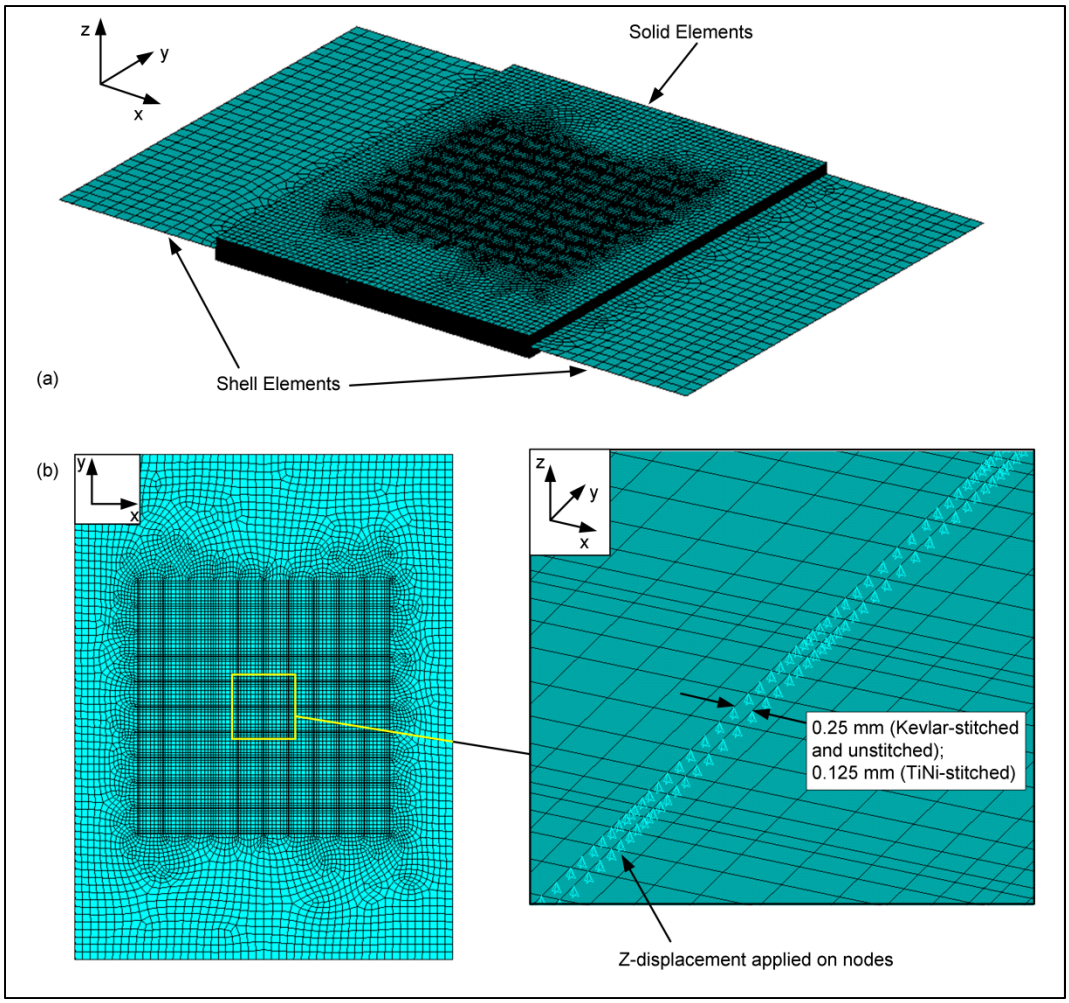

Figure 5.6 a) Complete mesh; b) Refined solid mesh

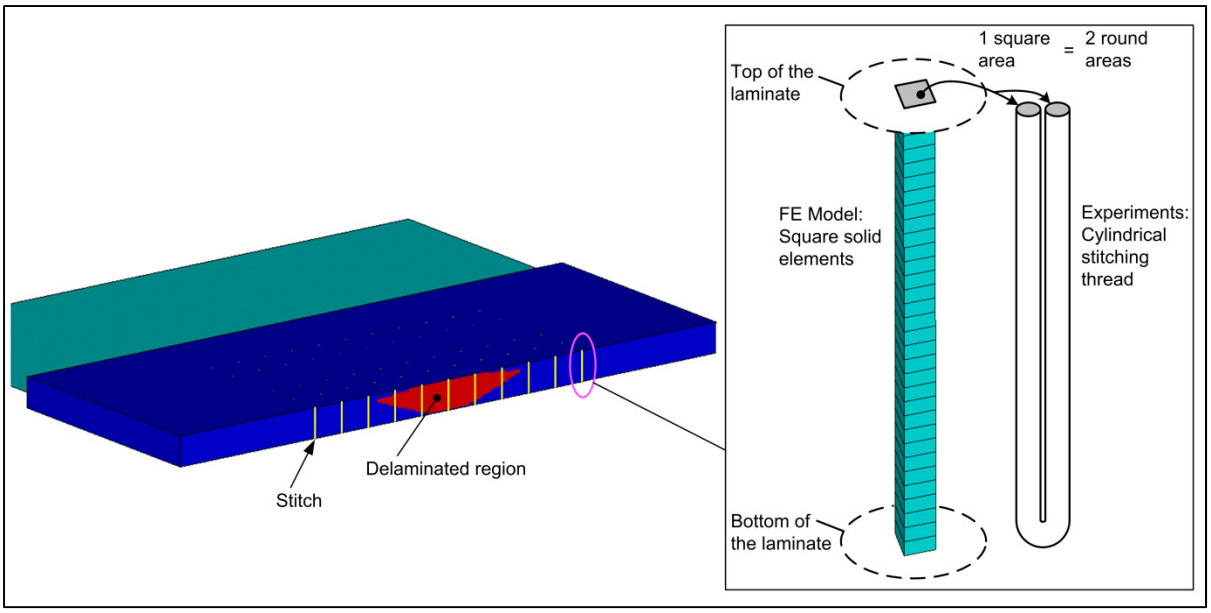

Figure 5.7 Cut view at the mid-length of the modeled plate (left) and detail of the modeled stitching thread with the square cross-section area equal to that of two cylindrical threads (right)

The z-displacement was applied at the top surface, mid-length of the plate, on two parallel lines of nodes in the central zone inside the grid mesh, and on one line of nodes outside the grid mesh, as shown in Fig. 5.6. The two parallel lines were distanced by 0.25 mm (Kevlar-stitched and unstitched) and 0.125 mm (TiNi-stitched). This allowed sharing the load and avoiding stress concentration in the region of higher interest (the impacted region, enclosed into the grid mesh), while lightening the mesh outside this zone. The x- and y-displacements as well as the z-rotation were blocked on one node of one support line to prevent rigid body motion. To avoid over-constrain the plate in the region of interest, the z-displacement was not applied on the entire width of the plate, but only on nodes whose reaction forces were acting in the same direction as the displacement, as illustrated in Fig. 5.8. This procedure allowed accounting for the non-uniform z-displacement of the laminate near the free edges.

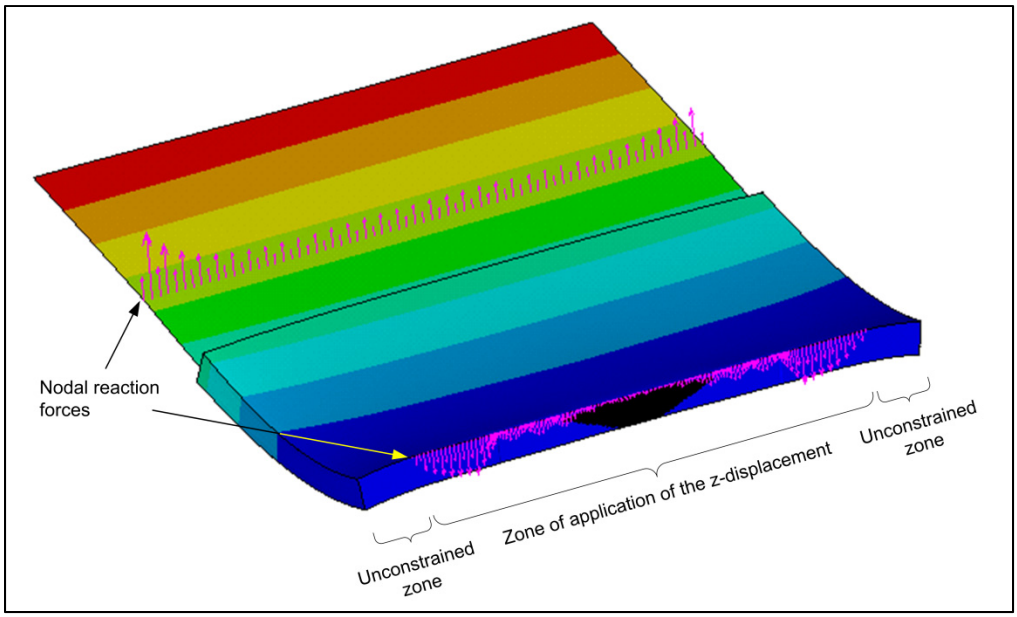

Figure 5.8 Deformed shape of the plate loaded in three-point bending (cut view at the mid-length); the displacement is applied on a partial zone along the width of the plate

The maximum face length of the solid elements was fixed at 10 times the thickness of the elements. As it can be seen in Fig. 5.6b, the grid mesh was refined in the vicinity of each grid corners, where the element face length was fixed at 0.25 mm (Kevlar-stitched and unstitched) and 0.125 mm (TiNi-stitched). The automatic tool for mesh checking was enabled during the mesh generation and before each nonlinear solution. The warning limits for the mesh check were kept at the default values of the software: aspect ratio: 20; parallel deviation of opposite edges: 100°; maximum corner angle: 165°; Jacobian ratio: 30; and Warping factor: 0.4.

The calculation algorithm presented in Fig. 5.9 is based on the progressive damage modeling technique developed by Shokrieh et al. [19]. The strength of this algorithm lies in its capacity to predict the damage progression with an acceptable level of accuracy, using only some basic engineering parameters as inputs (Young's moduli and the strengths of the composite material in tension, compression and shear). In addition, the exclusive presence of solid and shell elements in the present model eliminates some sources of convergence issues that could arise when cohesive elements are used for the modeling of the delamination progression [20].

The algorithm used in this work was previously validated by the authors for a simple plate in tension [18]. In this study, the displacement applied at the mid-length of the plate was increased by small increments, solving at each step and verifying the failure criteria for all the solid elements. Three failure criteria were considered: matrix failure, fiber failure and delamination. These are presented in Table 5.1a, along with their respective degradation factors [21]; σ and S stand for Stress and Strength, T and C for Tension and Compression, and E represents both modulus and strength in the progressive damage modeling equations. Following these rules, the appropriate mechanical properties of the broken elements were degraded. It is noted that the degradation factors for both matrix and fiber cracking depend on the sign of the stress (tensile or compressive), following the principle that under compressive loading, cracked material can still carry some load, unlike that under tensile loading [22]. This rule was used successfully by Camanho and Matthews [23] and Tserpes et al. [21].

In the case of the delamination failure, the degradation factor adopted for this work (0.1) was different from a near-zero value generally used in the literature [21]. Actually, it is known that the delamination does not necessarily result in a complete failure of the interface between two plies because of interlaminar fiber bridging [24]. Therefore, the use of a factor of 0.1 allowed accounting for some residual capability of the interface to bear a certain load. Besides, in the absence in the literature of any validated sets of degradation factors allowing differentiating the delamination in tension and compression, no difference between these two damage modes was considered in this work. This procedure allowed the damage propagation to be tracked throughout the simulation of the bending test. Large displacements were considered in the geometrically nonlinear analysis.

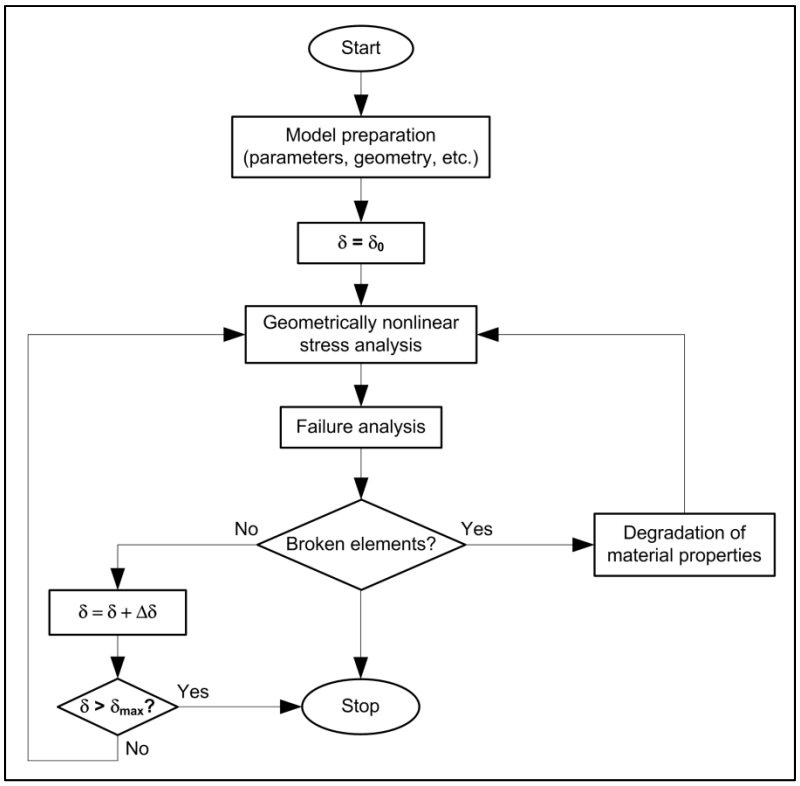

Figure 5.9 Algorithm of the numerical model

Table 5.1 a) Failure criteria and degradation factors; b) Mechanical properties of the carbon/epoxy material (in parentheses, properties assessed from the literature; otherwise as measured) and of the Kevlar and TiNi threads

(a)	Failure Criteria		Degradation Fact.
Matrix Tensile Failure	$\left(\frac{\sigma_{yy}^{T}}{S_{yy}^{T}}\right)^2+\left(\frac{\sigma_{xy}}{S_{xy}}\right)^2+\left(\frac{\sigma_{yz}}{S_{yz}}\right)^2 \geq 1$	$\rightarrow$	$E^d_{yy} = 0.2*E_{yy}$ $E^d_{xy} = 0.2*E_{xy}$ $E^d_{yz} = 0.2*E_{yz}$
Matrix Compr. Failure	$\left(\frac{\sigma_{yy}^{C}}{S_{yy}^{C}}\right)^2+\left(\frac{\sigma_{xy}}{S_{xy}}\right)^2+\left(\frac{\sigma_{yz}}{S_{yz}}\right)^2 \geq 1$	$\rightarrow$	$E^d_{yy} = 0.4*E_{yy}$ $E^d_{xy} = 0.4*E_{xy}$ $E^d_{yz} = 0.4*E_{yz}$
Fibre Failure	$\left(\frac{\sigma_{xx}^{T,C}}{S_{xx}^{T,C}}\right) \geq 1$	$\rightarrow$	$E^d_{xx} = 0.07*E_{xx}$ (T) $E^d_{xx} = 0.14*E_{xx}$ (C)
Delamination Failure	$\left(\frac{\sigma_{zz}^{T,C}}{S_{zz}^{T,C}}\right)^2+\left(\frac{\sigma_{xz}}{S_{xz}}\right)^2+\left(\frac{\sigma_{yz}}{S_{yz}}\right)^2 \geq 1$	$\rightarrow$	$E^d_{zz} = 0.1*E_{zz}$ $E^d_{xz} = 0.1*E_{xz}$ $E^d_{yz} = 0.1*E_{yz}$

(b) Carbon/epoxy laminate:			
Modulus		**Strength**	
E_{xx}:	128.3 GPa	S_{xT} (S_{xC}):	2000 (1200) MPa
E_{yy}, E_{zz}:	6.95 GPa	S_{yT}, S_{zT}:	14 MPa
G_{xy}, G_{xz} (G_{yz}):	2.88 (2.44) GPa	S_{yC}, S_{zC}:	56 MPa
ν_{xy}, ν_{xz} (ν_{yz}):	0.3 (0.42)	S_{xy}, S_{xz}, S_{yz}:	34 MPa

Kevlar Stitch:		**TiNi Stitch:**	
E_{xx}, E_{yy}, E_{zz}:	72 GPa	E_{aus}: 31.6 GPa	ε_L: 0.044
G_{xy}, G_{xz}, G_{yz}:	27.7 GPa[a]	σ_{AS}: 540 MPa	ν: 0.01[b]
ν_{xy}, ν_{xz}, ν_{yz}:	0.01[b]	σ_{AF}: 210 MPa	
		σ_{MS}: 410 MPa	
		σ_{MF}: 795 MPa	

[a] Calculated as $G = \frac{E}{2(1+\nu)}$

[b] Assumption

The mechanical properties of the unidirectional carbon/epoxy laminate are reported in Table 5.1b, with "x" being the fiber direction. The in-plane tensile and shear properties were determined experimentally according to the appropriate ASTM standards: D3039 (tensile) and D3518 (shear). The compressive strengths were assumed to be in accordance with what could be found in the literature (e.g. [25]). The Young's modulus and Poisson's coefficient in the "yz" direction were fixed following the assumption of transverse isotropy. All the mechanical properties in the composite model were assumed to be linear up to the rupture.

Table 5.1b also contains the mechanical properties of both the Kevlar and the TiNi threads. The Young's moduli of both threads were determined from tensile testing (see Fig. 5.2). The superelastic behavior of the TiNi thread was modeled using the ANSYS TB,SMA material law, which requires the following inputs: σ_{MS}, σ_{MF}, σ_{AS}, σ_{AF}, ε_L and E_{aus} (Fig. 5.10). The constants stand for: the starting and final stresses of the forward phase transformation, the starting and final stresses of the reverse phase transformation, the maximum superelastic plateau strain and the Young's modulus in the austenitic phase, respectively. These constants and the simulated superelastic tensile curve are shown in Fig. 5.10, as well as the experimental curves. Prior to solving the model, a pretension (initial strain) was imposed on the stitching threads' solid elements to account for the preload induced during stitching (round dot in Fig. 5.10). The initial stress state was then computed for the entire model and the resulting stresses were subtracted in all the subsequent calculations of the failure criteria. The subtraction of the initial stresses was made only in the directions whose mechanical properties are governed mainly by the matrix: y, z and yz. This operation reflects the particularities of the composite manufacturing process. Since the resin is infused into the already stitched carbon fabric panels, the cured matrix is free of stresses created by stitching contrary to the stacked carbon fabric plies. For the same reason, the Poisson ratios of both threads were set at 0.01, for neglecting the transverse dilatation of the stitch elements during the initial solution (application of the initial strain).

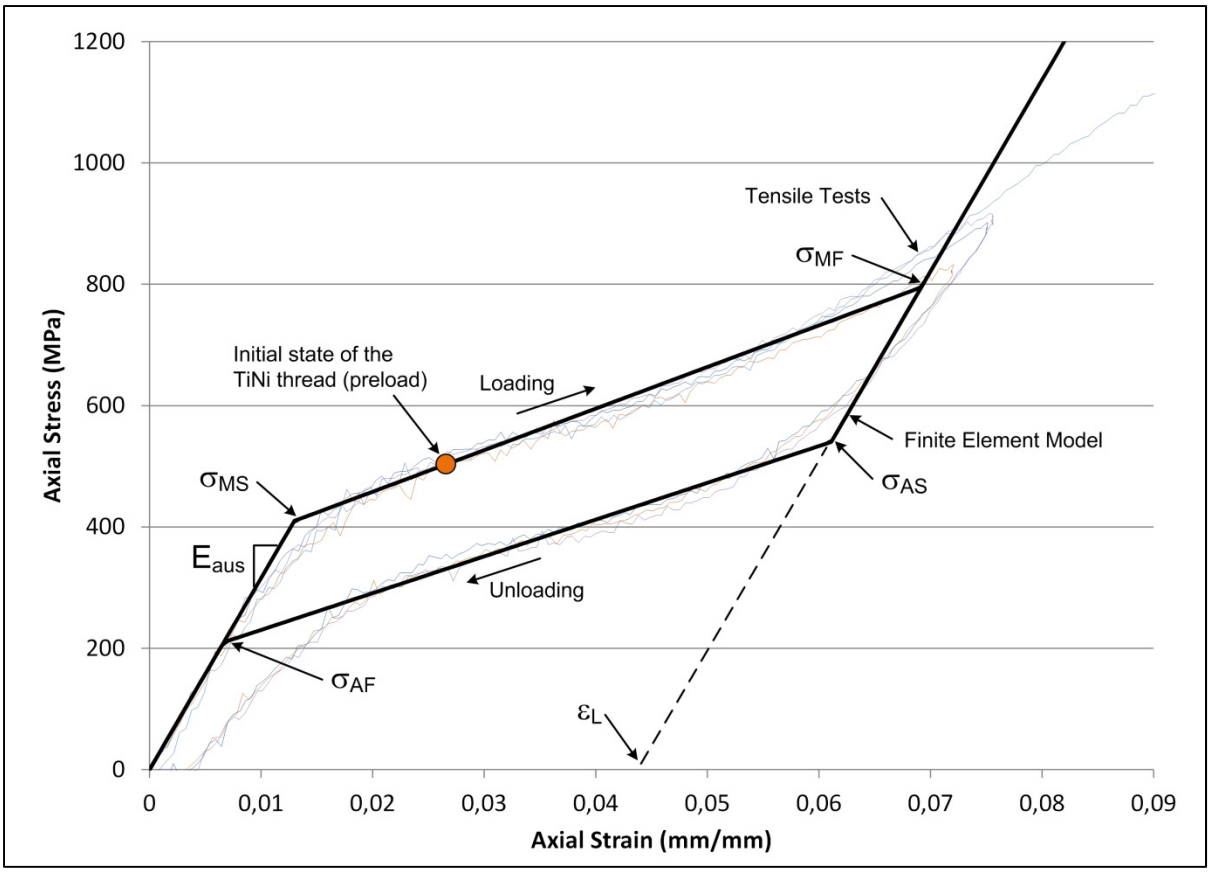

Figure 5.10 Characteristic constants and simulated tensile curve of the superelastic material model, superimposed with experimental tensile curves

An identical pre-damaged zone was considered in all the modeling cases, in order to simulate the effect of low velocity impact and to isolate the influence of stitching on the damage propagation. The shape of this zone was schematized in accordance with the B-scan observations, and the dimensions were as shown in Fig. 5.11. The dimensions of Fig. 5.11 were representative of one of the largest damaged zones measured among the unstitched specimens. Prior to launching the numerical algorithm simulating three-point bending, the mechanical properties of the solid elements confined in this zone were degraded according to the factors for delamination in Table 5.1a.

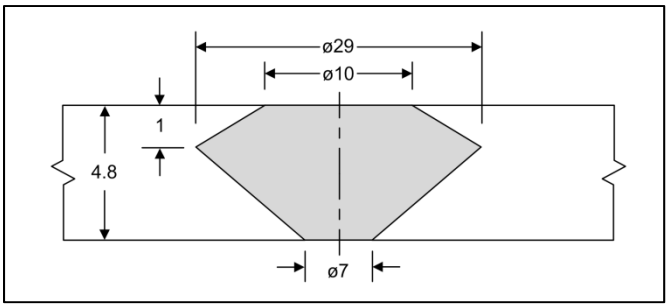

Figure 5.11 Typical shape and dimensions of an axisymmetric delaminated zone as measured by ultrasonic inspection (dimensions in mm)

5.6 Results and Discussion

5.6.1 Impact and Bending After Impact Tests

The effect of the stitched reinforcements on the impact-induced delamination was evaluated by measuring the volume of the impact-induced damaged zone. Table 5.2 presents the results for the unstitched, TiNi- and Kevlar-stitched specimens. The comparison between the stitched and the unstitched specimens shows that stitching by both threads allowed some reduction of the delaminated volume. The best performance was obtained with the Kevlar thread (-17%), but the TiNi thread also had a positive effect on reducing the damaged zone (-7%). Note however that the gain obtained with Ti-Ni thread was not statistically significant according to the Student's t-test with a 5% confidence threshold. Therefore, during the impact load, the Kevlar thread was more able to attenuate the impact-induced deformation than the TiNi thread, thus resulting in a smaller damaged volume. The apparent stronger performance of the Kevlar thread must however be relativized, since its initial stiffness was ten times that of the TiNi thread (Fig. 5.2).

Impacted specimens of all the three types were then submitted to three-point bending. The force-displacement response is presented in Fig. 5.12, as well as the three zones of the bending behavior: zone I corresponding to the linear response, zone II corresponding to the

gradual loss of stiffness due to damage propagation and zone III corresponding to the catastrophic stage of rupture in bending [26]. Even though the qualitative comparison of the three graphs shows that they look similar, with the force and the displacement being in similar ranges in every case, they differ in terms of the associated deformation energy.

The deformation energy in bending was measured as an area under the force-displacement curve, for all the specimens presented in Fig. 5.12. Only zones I and II of the curves were considered in this study, since zone III corresponds to catastrophic damage propagation, process which is out of the scope of this work. The results for the unstitched, TiNi- and Kevlar-stitched specimens are presented in Table 5.2. From this table, it can be observed that the Kevlar-stitched specimens require 20% more energy for deformation than the unstitched ones, while the TiNi-stitched specimens only require 13% more. It must be noted that this 13% increase of the bending energy presents a 6.5% probability of being false according to the Student's t-test, which is slightly higher than the generally accepted 5% confidence threshold.

Table 5.2 Experimental results for the volume of the delamination after impact (ultrasonic measurements) and the bending energy till failure (bending testing, zones I and II)

	Volume of the delamination (mm^3)	**Energy for rupture in bending (zones I+II) (J)**
Unstitched	1079 ± 98	19.5 ± 1.4
TiNi-stitched	1002 ± 47	22.1 ± 2.3
Kevlar-stitched	892 ± 104	23.4 ± 1.0

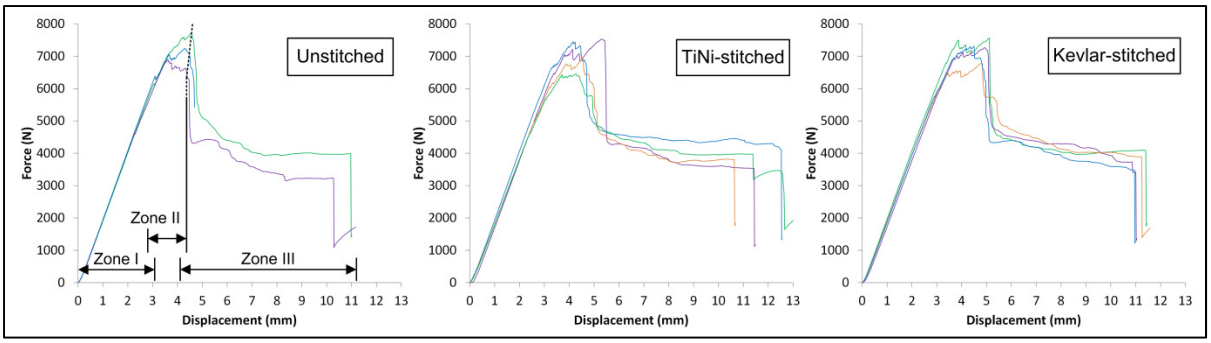

Figure 5.12 Force-displacement response in three-point bending for unstitched, TiNi- and Kevlar-stitched specimens

To quantify the delamination resistance of laminates, it is common practice to calculate the energy release rate (G) for the impact test [27] and for the delamination propagation [28]. This parameter represents the energy required to create a unit area of delamination. In this paper, the performance is presented in terms of the energy required to create a unit volume of damaged material, or energy per unit volume of damage (G_v). In this respect, all the performances discussed previously were weighted in respect to the volume of the damaged zone presented in Table 5.2. To accomplish this, the weighted performance of each specimen was calculated (in this study) as the energy related to: a) the apparition of a delaminated volume during the impact test; and b) the propagation of the existing damage during the post-impact bending test.

Equations 5.1 and 5.2 present the energy per unit volume of damage for the impact-induced damage and for the bending-induced damage propagation, respectively:

$$G_{v_{impact}} = \frac{E_{impact}}{V_{impact_f} - V_{impact_i}} \left[\frac{J}{mm^3}\right] \tag{5.1}$$

$$G_{v_{bending}} = \frac{E_{bending\ I+II}}{V_{bending_f} - V_{bending_i}} \left[\frac{J}{mm^3}\right] \tag{5.2}$$

where E_{impact}, V_{impact_i} and V_{impact_f} stand for the kinetic energy of the impactor (5 J) and the volume of the damage before and after the impact, respectively, $E_{bending\ I+II}$ represents the area under the F-d curve in the zones I and II of the bending test, and $V_{bending_i}$ and $V_{bending_f}$ stand for the volume of the damage before and after the bending test, respectively. The parameter $V_{impact_i} = 0$ (no damage prior to impact). The parameter $V_{bending_f}$ is calculated as the volume of the delamination at the rupture of the unstitched specimen in bending, which was obtained by numerical calculations. This value (~1700 mm^3, Fig. 5.14) is assumed to be identical for all the plates, stitched and unstitched, since the stitching reinforcement in its present configuration (less than 1% volume fraction) delays the post-impact damage propagation, without significantly increasing the global resistance of the plates (Fig. 5.12). No experimental verification of this assumption was possible in the framework of this work, due to inherent limitations of the ultrasound scan technique to penetrate through the thickness of the severely damaged specimens. The results of equations 5.1 and 5.2 are presented in Fig. 5.13. It must be noted that the scales of the two vertical axes are not of the same order of magnitude.

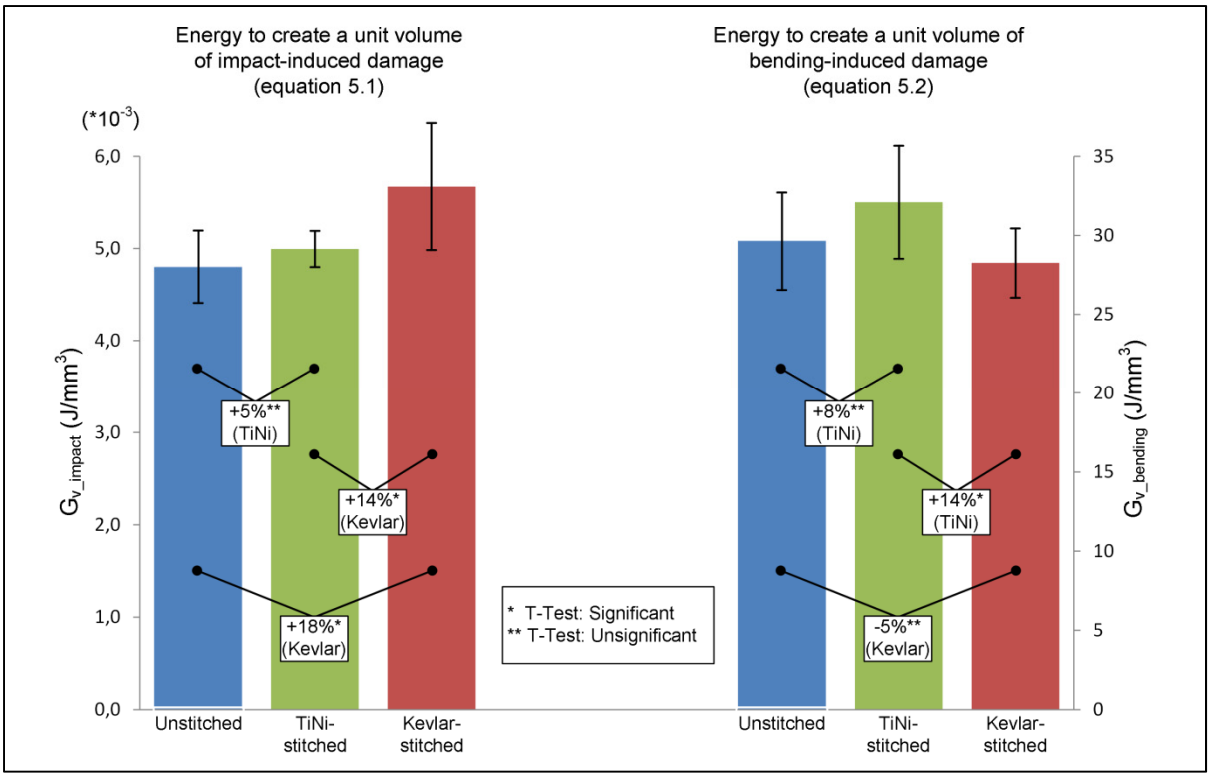

Figure 5.13 Energy required to create a unit volume of impact-induced damage (left) and for bending-induced delamination propagation (right)

Fig. 5.13 (left) shows that the Kevlar stitch allowed significant improvement of the performance during the impact test, with an increase of 18% and 14% of the energy density when compared to the unstitched and TiNi-stitched specimens, respectively. That is, it takes more impact energy to create a unit volume of delaminated material when Kevlar stitches are in the laminate. No significant effect was measured for the TiNi stitch in this test. However, the results from equation 5.2 (Fig. 5.13, right) show that both the TiNi-stitched and the unstitched laminates were more efficient than the Kevlar-stitched laminate at hindering the propagation of the delamination in the bending tests (+14% for the TiNi-stitched laminate). From this perspective, the strong performance of the Kevlar-stitched specimens in terms of the bending energy, as presented in Table 5.2, appears to be partially related to Kevlar's ability to reduce the apparition of damage during an impact load. The TiNi reinforcement was less effective at reducing the impact-induced damage, but more effective than Kevlar at preventing delamination propagation in bending. Therefore, it is suspected that a difference

does exist in the structural impact of the two stitching threads when the specimen is under bending load, even though no obvious change can be observed in the force-displacement curves (macroscopically). Globally, in terms of delamination, both types of stitching reinforcement seemed to be beneficial during impact, but this positive outcome could not necessarily be transposed to the flexural testing. The use of a numerical model for the study of the surroundings of the stitch will be of great help in elucidating the underlying phenomena.

5.6.2 Finite Element Modeling

The three different structures submitted to bending load (unstitched, TiNi- and Kevlar-stitched) were simulated with the finite element model. In all the cases modeled, the pre-damaged zone was assumed to be of identical dimensions, contrarily to what was measured experimentally, in order to evaluate the net impact of different types of reinforcement on the bending-induced delamination propagation. Fig. 5.14 presents the predicted force-displacement responses for the three cases. As observed experimentally, the three numerical curves are similar, confirming that no major change in the macroscopic behavior was induced by the insertion of stitches in the structure. The almost linear parts of the curves represent the zone I of the bending response, while the zone II is represented in all the cases by the gradual degradation of the plate stiffness. As it was observed in a previous work (see Fig. 5.15), the FE model stops at a certain displacement for the simulation involving Kevlar-stitched (2.5 mm) and TiNi-stitched (3.3 mm) reinforcement. This convergence failure was caused by highly distorted elements due to the degradation of the mechanical properties of the broken elements. The unstitched model was intentionally stopped at a deflection of 3.7 mm without experiencing any highly distorted elements. This is an indication of the more invasive character of the Kevlar stitch when compared to the TiNi stitch, due to its larger diameter and stiffness. A refinement of the mesh could allow the displacement to continue for the problematic model, but the computational time would then become prohibitive.

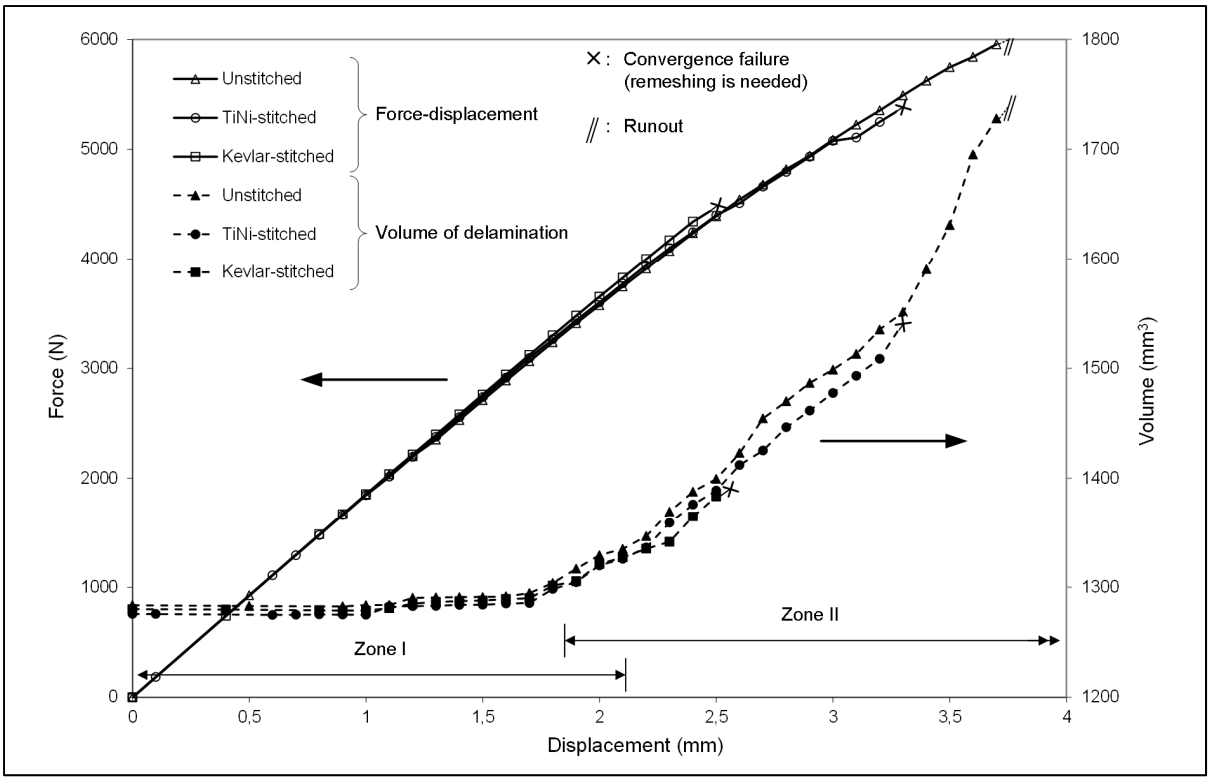

Figure 5.14 Predicted force-displacement response in bending for the three structures. The Kevlar-stitched and the TiNi-stitched models stopped at 2.5 and 3.3 mm in deflection, respectively, because of highly distorted elements (marked as 'x'); the unstitched model was intentionally stopped at 3.7 mm (marked as '//')

The damage propagation, in terms of the increasing volume of delaminated elements, was calculated as a function of flexural deflection for the three different structures considered. The result is also presented in Fig. 5.14 (secondary vertical axis). From this graph it can be stated that the insertion of TiNi- and Kevlar–stitched reinforcement with the present configuration has no major effect on the overall volume of composite material that can be considered as delaminated. It should also be noted that a drastic increase in the delaminated volume, which starts at 2 mm of displacement, does not significantly impact on the global force-displacement behavior of the actual structure. The reason for that lack of impact is that the volume of the delimination remains much smaller than that of the deformed structure.

A deeper investigation was carried out on the propagation of internal damage, by tracking the state of delamination throughout the simulation. The ability of the model to predict accurate propagation of delamination was validated in another study [26]. In Fig. 5.15 is presented an example of both the predicted and the measured delaminated regions, for an unstitched specimen loaded in bending. Images a), b), c) and d) represent the state of delamination at four displacement levels, from the ultrasonics and the FE model. The color scale of the model represents the value of the delamination criterion as described in Table 5.1, going from blue (low-stress level) to red (delaminated interface). The reader is referred to [26] for more details.

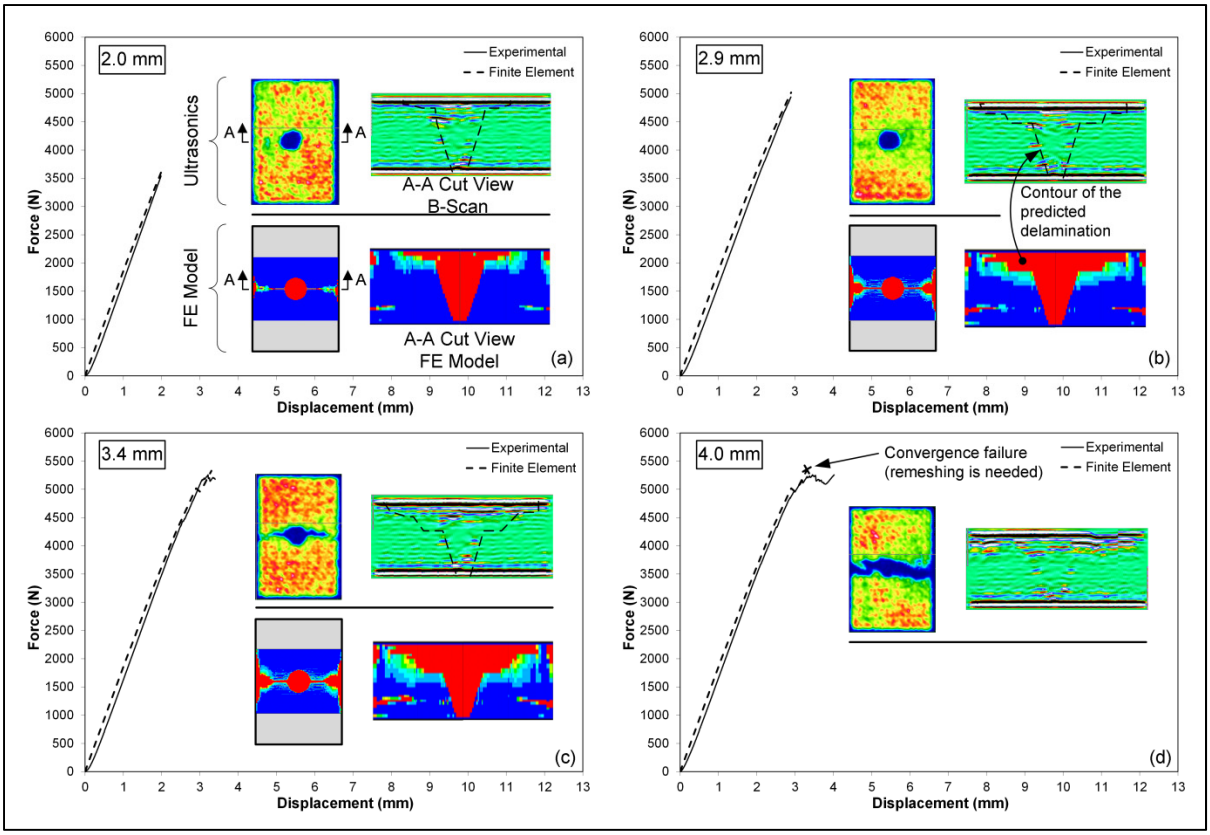

Figure 5.15 Propagation of the delamination at the mid-length of the plate, as measured by ultrasonics and as predicted by FE modeling [26]

Fig. 5.16 shows the propagation of the delamination on the cutting plane located at the mid-length of the plate for the three structures considered. In this figure, each image represents

half of the cutting plane (as circled by the dashed line in the upper part of the figure). It is clear from this figure that the presence of the stitching thread influences the propagation of the delamination, even though no difference could be detected on the force (delamination volume) -displacement curves of Fig. 5.14. In both of the stitched structures, the damage propagates laterally towards the free edge as generally observed, but tends to also propagate along the stitch thread through the laminate's thickness. This stress concentration effect seems to be more pronounced for the Kevlar thread than for the TiNi thread. Indeed, the damage penetrates more deeply through the thickness of the Kevlar-reinforced structure than in the TiNi-reinforced plate, for the same displacement. However, in a zone between the stitches, the Kevlar thread seems to delay the through-thickness propagation of the damage, a phenomenon that cannot be observed in the TiNi-stitched plate.

These two last observations may be explained by the different mechanical properties of the two stitching threads used. The lower stiffness of the TiNi thread makes it a weaker reinforcement than the Kevlar thread, but the stress concentration effect in the vicinity of the thread is thus reduced, due to the lower mismatch between the mechanical properties of the thread and the laminate. Moreover, the damping capability of the superelastic material, as implemented in the model for the case of the TiNi thread, may allow the damage propagation along the stitch to be reduced. In any case, the damage propagation along the stitch could result in the debonding of the thread, which is a known damage mechanism in stitched laminates [29, 30]. It is interesting to note that despite the different delamination schemes presented in Fig. 5.16, the overall volume of the delaminated elements remains the same for the three cases, as discussed previously. Therefore the insertion of reinforcement through the thickness of the laminate may locally impact how the delamination progresses depending on the properties of the stitching thread, without necessarily affecting the global damage extension.

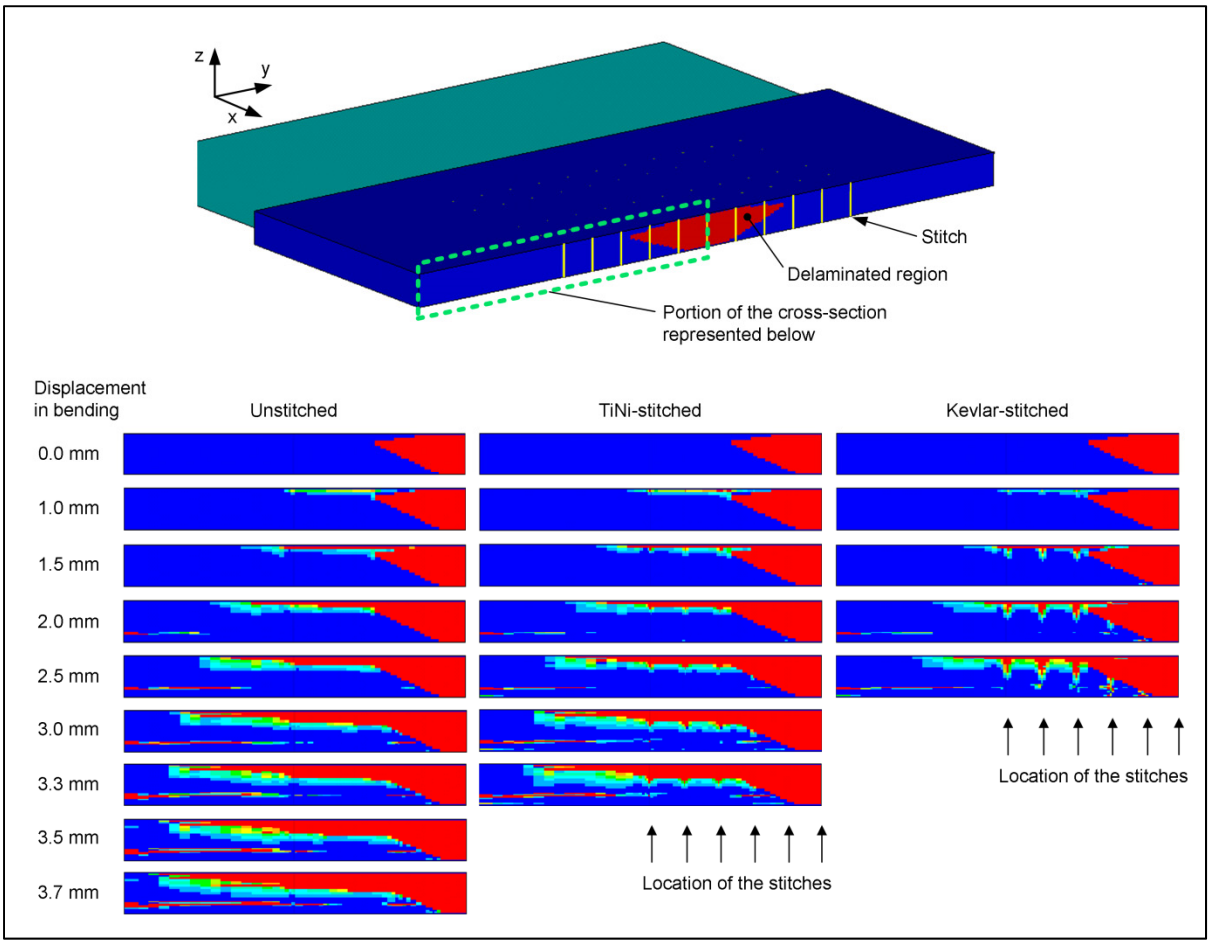

Figure 5.16 Numerical prediction of the propagation of the delamination for the unstitched, TiNi- and Kevlar-stitched plates

5.7 Conclusions

In this work the propagation of impact-induced damage was studied experimentally and numerically for three different carbon/epoxy structures: unstitched, TiNi- and Kevlar-stitched laminates. The TiNi thread had superelastic properties and the linearly elastic Kevlar thread was used as a reference. The specimens were submitted to low–velocity impact tests to induce embedded damage. The performance of the three specimen types was first evaluated in terms of the volume of the delaminated material after impact and the energy provided to the specimens during the zones I and II of the flexural tests. Considering the unstitched

specimen as a reference, the TiNi stitch was less effective than the Kevlar stitch at reducing the volume of the impact-induced delaminated zone (-7% vs -17%), whereas the gap was slightly reduced for the deformation energy in three-point bending (+13% for TiNi vs +20% for Kevlar). The results were then recalculated in terms of the energy per unit volume of impact-induced damage, and the energy per unit volume of bending-induced damage propagation. By comparing the resulting energy densities, it is clear that the Kevlar stitch allowed more significant improvement of composite resistance to the impact-induced damage than the unstitched (+18%) and the TiNi-stitched (+14%) laminates. However, this gain was completely canceled during the bending test, where the TiNi-stitched and the unstitched plates were more effective (+14%) than the Kevlar-stitched plates in terms of hindering the damage propagation. That is, in the present stitching configuration, the superelastic TiNi as reinforcement was more effective during bending than during low–velocity impact, while the Kevlar reinforcement was more effective during the impact test than during bending. In this respect, the performance of the TiNi stitch can be considered quite encouraging, since the diameter of Ti-Ni thread was half of that of the Kevlar thread.

To assess the influence of the type of reinforcement on the post-impact delamination propagation under flexural load, the three different structures (stitched and unstitched) were modeled and the propagation of the delamination was studied. Identical prior-to-bending delaminated volume was considered, to isolate the influence of the mechanical properties of the threads. The results of the finite element simulation showed that both types of stitching threads (Kevlar and Ti-Ni) promoted localized through-thickness damage propagation along the stitches, from the upper plies towards the adjacent plies. This phenomenon was more pronounced for the Kevlar thread, due to the higher mismatch between the properties of the thread and those of the laminate through the thickness: Kevlar is 10 times stiffer than the laminate while TiNi is 4.5 times stiffer in the austenitic phase and has a similar to the laminate stiffness when stretched to the martensitic phase (superelastic plateau). The lower stiffness of the superelastic TiNi thread thus induced lower stress concentration along the stitch compared to the Kevlar thread. However, for the same plate deflection, the overall through-thickness damage propagation was hindered by the presence of the Kevlar stitches

more than in the case of unstitched and TiNi-stitched laminates. The stiffness of the stitching thread thus seems to have a positive effect on one hand, while being detrimental on the other. This observation shows the usefulness of a numerical study when subtle behaviors in the structure cannot be identified with common experimental work such as bending tests and ultrasonic imaging alone.

In conclusion, the experimental work indicates that while the use of the superelastic stitching thread did not result in a significant gain of the resistance to delamination propagation in the three-point bending tests, it was not detrimental either. In addition, the performance of the Ti-Ni thread was much better than that of the Kevlar despite the smaller thread diameter and stiffness. The numerical study showed that both stitching threads create conditions for localized propagation of the damage along the stitches, but this phenomenon was less pronounced for the TiNi thread.

Consequently, it can be stated that the best performance in post-impact bending of stitched laminates does not necessarily require high stiffness of a stitching thread, but there is a certain trade-off between its ability to support the out-of-plane loads and to minimize the stiffness mismatch between the stitch and the surrounding composite material. For this reason, the use of superelastic (TiNi) stitching appears to be a promising avenue, since it could allow enhancing the performance of composite structures in bending with less invasive reinforcement elements (smaller thread dimensions, lower added mass, lower stress concentration). Twisted or braided Kevlar thread could also be tested further, since a braid should present more compliant tensile behavior than a simple thread. In future work, the numerical study could be extended, for instance, to the optimization of stitching configuration by varying some parameters (thread diameter, stitching pitch) and the thread properties (pretension and parameters of the superelastic behavior). The mesh of the FE model could also be refined in the vicinity of the mid-length of the plate, since this is the most loaded part of the structure. This effort should avoid the apparition of highly deformed elements and thus allow displacement to progress further that what was possible in this study.

5.8 Acknowledgements

The authors would like to thank the CREPEC (Centre de Recherche en Plasturgie et Composites) for providing logistical support for this project. We are also thankful to Prof. Larry Lessard from McGill University (Montreal, Qc) for access to McGill's drop-weight impact machine and to Prof. Martin Viens from ETS and to Mr Harold Hébert from the Industrial Materials Institute (Boucherville, Qc) for their support in the realization and interpretation of ultrasonic measurements.

5.9 References

[1] Mouritz AP, Bannister MK, Falzon PJ, Leong KH. Review of applications for advanced three-dimensional fibre textile composites. Composites Part A: Applied Science and Manufacturing. 1999;30:1445-61.

[2] Greenhalgh E, Hiley M. The assessment of novel materials and processes for the impact tolerant design of stiffened composite aerospace structures. Composites Part A: Applied Science and Manufacturing. 2003;34:151-61.

[3] Yoshimura A, Nakao T, Yashiro S, Takeda N. Improvement on out-of-plane impact resistance of CFRP laminates due to through-the-thickness stitching. Composites Part A: Applied Science and Manufacturing. 2008;39:1370-9.

[4] Aymerich F, Priolo P. Characterization of fracture modes in stitched and unstitched cross-ply laminates subjected to low-velocity impact and compression after impact loading. International Journal of Impact Engineering. 2008;35:591-608.

[5] Scarponi C, Perillo AM, Cutillo L, Foglio C. Advanced TTT composite materials for aeronautical purposes: Compression after impact (CAI) behaviour. Composites Part B: Engineering. 2007;38:258-64.

[6] Byun J-H, Song S-W, Lee C-H, Um M-K, Hwang B-S. Impact properties of laminated composites with stitching fibers. Composite Structures, Fifteenth International Conference on Composite Materials - ICCM-15. 2006;76:21-7.

[7] Xiaoquan C, Al-Mansour AM, Zhengneng L, Chenghe K. Compression strength of stitched laminates after low-velocity impact. Journal of Reinforced Plastics and Composites. 2005;24:935-47.

[8] Dransfield KA, Jain LK, Mai Y-W. On the effects of stitching in CFRPs - I. Mode I delamination toughness. Composites Science and Technology. 1998;58:815-27.

[9] Jain LK, Dransfield KA, Mai Y-W. On the effects of stitching in CFRPs - II. Mode II delamination toughness. Composites Science and Technology. 1998;58:829-37.

[10] Sankar BV, Sharma SK. Mode II delamination toughness of stitched graphite/epoxy textile composites. Composites Science and Technology. 1997;57:729-37.

[11] Wood MDK, Sun X, Tong L, Katzos A, Rispler AR, Mai Y-W. The effect of stitch distribution on Mode I delamination toughness of stitched laminated composites - experimental results and FEA simulation. Composites Science and Technology. 2007;67:1058-72.

[12] Wood MDK, Sun X, Tong L, Luo Q, Katzos A, Rispler A. A New ENF Test Specimen for the Mode II Delamination Toughness Testing of Stitched Woven CFRP Laminates. Journal of Composite Materials. 2007;41:1743-72.

[13] Yoshimura A, Yashiro S, Okabe T, Takeda N. Characterization of tensile damage progress in stitched CFRP laminates. Advanced Composite Materials: The Official Journal of the Japan Society of Composite Materials. 2007;16:223-44.

[14] Aymerich F, Priolo P, Sun CT. Static and fatigue behaviour of stitched graphite/epoxy composite laminates. Composites Science and Technology. 2003;63:907-17.

[15] Lau K-T, Ling H-Y, Zhou L-M. Low velocity impact on shape memory alloy stitched composite plates. Smart Materials and Structures. 2004;13:364-70.

[16] Vachon P-L, Brailovski V, Terriault P. Suppression of delamination propagation in carbon/epoxy laminates by the use of superelastic stitching wires: preliminary results. In: Design, Manufacturing and Applications of Composites, Proceedings of the Eight Joint Canada-Japan Workshop on Composites. Montreal, Quebec, Canada: DEStech Publications inc.; 2010. p. 286-96.

[17] Nilsson S, Bredberg A, Asp LE. Effects of CFRP laminate thickness on bending after impact strength. Plastics, Rubber and Composites. 2009;38:61-6.

[18] Vachon P-L, Brailovski V, Terriault P. Modeling of Delamination Initiation and Propagation in Composite Laminates Under Monotonic Tensile Loading Using the Progressive Damage Modeling Technique. Science and Engineering of Composite Materials. 2009;16:99-114.

[19] Shokrieh MM, Lessard LB. Progressive fatigue damage modeling of composite materials, Part I: Modeling. Journal of Composite Materials. 2000;34:1056-80.

[20] Alfano G, Crisfield MA. Finite element interface models for the delamination analysis of laminated composites: Mechanical and computational issues. International Journal for Numerical Methods in Engineering. 2001;50:1701-36.

[21] Tserpes KI, Labeas G, Papanikos P, Kermanidis T. Strength prediction of bolted joints in graphite/epoxy composite laminates. Composites Part B: Engineering. 2002;33:521-9.

[22] Tan SC, Perez J. Progressive failure of laminated composites with a hole under compressive loading. Journal of Reinforced Plastics and Composites. 1993;12:1043-57.

[23] Camanho PP, Matthews FL. Progressive damage model for mechanically fastened joints in composite laminates. Journal of Composite Materials. 1999;33:2248-80.

[24] de Moura MFSF, Campilho RDSG, Amaro AM, Reis PNB. Interlaminar and intralaminar fracture characterization of composites under mode I loading. Composite Structures. 2010;92:144-9.

[25] Shokrieh MM, Lessard LB. Progressive fatigue damage modeling of composite materials, Part II: Material characterization and model verification. Journal of Composite Materials. 2000;34:1081-116.

[26] Vachon P-L, Brailovski V, Terriault P. Prediction of the Propagation of Impact-Induced Delamination in Carbon/Epoxy Laminates. Composite Structures. 2013;95:227-235.

[27] Caprino G, Lopresto V, Langella A, Durante M. Irreversibly absorbed energy and damage in GFRP laminates impacted at low velocity. Composite Structures. 2011;93:2853-60.

[28] Delfosse D, Poursartip A. Energy-based approach to impact damage in CFRP laminates. Composites Part A (Applied Science and Manufacturing). 1997;28A:647-55.

[29] Cox BN. Constitutive model for a fiber tow bridging a delamination crack. Mechanics of Composite Materials and Structures. 1999;6:117-38.

[30] Cartie DDR, Cox BN, Fleck NA. Mechanisms of crack bridging by composite and metallic rods. Composites Part A: Applied Science and Manufacturing. 2004;35:1325-36.

CONCLUSION GÉNÉRALE

Ce projet de recherche visait principalement à développer une nouvelle technologie de renfort interlaminaire pour les stratifiés carbone/époxy. L'approche de tolérance au dommage qui est privilégiée dans le milieu aéronautique commande une meilleure connaissance des mécanismes d'apparition du délaminage, mais également des méthodes permettant de contrôler sa propagation. La technique d'insertion de renforts par couture existe déjà depuis une trentaine d'années et elle a démontré son efficacité. L'idée maîtresse de ce projet consistait donc en la combinaison de cette méthode bien connue avec la technologie des alliages à mémoire de forme. Ainsi, l'utilisation d'un fil en AMF superélastique comme renfort cousu à travers les couches de fibres, avant infusion de la résine, devait permettre l'amélioration de la résistance au délaminage des composites carbone/époxy.

La fabrication des échantillons renforcés de TiNi s'est effectuée avec succès, comme en font foi les images de microscopie optique permettant de voir une vue de coupe de la plaque et du fil cousu à l'intérieur. Les fils traversent la plaque de composite de façon à former un point « modified lock stitch », tel que prévu. Il est donc possible de fabriquer des plaques renforcées de couture en TiNi présentant une géométrie semblable à celle des plaques renforcées de Kevlar, qui sont communément utilisées en recherche.

Les essais d'impact à faible vitesse ont montré une performance encourageante des renforts superélastiques, en termes de volume de la zone endommagée. Ainsi, ces renforts permettent une diminution de 10% du volume délaminé comparativement aux échantillons non renforcés, et ce, avec des fils d'un diamètre relativement faible (0.1 mm). À titre de comparaison, les renforts de Kevlar ont contribué à diminuer de 27% la zone endommagée, avec un diamètre de fil deux fois plus grand et une rigidité nettement plus importante. Cependant, un point intéressant à souligner est que cette dernière performance ne se répercute pas nécessairement sur les résultats de compression résiduelle après impact, puisque l'écart entre les deux types d'échantillons renforcés se rétrécit grandement dans ce cas (+1% pour le TiNi et +8% pour le Kevlar).

L'essai de flexion trois-points a permis d'amener un élément intéressant à cette étude : la propagation du délaminage durant le chargement. En effet, ce phénomène était absent des essais de compression puisque la rupture était alors brutale. La caractérisation de l'état d'endommagement des plaques au cours de l'essai de flexion a montré que l'on pouvait séparer la courbe Force-Déplacement en trois zones distinctes, dont seulement les deux premières ont été étudiées. Pour mesurer la performance en flexion des trois structures, l'énergie de déformation calculée à partir des courbes Force-Déplacement a été relativisée par rapport au volume de la zone endommagée. Le paramètre qui en découle s'apparente au taux de restitution de l'énergie de déformation, ou ténacité (G), qui est souvent utilisé pour caractériser les matériaux composites. Ce paramètre a été calculé également pour les essais d'impact, afin de comparer les performances lors des deux types d'essais.

D'abord, les renforts superélastiques (TiNi) ont permis d'augmenter légèrement la ténacité moyenne lors des deux types d'essais (+5% impact, +6% flexion), mais avec des écart-types ne permettant pas de conclure avec assurance. Pour leur part, les renforts de Kevlar ont augmenté significativement la ténacité volumique lors de l'impact (+18%), alors que ce gain s'est complètement volatilisé lors des essais de flexion (-8%). De plus, si l'on compare les deux structures renforcées entre elles (TiNi et Kevlar), on constate que la supériorité des coutures de Kevlar lors de l'impact (+14%) s'inverse lors de la flexion, alors que la performance des coutures de TiNi dépasse de 16% celle du Kevlar. Par conséquent, on peut en conclure que la performance du renfort lors de l'impact n'est pas nécessairement garante d'une meilleure performance durant la vie utile de la structure, où les mécanismes de propagation du délaminage sont en fonction. Sur cet aspect, les renforts de TiNi ont montré un comportement satisfaisant et prometteur.

Outre le développement de cette technologie de renfort, le projet visait également à produire un modèle numérique polyvalent pouvant être utilisé en tant qu'outil complémentaire aux essais expérimentaux. Le modèle, entièrement paramétré, a été élaboré sur le logiciel commercial ANSYS de façon à pouvoir simuler divers cas de chargement sur une plaque

composite. La simulation numérique de l'essai de flexion trois-points a permis de confirmer la capacité du modèle à représenter fidèlement la propagation du délaminage pour un cas de chargement complexe, soit la flexion d'un échantillon pré-endommagé. Les images numériques du délaminage prises à différents niveaux de déplacement montrent les mêmes schémas de propagation que ce qui a été observé par la méthode des ultrasons, pour les échantillons non renforcés.

Par ailleurs, l'étude par éléments finis des deux structures composites renforcées (TiNi et Kevlar) a également permis d'identifier des différences subtiles dans le comportement interne de ces structures. En effet, bien que les réponses en force et en déplacement des deux plaques se soient montrées similaires, il est apparu que les deux types de renforts favorisaient la propagation du délaminage le long des coutures, mais à des degrés divers. Les fils de TiNi, de par leur comportement superélastique et leur rigidité semblable à celle du stratifié, semblent engendrer moins de fissures dans leur entourage immédiat que les fils de Kevlar, beaucoup plus rigides. En d'autres termes, pour un même déplacement en flexion, le front de délaminage se propage plus profondément le long des fils de Kevlar. Toutefois, entre les insertions de couture, le Kevlar semble plus efficace que le TiNi à freiner la propagation interlaminaire du délaminage. Néanmoins, si l'on considère le volume global de matériau délaminé durant l'essai de flexion simulé, celui-ci demeure similaire dans tous les cas, que l'échantillon soit renforcé ou non.

À la lumière de ces résultats, il apparaît donc clair que le modèle développé au cours de cette étude est un outil pratique et fiable qui pourra éventuellement être adapté à d'autres cas d'études, notamment pour l'optimisation des paramètres de couture : diamètre du fil, longueur de point et distance entre les lignes de couture, prétension dans le fil. Pour maximiser l'efficacité de ce travail d'optimisation, l'utilisation d'un ordinateur dédié au calcul par éléments finis et possédant beaucoup de mémoire vive (e.g. 16 Go et plus), ou le recours à un ordinateur en grappe (cluster) devrait être envisagé.

RECOMMANDATIONS

Les recommandations qui suivent visent à guider les actions futures dans le cas où une étude subséquente viendrait prolonger ou compléter ce projet de recherche :

- Les essais de flexion devraient être menés sur un montage à quatre points de façon à séparer la zone du moment maximal et les zones d'écrasement aux points d'application de la charge;

- L'implémentation d'éléments de contact dans le modèle pourrait être testée, pour modéliser les supports de flexion et les tiges d'application du chargement. Cela permettrait de rapprocher le cas simulé de la réalité expérimentale;

- Il serait intéressant de mener un travail d'optimisation des paramètres utilisés lors de l'inspection par ultrasons. Ainsi, une combinaison appropriée de paramètres logiciels et de choix de sonde permettrait probablement d'obtenir des images C-Scan et B-Scan de meilleure qualité, en diminuant ou en éliminant la zone de signal saturé aux surfaces de l'échantillon;

- Une étude numérique complémentaire pourrait être menée sur une cellule unitaire, comprenant un seul renfort superélastique et le matériau composite environnant, en tenant compte de la forme réelle de la couture telle qu'observée par microscopie optique;

- La caractérisation complète du matériau composite en traction, en compression et en cisaillement, dans le plan et interlaminaire, permettrait d'éliminer certaines hypothèses posées dans le modèle numérique;

- L'optimisation des paramètres de couture tels que le diamètre du fil, la distance entre les points de couture et la prétension dans le fil permettrait de raffiner la solution technologique proposée dans cette thèse;

- L'utilisation de la propriété de mémoire de forme au chauffage pourrait également faire l'objet d'une étude expérimentale et numérique. Ce type de renforts ajouterait l'élément « activation localisée » à la technologie de renforts testée dans ce projet;

- L'utilisation d'un renfort de géométrie différente pourrait être envisagée (e.g. fil tressé), de façon à diminuer les concentrations de contrainte à l'interface fil/matrice.

BIBLIOGRAPHIE

3Tex. 2007. « 3Tex Technologies ». In *3Tex Inc.* < http://www.3tex.com >. Consulté le 4 juin 2012.

Abrate, Serge. 1998. *Impact on composite structures*. 124. Cambridge, UK: Cambridge University Press, 289 p.

Airbus. 2012. « Technology and innovation ». In *A350 XWB*. < http://www.airbus.com/aircraftfamilies/passengeraircraft/a350xwbfamily/technology-and-innovation/ >. Consulté le 14 juin 2012.

Alfano, G., et M. A. Crisfield. 2001. « Finite element interface models for the delamination analysis of laminated composites: Mechanical and computational issues ». *International Journal for Numerical Methods in Engineering,* vol. 50, n° 7, p. 1701-1736.

American Society for Testing and Materials. 2005a. *Compressive Residual Strength Properties of Damaged Polymer Matrix Composite Plates*. ASTM D7137. West Conshohocken, PA: ASTM International.

American Society for Testing and Materials. 2005b. *Measuring the Damage Resistance of a Fiber-Reinforced Polymer Matrix Composite to a Drop-Weight Impact Event*. ASTM D7136. West Conshohocken, PA: ASTM International.

Aymerich, F.1, R.1 Onnis et P.1 Priolo. 2006. « Analysis of the effect of stitching on the fatigue strength of single-lap composite joints ». *Composites Science and Technology,* vol. 66, n° 2, p. 166-75.

Aymerich, F.1, et P.1 Priolo. 2008. « Characterization of fracture modes in stitched and unstitched cross-ply laminates subjected to low-velocity impact and compression after impact loading ». *International Journal of Impact Engineering,* vol. 35, n° 7, p. 591-608.

Aymerich, F., R. Onnis et P. Priolo. 2005. « Analysis of the fracture behaviour of a stitched single-lap joint ». *Composites Part A: Applied Science and Manufacturing,* vol. 36, n° 5, p. 603-614.

Aymerich, F., P. Priolo et C.T. Sun. 2003. « Static and fatigue behaviour of stitched graphite/epoxy composite laminates ». *Composites Science and Technology,* vol. 63, n° 6, p. 907-917.

Baker, Alan, Stuart Dutton et Donald Kelly (Eds). 2004. *Composite materials for aircraft structures*, 2nd. 111. Reston: American Institute of Aeronautics and Astronautics, 599 p.

Bogdanovich, Alexander, et Dmitri Mungalov. 2003. « Recent Advancements in Manufacturing 3-D Braided Preforms and Composites ». In *ACUN-4 Composite systems - macrocomposites, microcomposites, nanocomposites*. (Sydney, Australia, 21-25 juillet 2002), p. 61-72. S. Bandyopadhyay et al.

Bombardier. 2011. « Composite Structure ». In *Bombardier Learjet 85*. < http://www.learjet85.com/en/technology/composite-structure.html >. Consulté le 14 juin 2012.

Brailovski, V., S. Prokoshkin, P. Terriault et F. Trochu. 2003. *Shape Memory Alloys: Fundamentals, Modeling and Applications*. Montréal (Qué.): École de technologie supérieure, 844 p.

Brewer, J.C., et P.A. Lagace. 1988. « Quadratic stress criterion for initiation of delamination ». *Journal of Composite Materials,* vol. 22, n° 12, p. 1141-55.

Byun, Joon-Hyung, Sung-Wook Song, Chang-Hoon Lee, Moon-Kwang Um et Byung-Sun Hwang. 2006. « Impact properties of laminated composites with stitching fibers ». *Composite Structures, Fifteenth International Conference on Composite Materials - ICCM-15,* vol. 76, n° 1-2, p. 21-27.

Camanho, P. P., C. G. Davila et M. F. De Moura. 2003. « Numerical simulation of mixed-mode progressive delamination in composite materials ». *Journal of Composite Materials,* vol. 37, n° 16, p. 1415-1438.

Camanho, P.P., et F.L. Matthews. 1999. « Progressive damage model for mechanically fastened joints in composite laminates ». *Journal of Composite Materials,* vol. 33, n° 24, p. 2248-2280.

Campbell, F.C. 2010. *Structural Composite Materials*. Ohio, 621 p.

Chang, Fu-Kuo, et Kuo-Yen Chang. 1987. « Progressive damage model for laminated composites containing stress concentrations ». *Journal of Composite Materials,* vol. 21, n° 9, p. 834-855.

Chang, P., A. P. Mouritz et B. N. Cox. 2006. « Properties and failure mechanisms of z-pinned laminates in monotonic and cyclic tension ». *Composites Part A: Applied Science and Manufacturing,* vol. 37, n° 10, p. 1501-1513.

Chen, Leishan, Peter G. Ifju et Bhavani V. Sankar. 2005. « Analysis of mode I and mode II tests for composites with translaminar reinforcements ». *Journal of Composite Materials,* vol. 39, n° 15, p. 1311-1333.

Chou, S. C., O. Orringer et J. H. Rainey. 1976. « Post-failure behavior of laminates. I. No stress concentration ». *Journal of Composite Materials,* vol. 10, n° 4, p. 371-81.

Chun, Heoung-Jae, Hyung-Woo Kim et Joon-Hyung Byun. 2006. « Effects of through-the-thickness stitches on the elastic behavior of multi-axial warp knit fabric composites ». *Composite Structures,* vol. 74, n° 4, p. 484-494.

Corigliano, A., et S. Mariani. 2001. « Simulation of damage in composites by means of interface models: Parameter identification ». In *Workshop `Recent Advances in Continuum Damage Mechanics for Composites', 20-22 Sept. 2000*. (UK), 15. 5068. Vol. 61, p. 2299-315. Coll. « Compos. Sci. Technol. (UK) »: Elsevier. < http://dx.doi.org/10.1016/S0266-3538(01)00123-3 >.

De Paiva, Jane Maria Faulstich, Sergio Mayer et Mirabel Cerqueira Rezende. 2005. « Evaluation of mechanical properties of four different carbon/epoxy composites used in aeronautical field ». *Materials Research,* vol. 8, n° 1, p. 91-97.

Degrieck, Joris, et Wim Van Paepegem. 2001. « Fatigue damage modeling of fibre-reinforced composite materials: Review ». *Applied Mechanics Reviews,* vol. 54, n° 4, p. 279-300.

Dickinson, L.C.1, G.L. Farley et M.K. Hinders. 1999. « Prediction of effective three-dimensional elastic constants of translaminar reinforced composites ». *Journal of Composite Materials,* vol. 33, n° 11, p. 1002-29.

Diehl, Ted. 2008. « On using a penalty-based cohesive-zone finite element approach, Part I: Elastic solution benchmarks ». *International Journal of Adhesion and Adhesives,* vol. 28, n° 4–5, p. 237-255.

Dransfield, Kimberley A., Lalit K. Jain et Yiu-Wing Mai. 1998. « On the effects of stitching in CFRPs - I. Mode I delamination toughness ». *Composites Science and Technology,* vol. 58, n° 6, p. 815-827.

Dransfield, Kimberley, Caroline Baillie et Yiu-Wing Mai. 1994. « Improving the delamination resistance of cfrp by stitching-a review ». *Composites Science and Technology,* vol. 50, n° 3, p. 305-317.

Facchinello, Yann. 2011. « Développement de la technologie de laminage à tiède pour la mise en forme d'alliage à mémoire de forme Ti-Ni ». Mémoire de maîtrise en génie mécanique. Montréal, École de technologie supérieure, 132 p.

Fleming, D.C. 2001. « Delamination modeling of composites for improved crash analysis ». *Journal of Composite Materials,* vol. 35, n° 19, p. 1777-1792.

Gauthier, François-Simon, Pierre-Luc Vachon, Vladimir Brailovski et Patrick Terriault. 2006. « Development of a numerical model for the optimization of damage controlling carbon/epoxy composites containing SMA wires ». In *Fifth Canada-US CanSmart Workshop*. (Toronto, Oct. 13-14 2005).

Gerlach, Robert, Clive R. Siviour, Jens Wiegand et Nik Petrinic. 2012. « In-plane and through-thickness properties, failure modes, damage and delamination in 3D woven carbon fibre composites subjected to impact loading ». *Composites Science and Technology,* vol. 72, n° 3, p. 397-411.

Glaessgen, E.H., I.S. Raju et C.C. Poe Jr. 2002. « Analytical and experimental studies of the debonding of stitched and unstitched composite joints ». *Journal of Composite Materials,* vol. 36, n° 23, p. 2599-2622.

Goyal, Vinay K., Navin R. Jaunky, Eric R. Johnson et Damodar R. Ambur. 2004. « Intralaminar and interlaminar progressive failure analyses of composite panels with circular cutouts ». *Composite Structures,* vol. 64, n° 1, p. 91-105.

Greenhalgh, Emile, et Matthew Hiley. 2003. « The assessment of novel materials and processes for the impact tolerant design of stiffened composite aerospace structures ». *Composites Part A: Applied Science and Manufacturing,* vol. 34, n° 2, p. 151-161.

Hashin, Z. 1980. « Failure criteria for unidirectional fiber composites ». *Transactions of the ASME. Journal of Applied Mechanics,* vol. 47, n° 2, p. 329-34.

Hess, H., Y.C. Roth et N. Himmel. 2007. « Elastic constants estimation of stitched NCF CFRP laminates based on a finite element unit-cell model ». *Composites Science and Technology,* vol. 67, n° 6, p. 1081-1095.

Iannucci, L. 2006. « Progressive failure modelling of woven carbon composite under impact ». *International Journal of Impact Engineering,* vol. 32, n° 6, p. 1013-1043.

Institut für Verbundwerkstoffe. 2012. « Research & Development - Projects ». < http://www.ivw.uni-kl.de/index.php?id=88&L=1 >. Consulté le 12 juin 2012.

Instron. 2012. « Impact Testing for Composites ». < http://www.instron.tm.fr/wa/product/Composites-Impact-Testing.aspx >.

Jain, Lalit K., Kimberley A. Dransfield et Yiu-Wing Mai. 1998. « On the effects of stitching in CFRPs - II. Mode II delamination toughness ». *Composites Science and Technology,* vol. 58, n° 6, p. 829-837.

Kaw, Autar K. 2006. *Mechanics of Composite Materials*. CRC Press, Taylor and Francis Group, 466 p.

Lau, Kin-Tak, Hang-Yin Ling et Li-Min Zhou. 2004. « Low velocity impact on shape memory alloy stitched composite plates ». *Smart Materials and Structures,* vol. 13, n° 2, p. 364-370.

Lopresto, V., V. Melito, C. Leone et G. Caprino. 2006. « Effect of stitches on the impact behaviour of graphite/epoxy composites ». *Composites Science and Technology,* vol. 66, n° 2, p. 206-214.

Lorriot, Th., G. Marion, R. Harry et H. Wargnier. 2003. « Onset of free-edge delamination in composite laminates under tensile loading ». *Composites Part B: Engineering,* vol. 34, n° 5, p. 459-471.

Mandell, John F., Douglas S. Cairns, Daniel D. Samborsky, Robert B. Morehead et Darrin J. Haugen. 2003. « Prediction of delamination in wind turbine blade structural details ». *Journal of Solar Energy Engineering, Transactions of the ASME Wind Energy,* vol. 125, n° 4, p. 522-530.

Massabo, R., D.R. Mumm et B.N. Cox. 1998. « Characterizing mode II delamination cracks in stitched composites ». *International Journal of Fracture,* vol. 92, n° 1, p. 1-38.

Mignery, L. A., T. M. Tan et C. T. Sun. 1985. « The use of stitching to suppress delamination in laminated composites ». In *Delamination and debonding of materials, ASTM STP 876*, W. S. Johnson. 6019. p. 371-385. Philadelphia: American Society for Testing and Materials.

Mikhaluk, D.S., T.C. Truong, A.I. Borovkov, S.V. Lomov et I. Verpoest. 2008. « Experimental observations and finite element modelling of damage initiation and evolution in carbon/epoxy non-crimp fabric composites ». *Engineering Fracture Mechanics,* vol. 75, n° 9, p. 2751-66.

Mouritz, A. P., M. K. Bannister, P. J. Falzon et K. H. Leong. 1999. « Review of applications for advanced three-dimensional fibre textile composites ». *Composites Part A: Applied Science and Manufacturing,* vol. 30, n° 12, p. 1445-1461.

Mouritz, A. P., P. Chang et B. N. Cox. 2007. « Flexural properties of z-pinned laminates ». *Composites Part A (Applied Science and Manufacturing),* vol. 38, n° 2, p. 244-51.

Mouritz, A. P., et B. N. Cox. 2010. « A mechanistic interpretation of the comparative in-plane mechanical properties of 3D woven, stitched and pinned composites ». *Composites Part A: Applied Science and Manufacturing,* vol. 41, n° 6, p. 709-728.

Mouritz, A.P. 2007. « Review of z-pinned composite laminates ». *Composites Part A: Applied Science and Manufacturing,* vol. 38, n° 12, p. 2383-2397.

Mouritz, A.P., et B.N. Cox. 2000. « Mechanistic approach to the properties of stitched laminates ». *Composites Part A: Applied Science and Manufacturing,* vol. 31, n° 1, p. 1-27.

Mouritz, A.P., K.H. Leong et I. Herszberg. 1997. « Review of the effect of stitching on the in-plane mechanical properties of fibre-reinforced polymer composites ». *Composites Part A: Applied Science and Manufacturing,* vol. 28, n° 12, p. 979-991.

Ogale, A., et P. Mitschang. 2004. « Tailoring of textile preforms for fibre-reinforced polymer composites ». *Journal of Industrial Textiles,* vol. 34, n° 2, p. 77-96.

Papanikos, P., K.I. Tserpes, G. Labeas et Sp. Pantelakis. 2005. « Progressive damage modelling of bonded composite repairs ». *Theoretical and Applied Fracture Mechanics,* vol. 43, n° 2, p. 189-198.

Papanikos, P., K.I. Tserpes et S. Pantelakis. 2003. « Modelling of fatigue damage progression and life of CFRP laminates ». *Fatigue and Fracture of Engineering Material and Structures,* vol. 26, n° 1, p. 37-47.

Park, Yong-Bin, Byeong-Hee Lee, Jin-Hwe Kweon, Jin-Ho Choi et Ik-Hyeon Choi. 2012. « The strength of composite bonded T-joints transversely reinforced by carbon pins ». *Composite Structures,* vol. 94, n° 2, p. 625-634.

Partridge, Ivana K. 2008. « Damage Tolerance in Composite Structures ». In *Automotive Engineering*. p. 241-252. Coll. « Series in Material Science and Engineering »: Taylor & Francis. < http://dx.doi.org/10.1201/9781420011906.ch18 >. Consulté le 2012/07/05.

Pereira, A.B., et A.B. de Morais. 2004. « Mode I interlaminar fracture of carbon/epoxy multidirectional laminates ». *Composites Science and Technology,* vol. 64, n° 13-14, p. 2261-2270.

Pipes, R. B., et N. J. Pagano. 1970. « Interlaminar stresses in composite laminates under uniform axial extension ». *Journal of Composite Materials,* vol. 4, p. 538-548.

Riccio, A. 2005. « Effects of geometrical and material features on damage onset and propagation in single-lap bolted composite joints under tensile load: Part II - Numerical studies ». *Journal of Composite Materials,* vol. 39, n° 23, p. 2091-2113.

Rugg, K. L., B. N. Cox et R. Massabò. 2002. « Mixed mode delamination of polymer composite laminates reinforced through the thickness by z-fibers ». *Composites Part A: Applied Science and Manufacturing,* vol. 33, n° 2, p. 177-190.

Rys, Tomek, Bhavani V. Sankar et Peter G. Ifju. 2010. « Investigation of fracture toughness of laminated stitched composites subjected to mixed mode loading ». *Journal of Reinforced Plastics and Composites,* vol. 29, n° 3, p. 422-430.

Sankar, B. V., et S. K. Sharma. 1997. « Mode II delamination toughness of stitched graphite/epoxy textile composites ». *Composites Science and Technology,* vol. 57, n° 7, p. 729-737.

Scarponi, C., A.M. Perillo, L. Cutillo et C. Foglio. 2007. « Advanced TTT composite materials for aeronautical purposes: Compression after impact (CAI) behaviour ». *Composites Part B: Engineering,* vol. 38, n° 2, p. 258-264.

Shen, F., K.H. Lee et T.E. Tay. 2001. « Modeling delamination growth in laminated composites ». *Composites Science and Technology,* vol. 61, n° 9, p. 1239-51.

Shokrieh, Mahmood M. 1991. « Failure of laminated composite pinned connections ». Master Thesis. Canada, McGill University. < http://proquest.umi.com/pqdweb?did=748138281&Fmt=7&clientId=46962&RQT=309&VName=PQD >.

Shokrieh, Mahmood M., et Larry B. Lessard. 2000. « Progressive fatigue damage modeling of composite materials, Part I: Modeling ». *Journal of Composite Materials,* vol. 34, n° 13, p. 1056-1080.

Shokrieh, Mahmood M., et Roham Rafiee. 2005. « Simulation of fatigue failure in a full composite wind turbine blade ». *Composite Structures,* vol. In Press, Corrected Proof.

Simpson, J.C., et C. Boller. 2008. « Design and performance of a shape memory alloy-reinforced composite aerodynamic profile ». *Smart Materials and Structures,* vol. 17, n° 2, p. 025028.

Steeves, Craig A., et Norman A. Fleck. 2006. « In-plane properties of composite laminates with through-thickness pin reinforcement ». *International Journal of Solids and Structures,* vol. 43, n° 10, p. 3197-3212.

Tay, T. E. 2003. « Characterization and analysis of delamination fracture in composites: an overview of developments from 1990 to 2001 ». *Applied Mechanics Review,* vol. 56, n° 1, p. 1-32.

Tay, T. E., V. B. C. Tan et S. H. N. Tan. 2005. « Element-Failure: An Alternative to Material Property Degradation Method for Progressive Damage in Composite Structures ». *Journal of Composite Materials,* vol. 39, n° 18, p. 1659-1675.

The Boeing Company. 2008. « Boeing 787 from the ground up ». In *Aero*. < http://www.boeing.com/commercial/aeromagazine/articles/qtr_4_06/article_04_2.html >. Consulté le 14 juin 2012.

Tsai, Gwo-Chung, et Jun-Wei Chen. 2005. « Effect of stitching on Mode I strain energy release rate ». *Composite Structures,* vol. 69, n° 1, p. 1-9.

Tserpes, K.I., G. Labeas, P. Papanikos et Th. Kermanidis. 2002. « Strength prediction of bolted joints in graphite/epoxy composite laminates ». *Composites Part B: Engineering,* vol. 33, n° 7, p. 521-529.

Tserpes, K.I., P. Papanikos et Th. Kermanidis. 2001. « A three-dimensional progressive damage model for bolted joints in composite laminates subjected to tensile loading ». *Fatigue and Fracture of Engineering Materials and Structures,* vol. 24, n° 10, p. 663-675.

Uj, J. 2004. « A finite element model of delamination in cross-ply laminates ». *Journal of computational and applied mechanics,* vol. 5, n° 1, p. 151-155.

University of Latvia. 2012. « Stiffness Reduction of the Laminates ». In *Institute of Polymer Mechanics*. < http://www.pmi.lv/soft/stirel/index.htm >. Consulté le 20 juin 2012.

Van Paepegem, W., et J. Degrieck. 2001. « Experimental set-up for and numerical modelling of bending fatigue experiments on plain woven glass/epoxy composites ». *Composite Structures,* vol. 51, n° 1, p. 1-8.

Van Paepegem, W., J. Degrieck et P. De Baets. 2001. « Finite element approach for modelling fatigue damage in fibre-reinforced composite materials ». *Composites Part B: Engineering,* vol. 32, n° 7, p. 575-588.

Wei, J., et J.H. Zhao. 1991. « Three-dimensional finite element analysis on interlaminar stresses of symmetric laminates ». *Computers and Structures,* vol. 41, n° 4, p. 561-567.

Whitcomb, John D. 1988. « Three-dimensional analysis of a postbuckled embedded delamination ». *NASA Technical Paper*, n° 2823, p. 1-24.

Wood, Michael D.K., Xiannian Sun, Liyong Tong, Anthony Katzos, Adrian R. Rispler et Yiu-Wing Mai. 2007a. « The effect of stitch distribution on Mode I delamination toughness of stitched laminated composites - experimental results and FEA simulation ». *Composites Science and Technology,* vol. 67, n° 6, p. 1058-1072.

Wood, Michael D.K., Xiannian Sun, Liyong Tong, Quantian Luo, Anthony Katzos et Adrian Rispler. 2007b. « A New ENF Test Specimen for the Mode II Delamination

Toughness Testing of Stitched Woven CFRP Laminates ». *Journal of Composite Materials,* vol. 41, n° 14, p. 1743-1772.

Xiaoquan, Cheng, Ali M. Al-Mansour, Li Zhengneng et Kou Chenghe. 2005. « Compression strength of stitched laminates after low-velocity impact ». *Journal of Reinforced Plastics and Composites,* vol. 24, n° 9, p. 935-947.

Xu, Y., K. Otsuka, H. Nagai, H. Yoshida, M. Asai et T. Kishi. 2003. « A SMA/CFRP hybrid composite with damage suppression effect at ambient temperature ». *Scripta Materialia,* vol. 49, n° 6, p. 587-93.

Yoshimura, Akinori, Tomoaki Nakao, Shigeki Yashiro et Nobuo Takeda. 2008. « Improvement on out-of-plane impact resistance of CFRP laminates due to through-the-thickness stitching ». *Composites Part A: Applied Science and Manufacturing,* vol. 39, n° 9, p. 1370-1379.

Yoshimura, Akinori, Shigeki Yashiro, Tomonaga Okabe et Nobuo Takeda. 2007. « Characterization of tensile damage progress in stitched CFRP laminates ». *Advanced Composite Materials: The Official Journal of the Japan Society of Composite Materials,* vol. 16, n° 3, p. 223-244.

Zhang, X., L. Hounslow et M. Grassi. 2006. « Improvement of low-velocity impact and compression-after-impact performance by z-fibre pinning ». *Composites Science and Technology,* vol. 66, n° 15, p. 2785-2794.

Zhao, L.G., N.A. Warrior et A.C. Long. 2006. « Finite element modelling of damage progression in non-crimp fabric reinforced composites ». *Composites Science and Technology,* vol. 66, n° 1, p. 36-50.